P-119

NASA / USRA

HIGH ALTITUDE RESEARCH AIRCRAFT

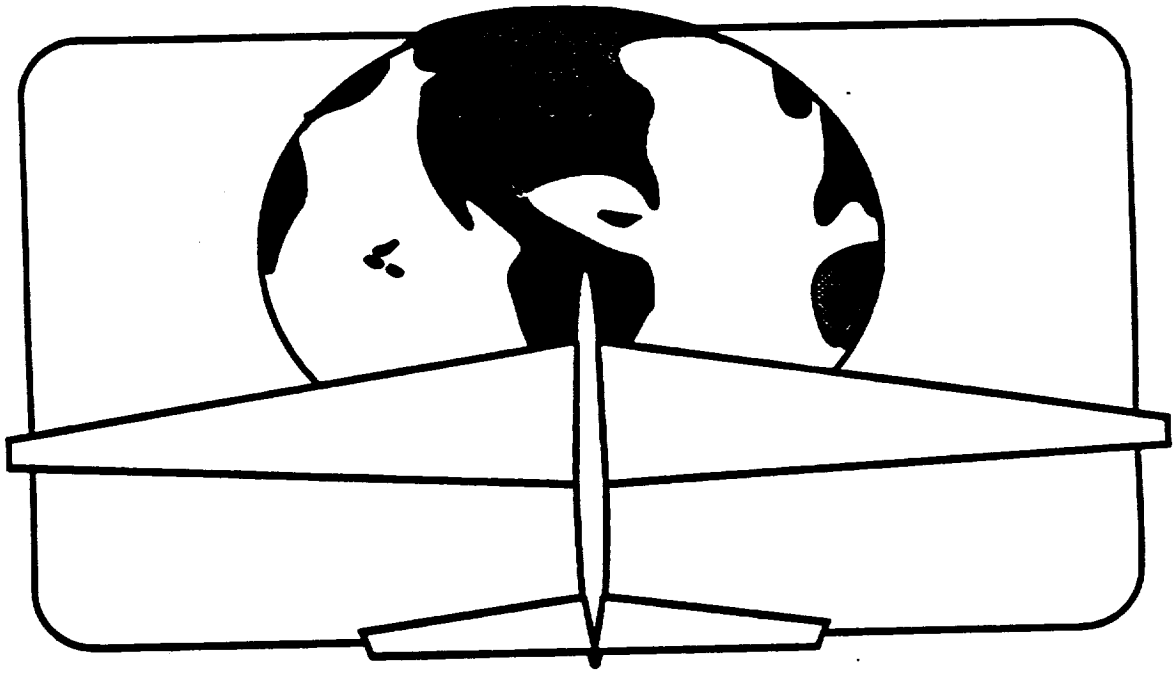

VOLUME 2

SUBMITTED - 1 JULY 1990

Advanced Aerospace Design Project
ARO 446/ ARO 463

Global Sentry:

NASA/USRA HIGH ALTITUDE RECONNAISSANCE AIRCRAFT DESIGN

California State Polytechnic University, Pomona
Winter/Spring 1990

PRELIMINARY STUDY OF A HIGH ALTITUDE RECONNAISSANCE AIRCRAFT

GLOBAL SENTRY

CAL POLY UNIVERSITY, POMONA

WINTER/SPRING 1990

Designers: Mona-Lisa Alexandru

Frank Martinez
(Aerodynamics)

Jim Tsou
(Structures)

Henry Do
(Structures)

Ashish Peters
(Performance)

Tom Chatsworth
(Stability and Control)

Ye Yu
(Maintainability)

Jaskiran Dhillon
(Cost Analysis)

Advisor: Prof. Paul A. Lord

SUMMARY

The Global Sentry is a high altitude reconnaissance aircraft design for the NASA/USRA design project. The Global Sentry uses proven technologies, light-weight composites, and meets the R.F.P. requirements in the following ways:

- capability of flying at an altitude of 130,000 ft
- sampling time of about 10 hours
- cruise range over 6,000 miles
- can be expanded for two pilots.

Chapter 2 describes the mission requirements for the Global Sentry. Chapter 3 and 4 discuss the configuration option and a description of the final design. Preliminary sizing analyses and the mass properties of the design are presented in Chapter 5. Chapter 6 describes the aerodynamic features of the Global Sentry, while Chapter 7 summarizes the stability and control characteristics designed into the flight control system. The performance characteristics are shown in Chapter 8. Chapter 9 discusses the propulsion installation and system layout. The Global Sentry structural design is the subject of Chapter 10, including a wing structural analysis. The cockpit, controls and display layouts are covered in Chapter 11. Manufacturing is covered in Chapter 12 and the subject of Chapter 13 is life cost estimation. Reliability is

discussed in Chapter 14. Conclusions about the current Global Sentry design are presented in Chapter 15, along with suggested areas for future engineering work.

TABLE OF CONTENTS

GENERALIZED SYMBOLS

SYMBOL	DEFINITION
a.c.	aerodynamic center
AR	wing span ratio
b	wing span
$\bar{c}$	mean geometric chord
c_l	airfoil lift coefficient
c_m	airfoil pitching moment
c_t	tip chord
c_r	root chord
C_D	airplane drag coefficient
C_L	airplane lift coefficient
I	mass moment of inertia
L	lift
L/D	lift-to drag ratio
M	free stream Mach number
n	airplane load factor
S	wing platform area
S_V	vertical tail area
t/c	thickness ratio at c
W	airplane weight

GREEK SYMBOLS

α	perturbed angle of attack and angle of attack

β	perturbed sideslip and sideslip
θ	perturbed pitch attitude and pitch attitude
Φ	perturbed roll attitude and roll attitude

SUBSCRIPTS

cr	critical
xx	about body x-axis
wet	wetted
yy	about body y-axis
zz	about body z-axis

ACRONYMS

DATCOM	Data Compendium
HUD	Heads Up Display
RFP	Request For Proposal
NASA	National Aeronautics And Space Administration
USRA	Universities Space Research Association

1. INTRODUCTION

Recent discoveries of the ozone holes over the Antarctic and Arctic has generated much concern in the world wide scientific community for the effect of solar radiation on the biosphere. The ozone layers, found in the upper atmosphere, play a fundamental role in global climate, and provide protection against harmful ultraviolet rays.

Scientists believe that a chlorine molecule, OClO, found in CFC (chlorofluorocarbons - man made chemicals) is destroying the ozone molecules- O_3. It is believed that during the winter months, a vortex forms over the North Pole which encapsulates cold air that in turn triggers the breakdown of CFC and the destruction of the ozone layers. In spring, when the Antarctic vortex brakes, ozone-poor air is transported into lower latitudes. Therefore, a global depletion is occurring, where 3% depletion was noted over the past decade. Figure 1.1, using data from Nimbus-7 total ozone mapping spectrometer(TOMS) over Australia, shows how the chemical destruction of ozone over Antarctica in early spring is having an impact on lower latitudes.

The ozone layers location is dependent on temperature, over the poles the ozone is located between 50,000 and 85,000 feet, where over the tropics is found at higher altitudes of above 100,000 ft. Since this range is outside the ER-2

aircraft operating envelope, NASA was promoted to start an investigation of the design requirements for a

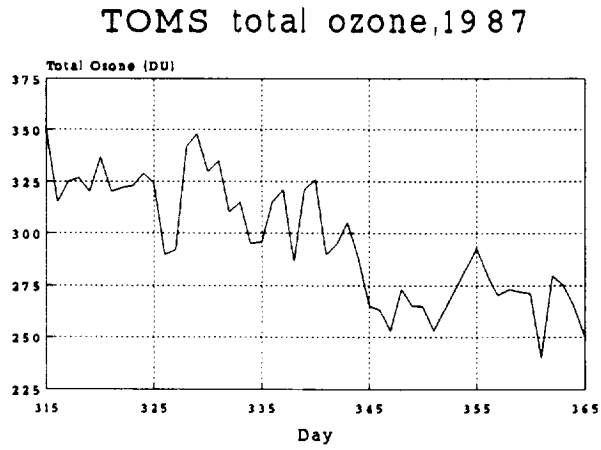

Figure 1.1

subsonic aircraft that would have the capability of achieving altitudes in excess of 130,000 feet. As part of this investigation and the NASA/USRA design project, California State Polytechnic University Pomona has been involved in the design of an aircraft that would meet these high altitude cruise and payload requirements.

2. MISSION DESCRIPTION

A common request for proposal (RFP) was developed from the very general mission requirements provided by NASA. The request for proposal was for a complete aircraft that meets the requirements in Table 2.1.

Table 2.1

RFP - Requirements	
Altitude	= cruise at 130,000 feet
Payload	= 3,000 lb.
Speed	= Mach .7
Range	= total transit: 6,000 miles cruise time:6 hours
crew	= one minimum
technology	- current

As directed by the RFP the basic mission profile can be seen in Figure 2.1. Taking in consideration that the range was 6000 nm and a sampling time of 6 hours at Mach .7 it was calculated that cruise range will be only about 3000 nm, which in turn will leave 3000 nm for climb and descent. By optimizing the climb through energy methods it was found that the sampling time will approximate 10 hours.

Mission Profile

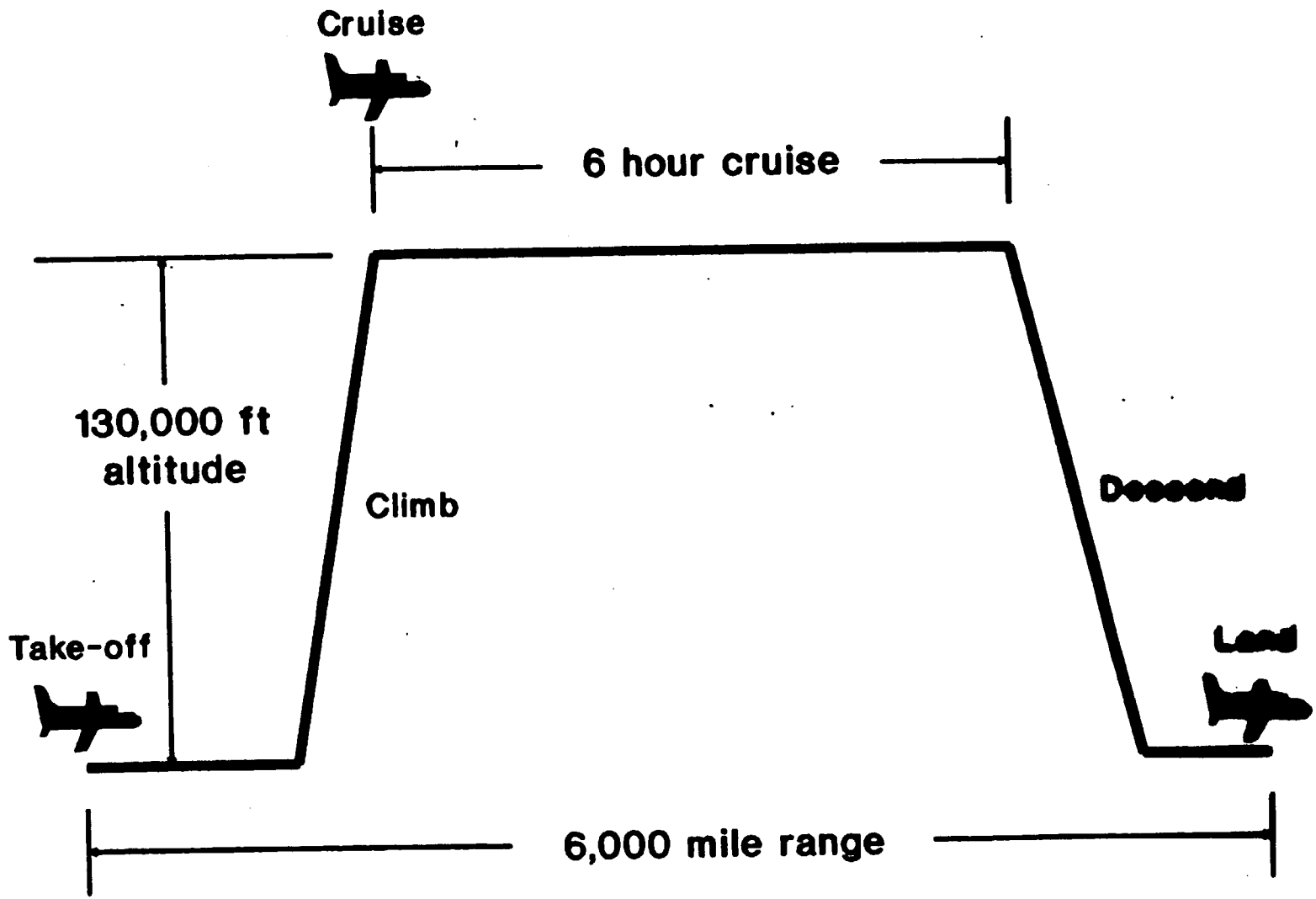

3. CONFIGURATION SELECTION

One of the critical design parameters was that at high altitudes the air density is very low, approximately 0.00003211 slugs/ft^3, as it can be seen in Figure 3.1. This low density at high altitude results in a very small dynamic pressure (q_∞<8.0) generating small lift per unit area and thereby requiring prohibitively large wing surface areas.

AIR DENSITY VS. ALTITUDE

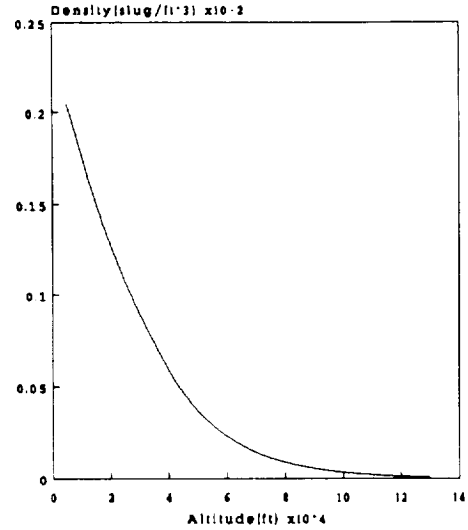

Figure 3.1

In order to maximize the lift a straight wing was desired. In primary analysis certain configurations were looked at such:

1. Conventional (tail aft)
2. Flying wing
3. Three surface (small canard-wing-h. tail)
4. Canard (wing aft)

First, the flying wing design was rejected because at such high altitude the plane would not be stable, also a flying wing has a high leading edge sweep which would reduce the lift drastically. Next, the three surface configuration was eliminated since the slight gain in the lower induced drag was offset by the lower stability in the system. And last, the canard configuration was dismissed since it has a lower L/D than a conventional design, also preliminary studies showed that there would be stability problems. Therefore, the conventional configuration was chosen and is discussed in this report.

4. CONFIGURATION DESCRIPTION

Figure 4.1 presents the front, top and side views of the Global Sentry configuration. The plane is a twin fuselage with a 6 degree of sweep at the leading edge (for stability purposes). Table 4.1 contains the tabulated geometry.

	SPECIFICATIONS		GEOMETRY	
Weights	W_{to}	60,127 lb	Fuselage Length	100 ft
	W_{empty}	37,534 lb	Max.Dia	6 ft
	$W_{payload}$	3,250 lb		
Rotor 3	Blades	6	Wing	Wing Loading
	Radius	13.5 ft	Area	20,008 ft^2
	Blade twist	55 @ .75R	Span	490 ft
		75 @ .3R	AR	12
	Advance ratio	1.2	Sweep(LE)	+6
	Efficiency	.71		
			Horiz.Tail Span	158 ft
Power Plant	Number	4	AR	1.91
	Type	Recipicating Spark Ignition		
	Cruise Power	1202.8 hp	Vert.Tail Span	24 ft
	Max. Power	1240 hp	AR	1.78
			Sweep	36.9

Table 4.1

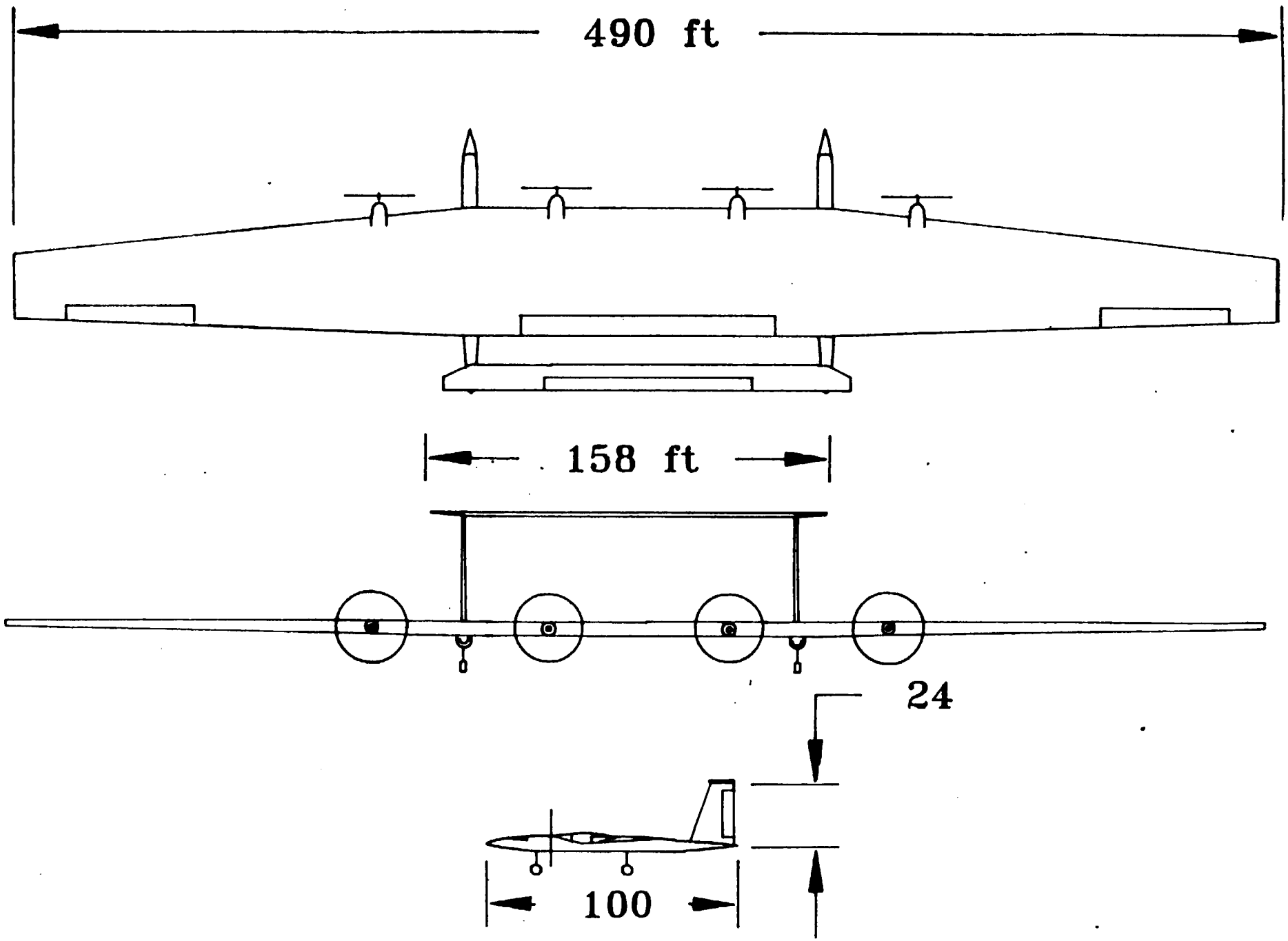
490 ft
158 ft
24
100

5.0 PRELIMINARY SIZING AND MASS PROPERTIES

5.1 CONSTRAINT ANALYSIS

An efficient aircraft not only satisfies all the RFP requirements but also operates at a point which is optimum for every phase of the mission. On of the tools used to derive such a point is obtained using a constraint diagram by performing several parametric analyses. These parameters include takeoff, landing, cruise and climbing. The resulting chart, Figure 5.1, was used to determine an optimum wing loading and the power loading. Initial aircraft dimensions were then determined and refined with more precise methods in each category. The final wing and power loading for the Global Sentry are 3.2 lb/sq ft., and 24.3 lb/hp respectively. The corresponding wing surface area was approximately 19017 sq. ft.

5.2 REFINED WEIGHT ESTIMATE

The refined weight estimate of the Global Sentry was determined with methodology given in Ref.5. Fuel fraction method was used to estimate the fuel weight. The preliminary dimensions for the aircraft were approximated from historical and preliminary analysis to be used in the weight method. This weight estimation technique evaluates the component weights with respect to the geometric properties of the component and the initial weight

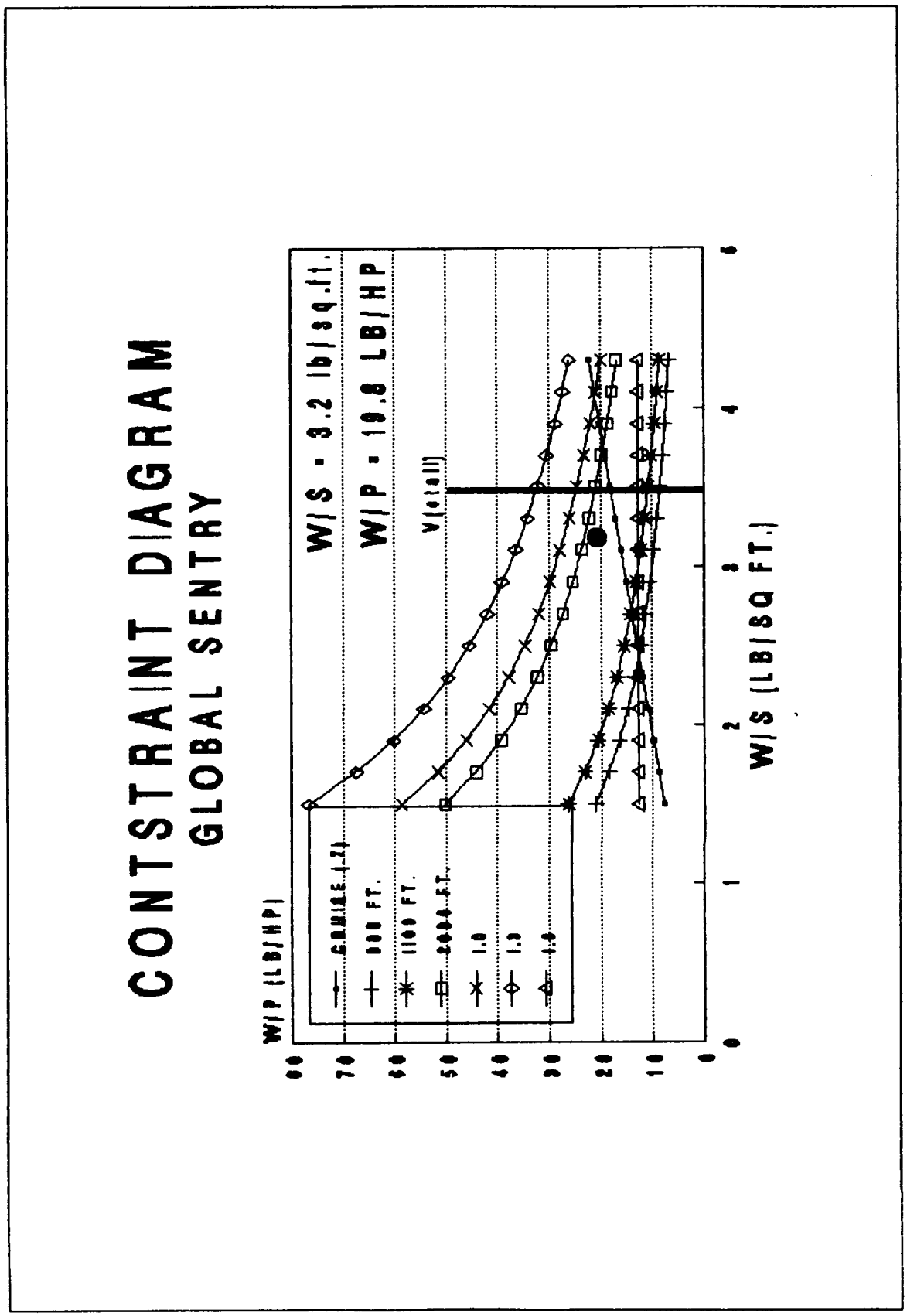
CONTSTRAINT DIAGRAM
GLOBAL SENTRY
W/S - 3.2 lb/sq.ft.
W/P - 19.8 LB/HP
V(stall)
W/P (LB/HP)
W/S (LB/SQ FT.)
0
10
20
30
40
50
60
70
1
2
3
4
5
6
CRUISE (.7)
500 FT.
1100 FT.
2000 FT.
1.0
1.3
1.6

Figure 5.1

approximation. This iterative process was done until the weight estimate was equal to the resulting weight estimate. A spreadsheet program was used to do this iterative process. The complete weight summary is given in Table 5.1 along with the empty weight breakdown.

5.3 CENTER OF GRAVITY

The center of gravity and its movement with respect to different loading conditions was evaluated for the Global Sentry. The location of the centers of gravity for the wing, fuselage, avionics, cargo, empennage, engines and landing gear were estimated with techniques given in Ref.5. A reference point of 6 feet above the bottom of the fuselage and the nose of the airplane was selected about which moments were calculated.

5.4 MOMENTS OF INERTIA

To evaluate the moments of inertia, the aircraft was broken up into small components and then the moments of inertia were taken about the desired axis. The analysis was performed for the conditions of maximum take-off weight. The results are summarized in Table 5.2.

Table 5.1
Component Weight Breakdown

COMPONENTS	WEIGHT(LBS)
AVIONICS	500
FUSELAGE	5344.5
CARGO	3250
ENGINES(4)	10704
VERTICAL TAIL	498.8
HORIZONTAL TAIL	954
LANDING GEAR	2213.6
WING	15876
FUEL	21481
EMPTY WEIGHT	36123
GROSS TAKEOFF WEIGHT	60,854

TABLE 5.2

MOMENTS OF INERTIA

PHASE	Ixx	Iyy	Izz	Ixz
Takeoff	1.003e8	1.068e7	1.106e8	7.115e4
+Cruise	1.003e8	1.062e7	1.105e8	6.319e4
-Cruise	1.003e8	1.055e7	1.104e8	6.918e4
Landing	1.003e8	1.054e7	1.104e8	9.400e4

*the units for moments of inertia are slug sqft.

6. Aerodynamics

6.1 Introduction

In this chapter, the aerodynamic properties of the Global Sentry will be discussed. The wing of the Global Sentry, as is true of any aircraft, is the main contributor to lift, and as a result, this chapter will concentrate on the design of the wing aerodynamics. In section 6.2, the reference geometry used in the aerodynamic calculations will be identified. Section 6.3 will deal with airfoil selection followed by the discussion of aircraft lift and drag in sections 6.3 and 6.4, respectively.

6.2 Reference Geometry

The reference data used in the calculation of the aerodynamic properties of the Global Sentry are as follows:

$$S_{ref} = 20{,}000 \text{ sq. ft.}$$

$$\text{MGC} = 34 \text{ ft.}$$

$$b = 490 \text{ ft.}$$

6.3 Airfoil Selection

One of the foremost factors influencing the design lift coefficient of the airfoil for the Global Sentry was the wing loading requirement. For instance, it was determined that the criterion of low design lift coefficient resulted in low values of wing loading which would only increase what seems to be an unrealistic wing span. On the other hand, analysis showed that high wing loadings resulted in design lift

coefficients of greater than 1.3 which are not practical with existing airfoil technology. This latter requirement would violate the RFP which states that the project should be feasible using current technology. Thus, a compromise between wing loading and design lift coefficient had to be met. This resulted in the selection of a design lift coefficient of 1.2.

In addition to the design lift coefficient, it was determined that the following criteria also had to be satisfied in selecting an airfoil for the Global Sentry:

- Maximize M_{crit}
- Maximize $C_{l_{MAX}}$
- Maximize C_{l_α}
- Maximize Fuel Volume
- Minimize C_d
- Minimize Wing Weight

It was concluded from sources such as Reference 3 that to maximize the critical Mach number the two criteria were:

(1) Employ a supercritical section

(2) Choose a thin airfoil

Also, it was determined that to optimize the maximum lift the criteria were: (1) Choose a thick airfoil

(2) Choose a highly cambered airfoil

(3) Employ a section with a high degree of camber

Based on the requirements listed above a supercritical airfoil section, the Eppler 989, was selected to fulfill these requirements. The airfoil section along with its corresponding lift curve and drag polar obtained from Reference 4 are shown in Figures 6.1 , 6.3, and 6.4, respectively.

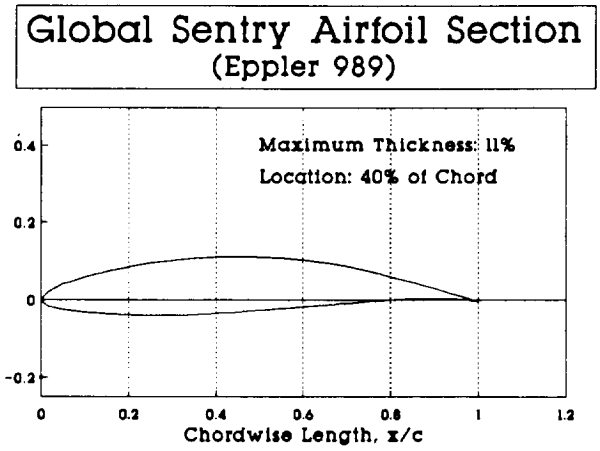

Figure 6.1: Global Sentry airfoil section

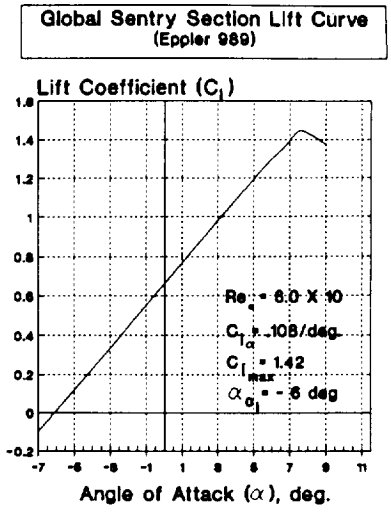

Figure 6.2: Global Sentry lift curve

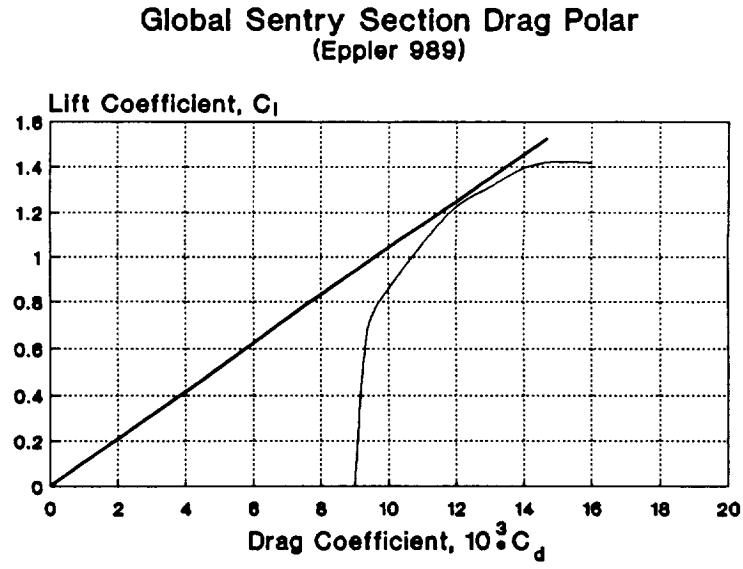

Figure 6.3: Global Sentry drag polar

6.4 Lift Determination

Lift characteristics of the Global Sentry were calculated using the methods outlined in References 1,3, and 4. The results appear in Figure 6.4. The results indicate that the maximum lift coefficient of the wing is 1.29 at an angle of attack of 12.6 degrees.

The large lifting surface of the Global Sentry is such that no high lift devices need to be employed from an aerodynamics perspective. The wing alone can provide the lift required for low speed take-off and landing when such devices need sometimes to be employed.

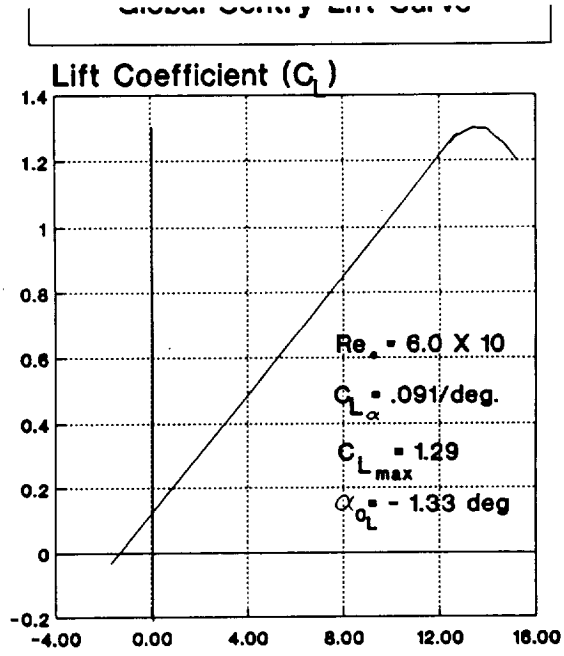

Figure 6.4: Global Sentry Lift Curve

6.5 Drag Estimation

The drag polar for the Global Sentry was determined using the component build up method outlined in Reference 5. The wetted areas of the aircraft were estimated by decomposing the structure into a series of simple geometric shapes whose areas could readily be calculated.

The results of the calculations are shown in Figure 6.5. The parasite drag coefficient of the plane was found to have a value of .0146. In addition, it was estimated that the best lift to drag ratio has a value of 21. However, for cruise conditions, the lift to drag was found to have a value of 17.3 at a corresponding cruise lift coefficient of 1.2.

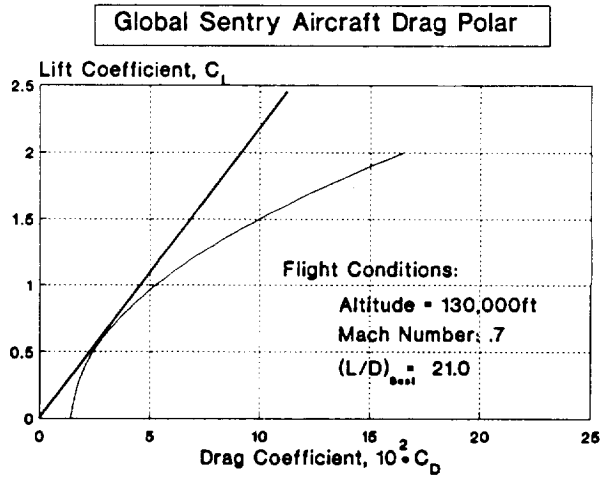

Figure 6.5: Global Sentry drag polar

7. STABILITY AND CONTROL

7.1 STABILITY DERIVATIVES

The stability and control dervatives for the Global Sentry have been determined for different stages in the mission using the program in Ref. 9 and methods from References 6 and 7. The descriptions of the flight conditions for which the stability analysis was performed are listed in Table 7.1. Flight conditions 1-4 correspond to flight after takeoff, at the beginning of cruise, at the end of cruise, and just before landing respectively. The corresponding non-dimensional stability derivatives are listed in Table 7.2.

TABLE 7.1 FLIGHT CONDITIONS FOR STABILITY ANALYSIS

	Flt. Cond.I	Flt. Cond.II	Flt. Cond.III	Flt. Cond. IV
Altitude:	Sea Level	130,000 ft.	130,000 ft.	Sea Level
Mach #:	0.2	0.7	0.7	0.2
Weight:	60,854 lb.	54,767 lb.	40,952 lb.	39,373 lb.
C.G.:	26.1 % C_R	26.4 % C_R	31.2 % C_R	32.2 % C_R
I_{xx}:	1.003×10^8	1.003×10^8	1.003×10^8	1.003×10^8
I_{yy}:	1.075×10^7	1.070×10^7	1.055×10^7	1.050×10^7
I_{zz}:	1.106×10^8	1.106×10^8	1.104×10^8	1.104×10^8
I_{xz}:	-7.15×10^4	-6.32×10^4	6.918×10^4	7.754×10^4

TABLE 7.2 GLOBAL SENTRY STABILITY DERIVATIVES

	F.C.I	F.C.II	F.C.III	F.C.IV
Longitudinal Derivatives				
C-D-alpha	0.02	0.6676	0.6676	0.02
C-D-u	0.0	0.0	0.0	0.0
C-L-i-H	0.419	0.5523	0.5523	0.419
C-m-i-H	-.4907	-.6435	-.6125	-.4601
C-l-alpha	5.9695	7.6354	7.6554	5.9695
C-L-u	0.0021	1.2944*	1.2944*	0.0021
C-L-q	4.3545	5.6008	4.7024	3.4579
C-L-delta-E	0.1369	0.1804	0.1804	0.1369
C-L-alpha-dot	0.3979	0.6725	0.6402	0.3731
C-m-alpha	-.5398	-.5847	-.1571	-.104+
C-m-u	0.0	0.0	0.0	0.0
C-m-q	-2.1324	-2.8103	-2.4513	-1.7885+
C-m-delta-E	-.1603	-.2102	-.2001	-.4098
C-m-alpha-dot	-.4660	-.7836	-.7101	-.4098
Lateral-Directional Derivatives				
C-y-beta	-.0796+	-.0829+	-.0829+	-.0796+
C-y-p	-.0043	-.0024	-.0025	.0024
C-y-r	0.0125+	0.0136+	0.013+	0.0117+
C-y-delta-A	0.0	0.0	0.0	0.0
C-y-delta-R	0.0264+	0.0276+	0.0276+	0.0264+
C-l-beta	-.0327	-.1127	-.1128	-.0327
C-l-p	-.6469	-.7713+	-.7713+	-.6469
C-l-r	0.0899	0.5370	0.5370	0.0899+
C-l-delta-A	0.1465	0.2020	0.2020	0.1465
C-l-delta-R	0.0008	0.0005	0.0005	0.0008
C-n-beta	0.056+	0.0065+	0.0062+	0.0052+
C-n-p	-.0037	-.1481	-.1482	-.0037
C-n-r	-.0082+	-.0605+	-.0604+	-.0081+
C-n-delta-A	-.0006	-.02	-.02	-.0006
C-n-delta-R	-.0024+	-.0026+	-.0025+	-.0023

* Value out of typical range for stability
+ Value on extreme of typical range

The original configuration of Global Sentry had no leading edge sweep so that the local velocity would be at a maximum for the best section lift coefficient. However, since the wing weight is a large percentage of the total aircraft weight, the center of gravity was located behind the aerodynamic center. Therefore, to enhance the longitudinal stability the wing was swept back 6 degrees, bringing the aerodynamic center to 33% of the root chord (behind the C.G. at landing).

In Table 7.2 it is seen that the variation of the lift coefficient with speed is the only longitudinal derivative at an unstable value. This can be explained by the extremely low air density at cruise altitude. By the end of the mission C-m-alpha and C-m-q are close to becoming positive. A study was done on the effect of changing the horizontal tail surface area. As seen in Figure 7.1, a 50% increase in the horizontal tail area does little to improve the stability, and any large weight additions to the aircraft would increase the wing loading and cause stall at the beginning of cruise at altitude.

It may also be noted that although no lateral-directional derivatives are unstable, there are several that are close to the point of neutral stability. Studies were performed on the effect of varying the vertical tail area and longitudinal

position and the results are shown in Figures 7.2 & 7.3 (the derivatives shown are those that are most sensitive to the change). Apparently, because of the large wing span and surface area large increases in both the vertical tail area and length do little to enhance the lateral-directional stability. Due to the fact that the wing span is extremely large relative to the rest of the Global Sentry geometry, there will be large deflections during flight. The results of a study on the effect of changing wing dihedral on the two most sensitive derivatives to this change is shown in Figure 7.4. C-y-beta remains stable for the entire range of dihedral change shown, but C-l-r attains an unstable value at about 8 degrees positive dihedral.

7.2 DYNAMIC STABILITY

Using Reference 8 the dynamic stability handling qualities were determined. The values are tabulated in Table 7.3 with the range of Level I handling qualities from MIL-F-8785C for a Class III aircraft.

Variation in C_{m_q} and C_{m_α} with % Change in Horizontal Tail Area

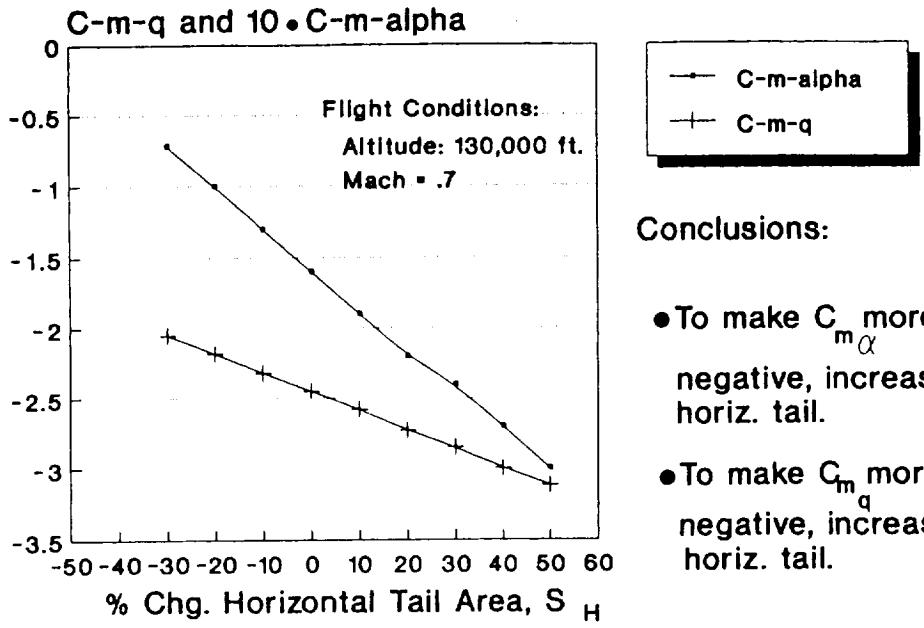

Conclusions:

- To make C_{m_α} more negative, increase horiz. tail.
- To make C_{m_q} more negative, increase horiz. tail.

Figure 7.1

Variation in C_{y_r} and C_{n_β} with % Change in Vertical Tail Length

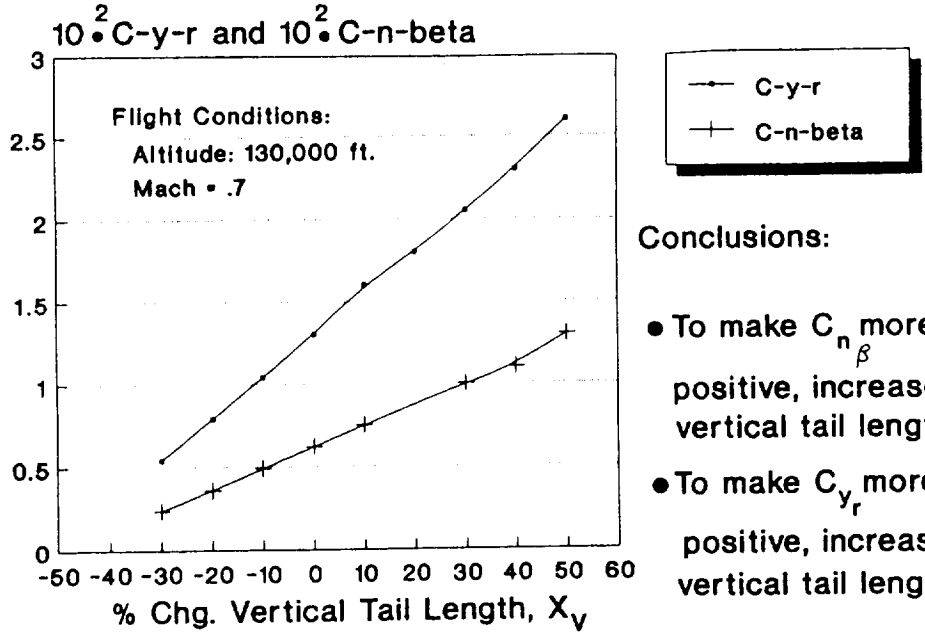

Conclusions:

- To make C_{n_β} more positive, increase vertical tail length.
- To make C_{y_r} more positive, increase vertical tail length.

Figure 7.2

Variation in C_{y_β} and C_{n_β} with % Change in Vertical Tail Area

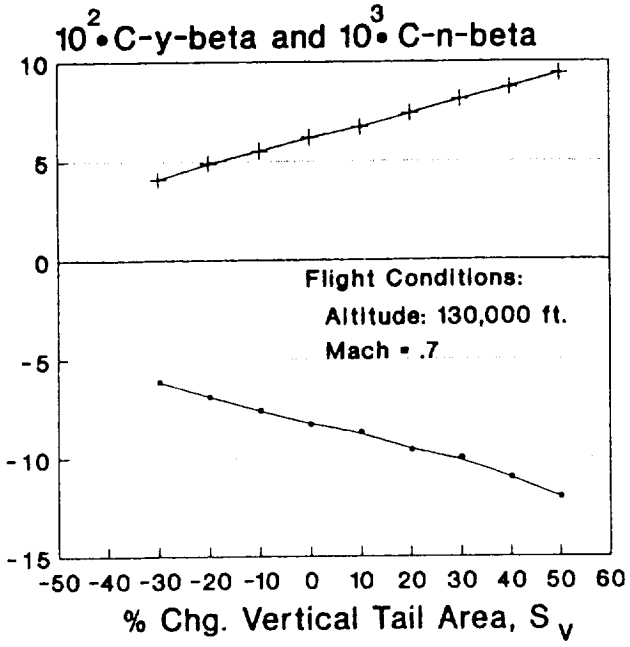

Conclusions:

- To make C_{n_β} more positive, increase vertical tail area.
- To make C_{y_β} more negative, increase vertical tail area.

Figure 7.3

Variation in C_{y_β} and C_{l_r} with Change in Wing Dihedral

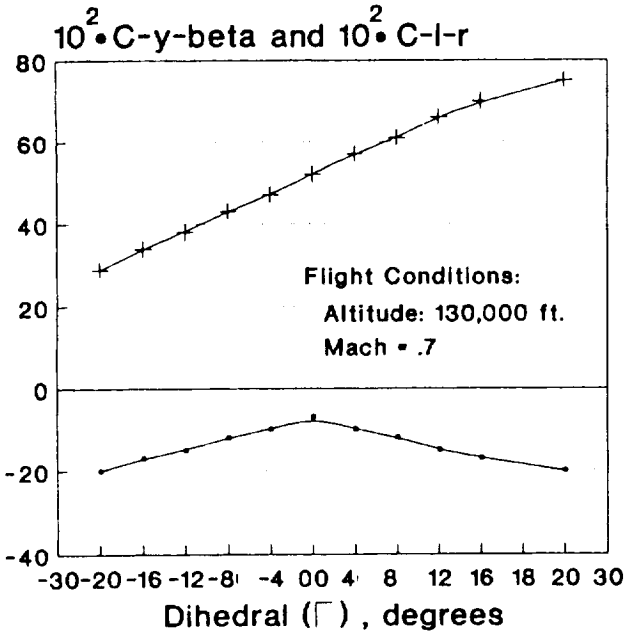

Conclusions:

- To make C_{l_r} more positive, increase wing dihedral.
- To make C_{y_β} more negative, increase or decrease wing dihedral.

Figure 7.4

TABLE 7.3 COMPARISON BETWEEN LEVEL I AIRCRAFT REQUIREMENTS AND GLOBAL SENTRY OUTPUTS

Regulated Parameter	Level I Requirements F.C.III/F.C.IV	Global Sentry F.C.III/F.C.IV
S.P. frequency (rad/sec)	0.7-4.5/1.3-8.2	.2102/.1775*
S.P. damping ratio	0.3-2.0/0.3-2.0	.865/.980
Phugoid damping	0.04 min/0.04 min	-.23/-.21*
D.R. frequency (rad/sec)	0.4 min/0.4 min	.1028/.0624*
D.R. damping	0.08 min/0.08 min	-.323/-.263*
Roll time constant (sec)	1.4 max/1.4 max	7.82/11.28*
Spiral Time Constant (sec)	20 min/20 min	645/941

* Value does not meet Level I requirements

As seen in Table 7.3 , Global Sentry meets only two of the level one requirements. The time responses of velocity, angle of attack and pitch due to a unit elevator step can be seen in Figure 7.5, which shows the instability of the plane.

7.3 STABILITY AUGMENTED SYSTEMS

Due to the instability of the Global Sentry in certain flight regimes the following Stability augmented systems were required: a displacement autopilot with pitch-rate feedback, a phugoid damper, and a Dutch roll damper. These were designed using methods from Reference 11 and Program CC

(Reference 12).

In Figure 7.6 the block diagram for the displacement autopilot with pitch-rate feedback is shown. The root locus plot of the aircraft pitch over elevator deflection transfer function is shown in Figure 7.7. For all gain values there would be closed loop poles in the right half plane (indicating instability). A rate gyro gain of 11 volt/deg/sec was chosen for a damping ratio of 0.92 on the inner loop. The root locus of the outer loop is shown in Figure 7.8. Here an amplifier gain of 0.5 volt/deg/sec was chosen to achieve a short period damping ratio of 0.89 which satisfies the Level I requirements. As seen in Figure 7.9 the new time responses all converge to steady state values.

A block diagram of the Velocity Control System of the Phugoid damper is shown in Figure 7.10. The root locus plot of the aircraft velocity over r.p.m. change transfer function is shown in Figure 7.11. For all gain values there would be poles in the right half plane. The root locus plot of the velocity control loop is seen in Figure 7.12. In order to get a phugoid damping ratio of 0.64 a gain of 0.5 was chosen (which corresponds to the product of C_{X_T} and the engine time lag constant). This satisfies Level I requirements for phugoid damping.

The unstable aircraft heading rate, roll, and sideslip responses to a unit rudder step for the Global Sentry with

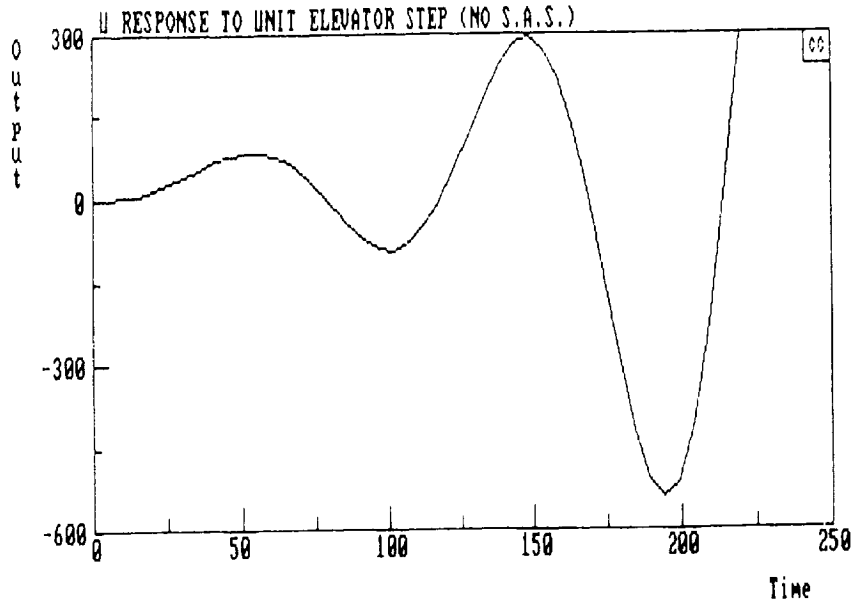
U RESPONSE TO UNIT ELEVATOR STEP (NO S.A.S.)
Output
300
0
-300
-600
0
50
100
150
200
250
Time

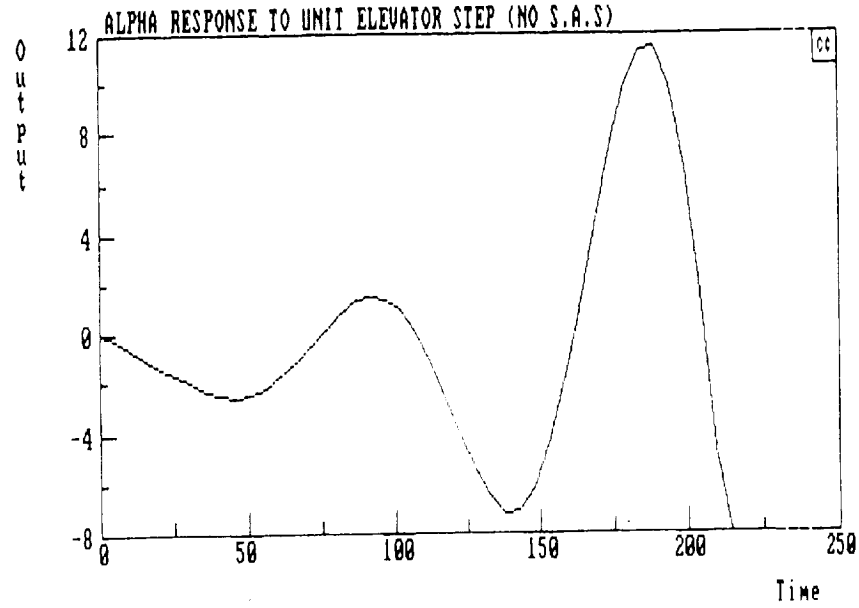
ALPHA RESPONSE TO UNIT ELEVATOR STEP (NO S.A.S)
Output
12
8
4
0
-4
-8
0
50
100
150
200
250
Time

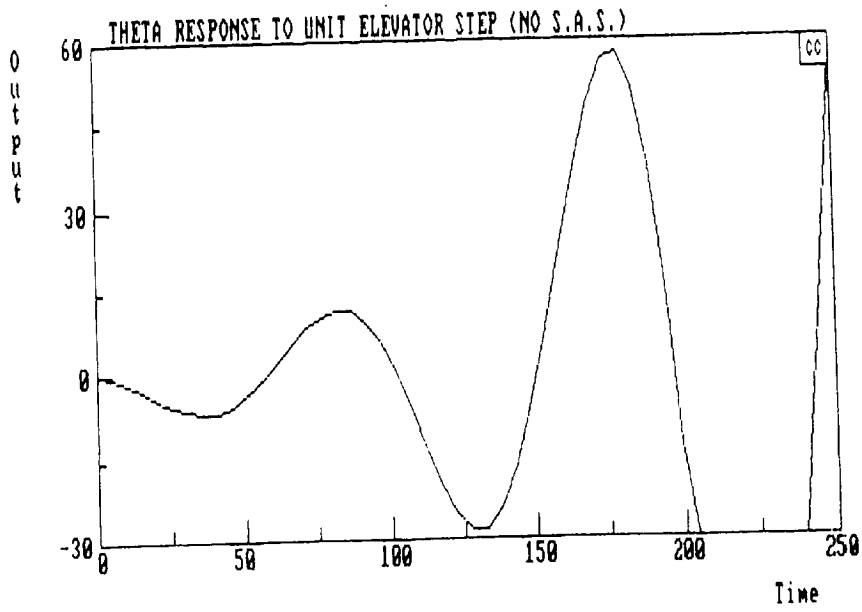
THETA RESPONSE TO UNIT ELEVATOR STEP (NO S.A.S.)
Output
60
30
0
-30
0
50
100
150
200
250
Time

Figure 7.5

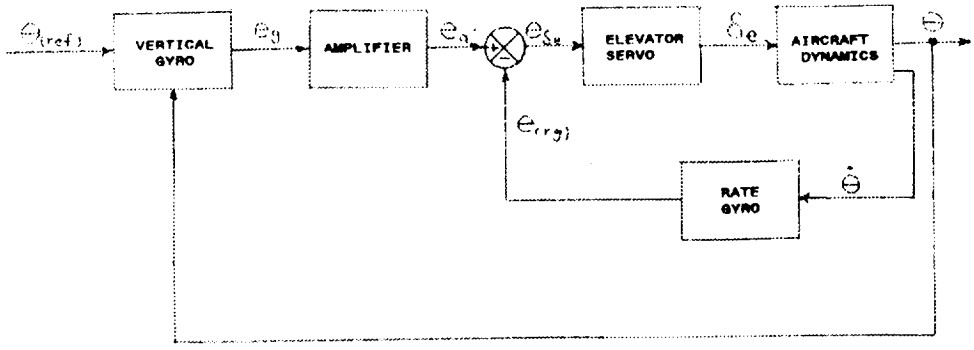

Figure 7.6

BASIC AUTOPILOT WITH PITCH RATE FEEDBACK

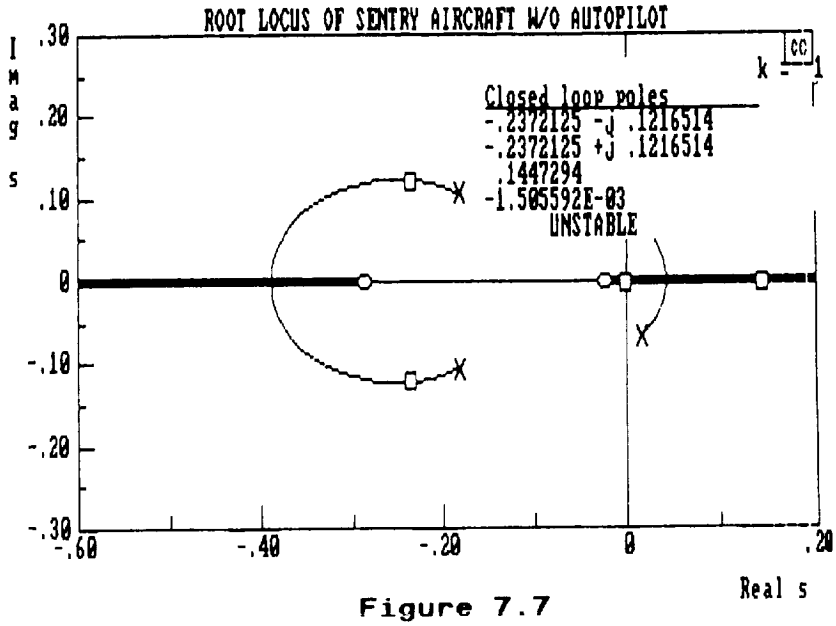

Figure 7.7

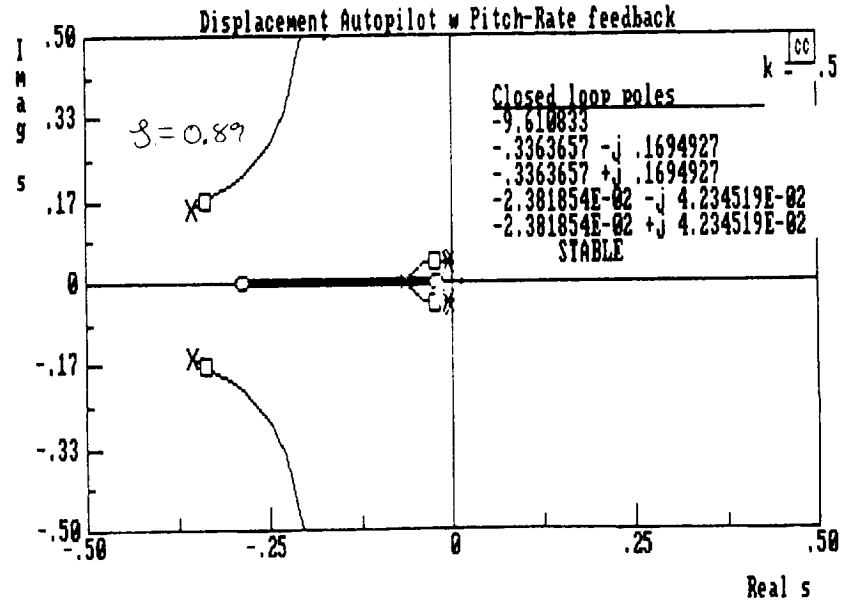

Figure 7.8

ORIGINAL PAGE IS
OF POOR QUALITY

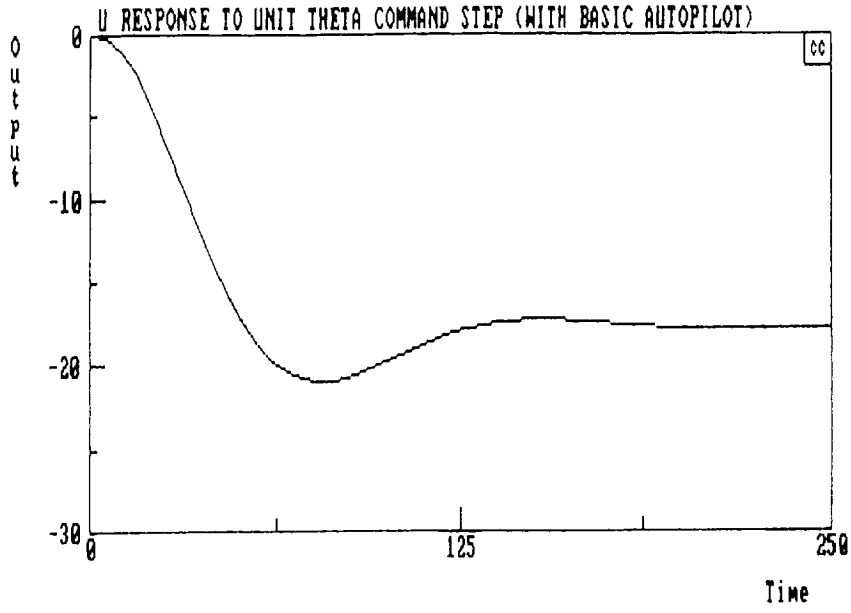
U RESPONSE TO UNIT THETA COMMAND STEP (WITH BASIC AUTOPILOT)
Output
0
-10
-20
-30
0
125
250
Time
cc

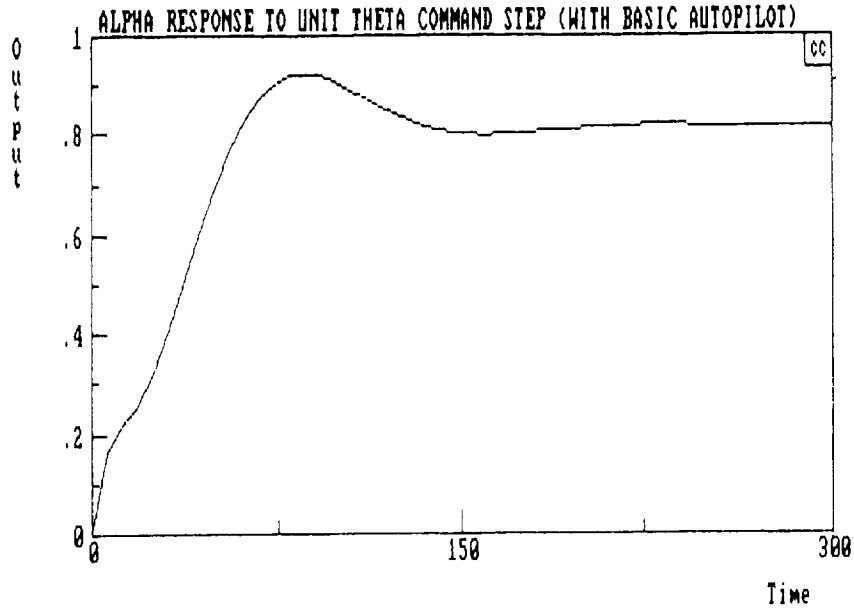
ALPHA RESPONSE TO UNIT THETA COMMAND STEP (WITH BASIC AUTOPILOT)
Output
1
.8
.6
.4
.2
0
0
150
300
Time
cc

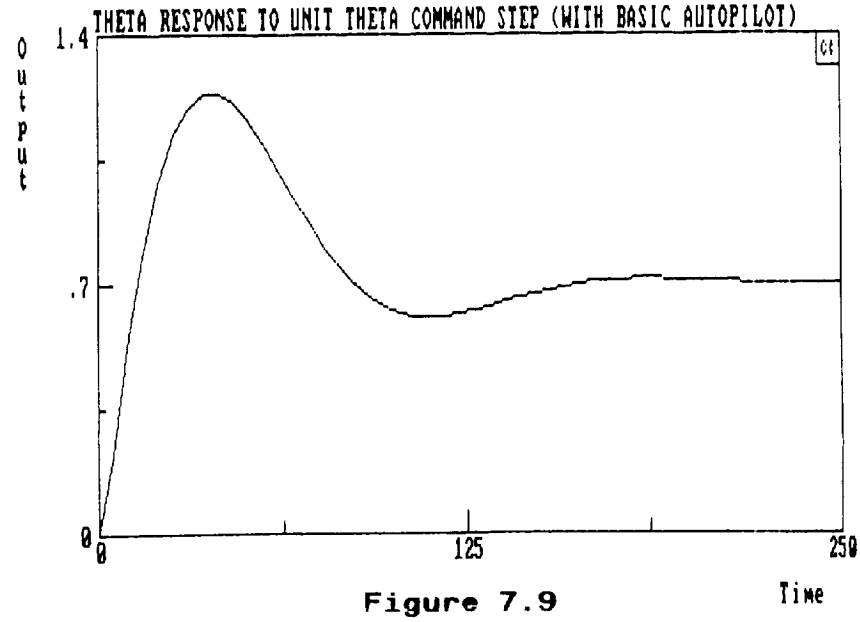
THETA RESPONSE TO UNIT THETA COMMAND STEP (WITH BASIC AUTOPILOT)
Output
1.4
.7
0
0
125
250
Time
cc

Figure 7.9

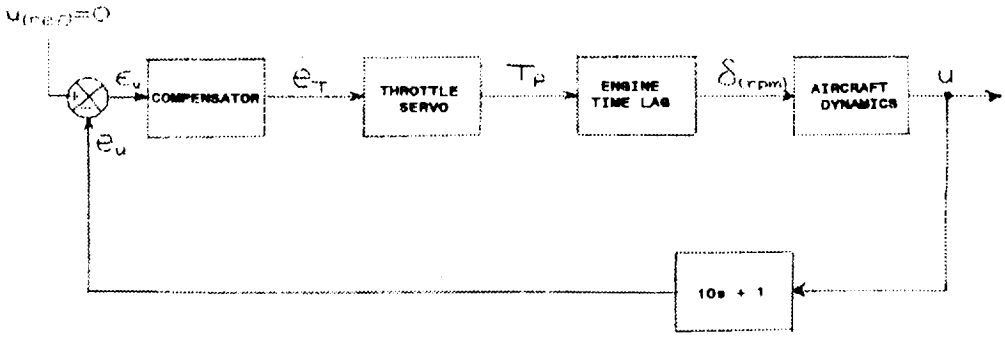

VELOCITY CONTROL SYSTEM (Phugoid Damper)

Figure 7.10

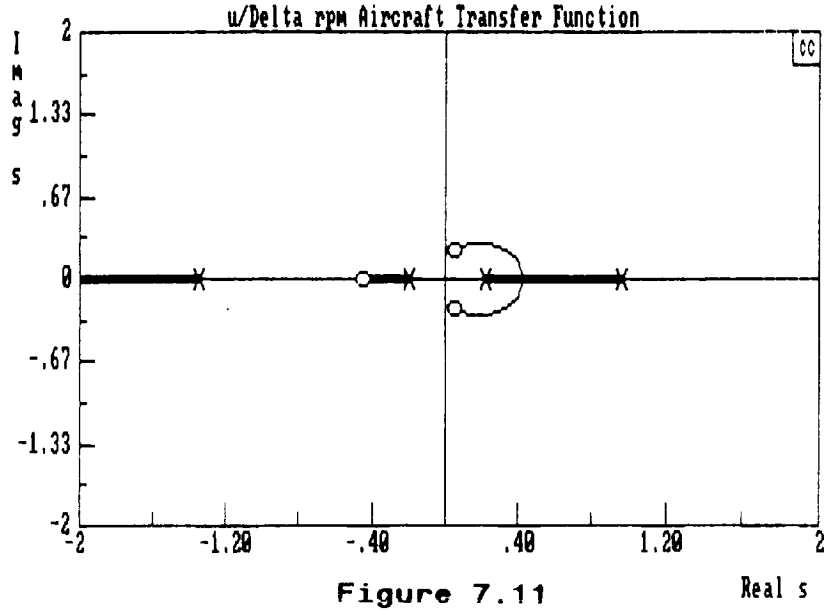

Figure 7.11

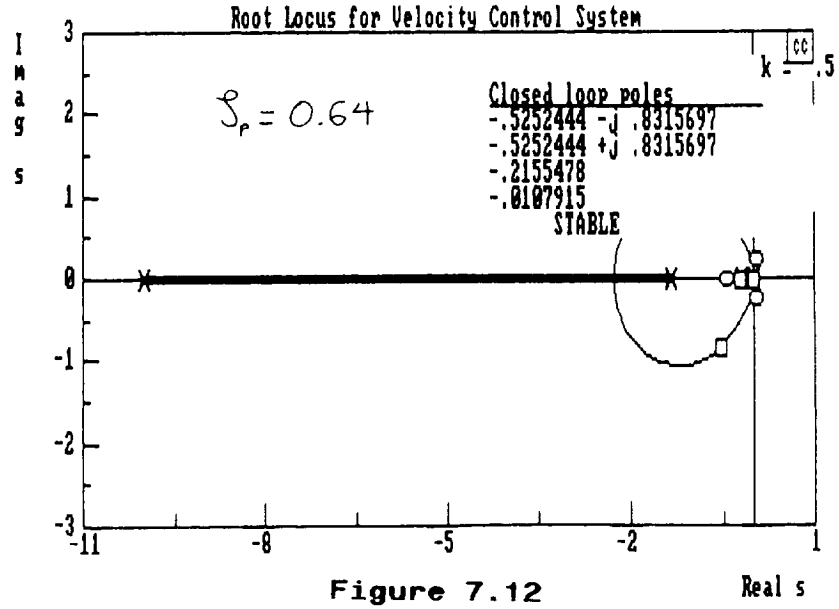

Figure 7.12

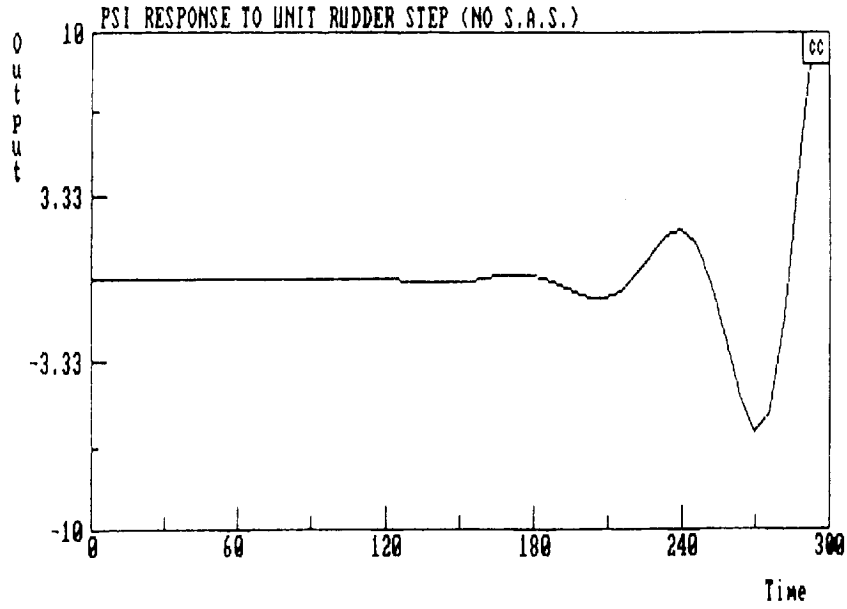
PSI RESPONSE TO UNIT RUDDER STEP (NO S.A.S.)
Output
10
3.33
-3.33
-10
0
60
120
180
240
300
Time
cc

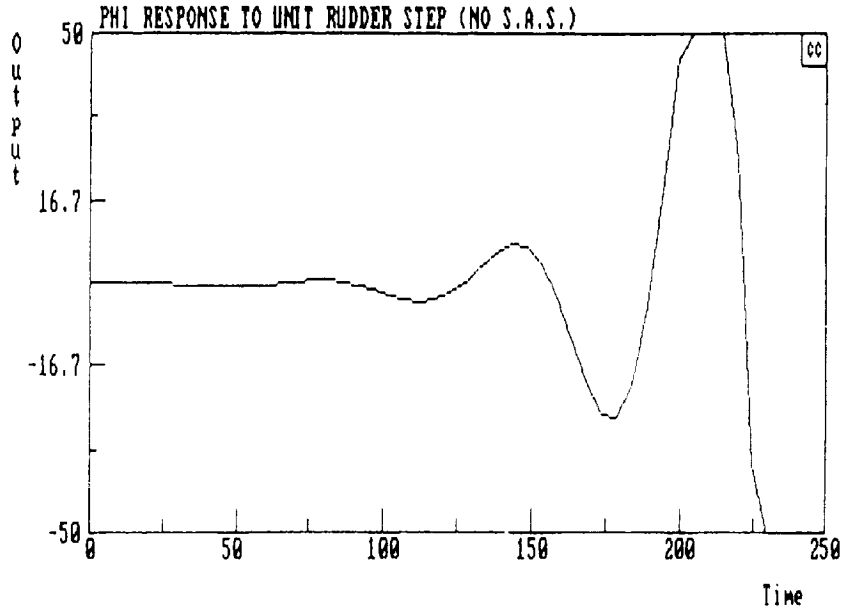
PHI RESPONSE TO UNIT RUDDER STEP (NO S.A.S.)
Output
50
16.7
-16.7
-50
0
50
100
150
200
250
Time
cc

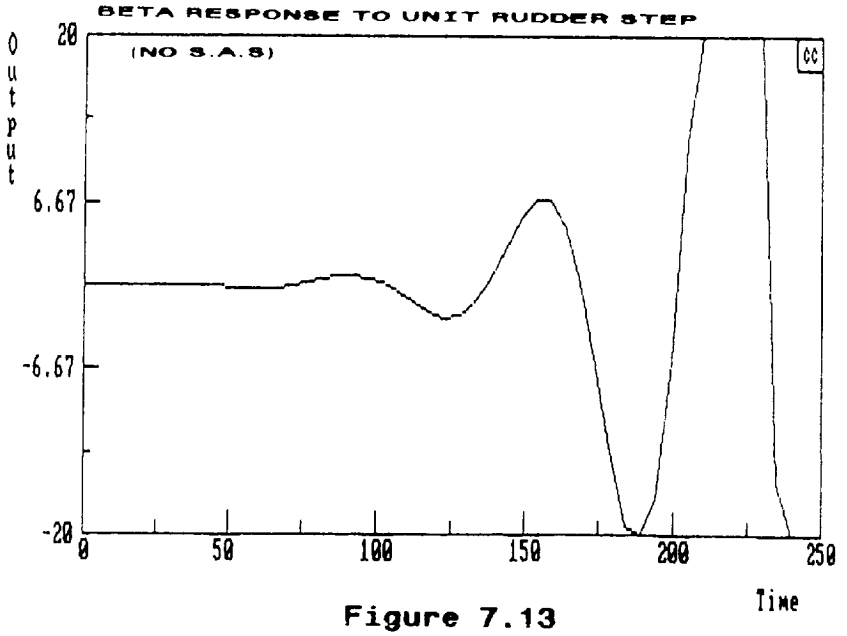
BETA RESPONSE TO UNIT RUDDER STEP
(NO S.A.S)
Output
20
6.67
-6.67
-20
0
50
100
150
200
250
Time
cc

Figure 7.13

Control Systems off can be seen in Figure 7.13. The block diagram of the Dutch Roll Damper is shown in Figure 7.14. The root locus plot for the Dutch Roll damper is seen in Figure 7.15. Figure 7.16 shows a close-up of the dominant poles - a yaw rate gyro gain of 2 was chosen to get a damping ratio of 0.78 and a frequency of 0.7, both of which satisfy Level I requirements. The time responses due to a unit rudder deflection for the Global Sentry with the Dutch Roll damper on can be seen in Figure 7.17. All values now attain steady state values. To better control the sideslip of the Global Sentry a coordination system is also used. In Figure 7.18 the block diagram of the coordination system using lateral acceleration is shown. From Figure 7.19 it is seen that an accelerometer gain of 1.5 was used to get a damping ratio of 0.78.

With the Global Sentry's S.A.S. all handling qualities fall into the Level I range. Using control systems was a practical alternative to increasing the stabilizer control surface areas which would increase the weight and drag of the aircraft, jeopardizing Global Sentry's chances of attaining a 130,000 foot altitude.

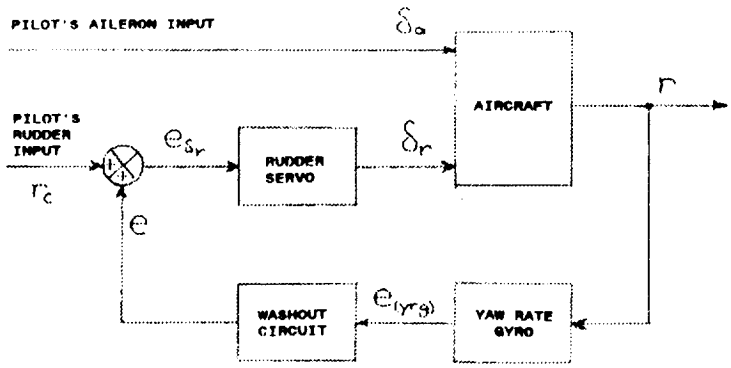

Figure 7.14 DUTCH ROLL DAMPER

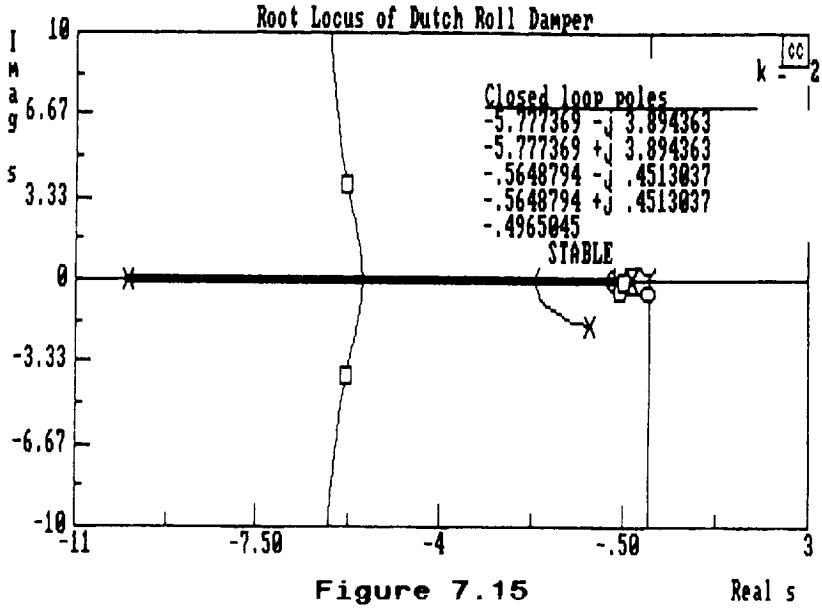

Figure 7.15

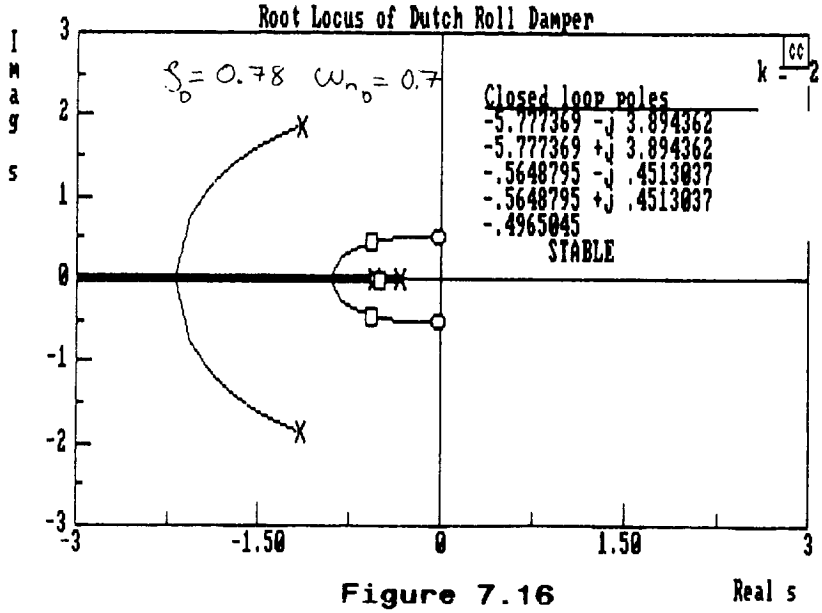

Figure 7.16

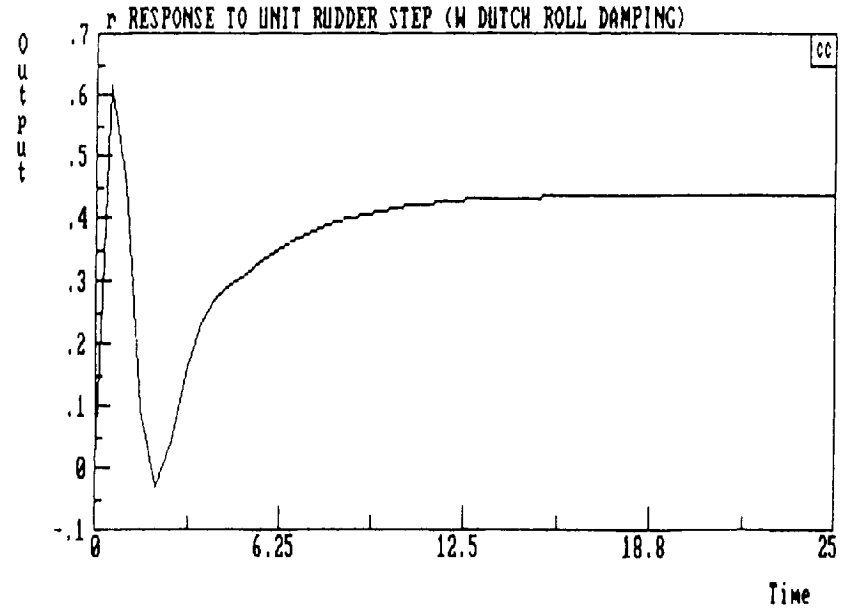
r RESPONSE TO UNIT RUDDER STEP (W DUTCH ROLL DAMPING)
Output
.7
.6
.5
.4
.3
.2
.1
0
-.1
0
6.25
12.5
18.8
25
Time
cc

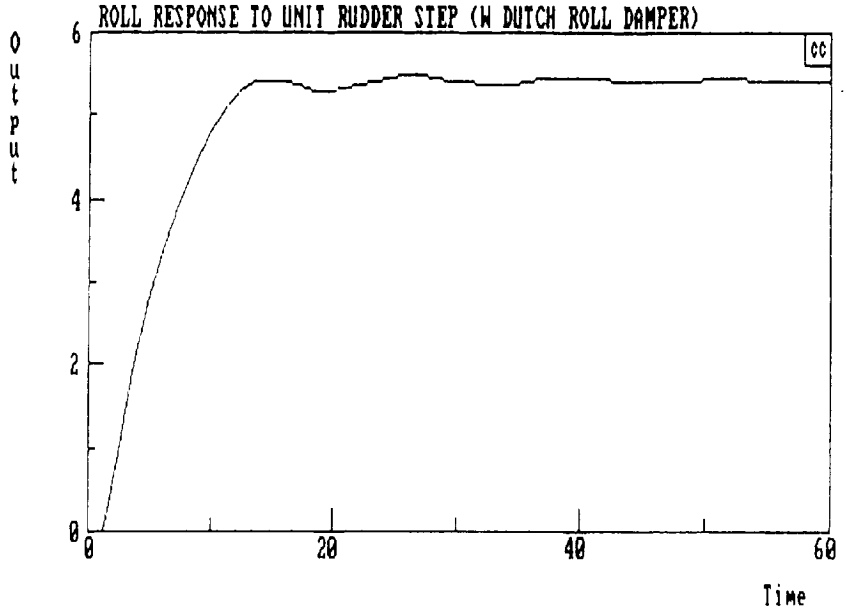
ROLL RESPONSE TO UNIT RUDDER STEP (W DUTCH ROLL DAMPER)
Output
6
4
2
0
0
20
40
60
Time
cc

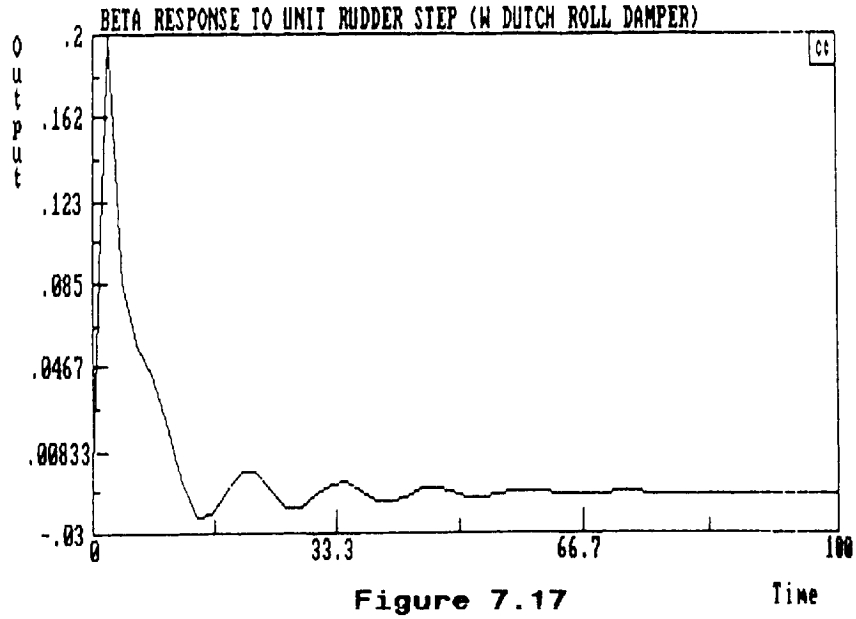
BETA RESPONSE TO UNIT RUDDER STEP (W DUTCH ROLL DAMPER)
Output
.2
.162
.123
.085
.0467
.00833
-.03
0
33.3
66.7
100
Time
cc

Figure 7.17

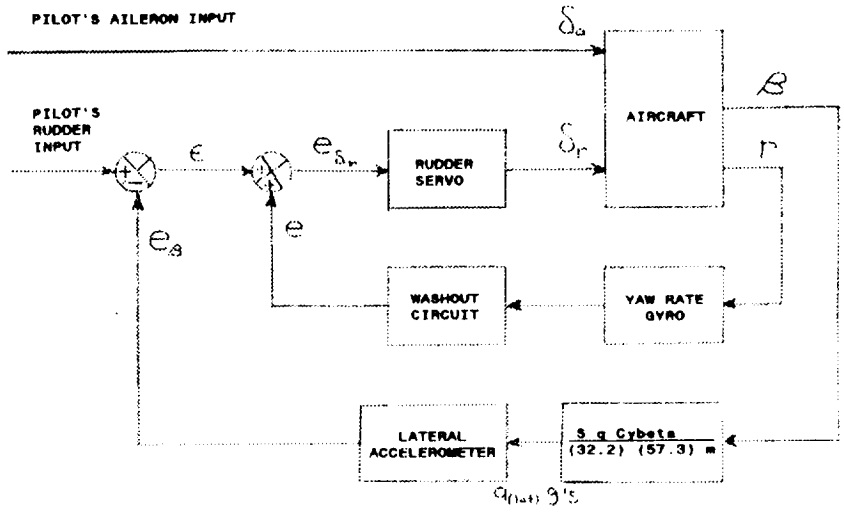

COORDINATION SYSTEM

Figure 7.18

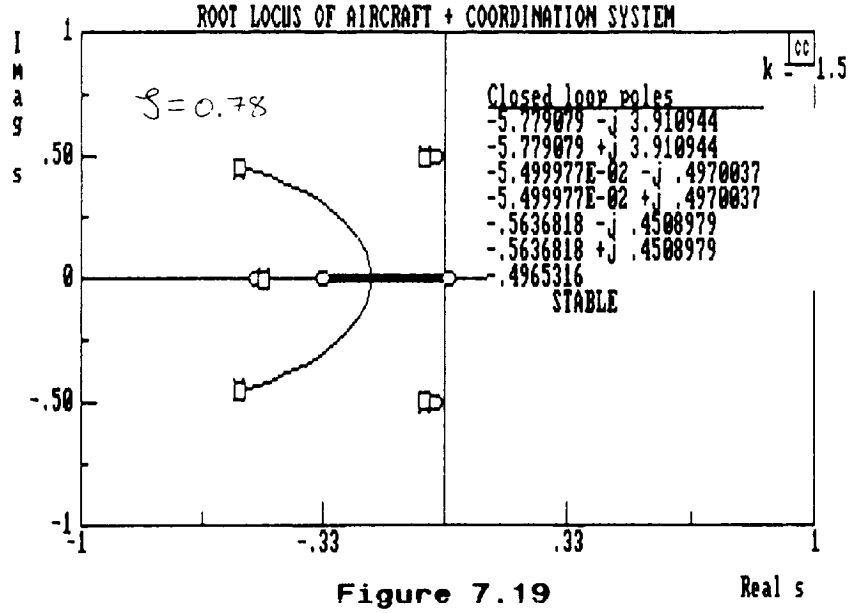

Figure 7.19

8.0 AIRCRAFT PERFORMANCE

8.1 INTRODUCTION

The Global Sentry aircraft is designed to operate in the atmosphere where it experiences the greatest range of temperature, density and pressure. As a result, the performance of the aircraft demands the optimized values during takeoff, climb, cruise, descent and landing. The performance calculations were done using methods in Reference 1. Computer programs were written to do most of the performance calculations.

8.2 OPERATING ENVELOPE

The operating envelope of an aircraft defines where in the airspace it must operate, using the aircraft limitations such as minimum dynamic pressure, maximum dynamic pressure, aerodynamic heating, sonic boom and engine limitations. Global Sentry's flight envelope is shown in Figure 8.1. It shows the relationship between the altitude and its attainable velocities. The left side of the flight envelope was determined by the stall and buffet characteristics of the aircraft. The right side of the envelope is limited by the available power and drag at respective altitudes. As a result the service ceiling of almost 140,000 feet is achieved at the velocity of 432 knots (see Fig. 8.2).

FLIGHT ENVELOPE
GLOBAL SENTRY

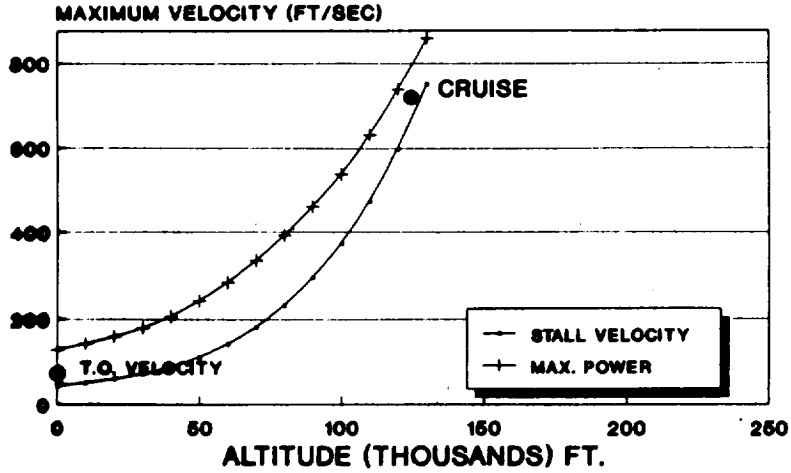

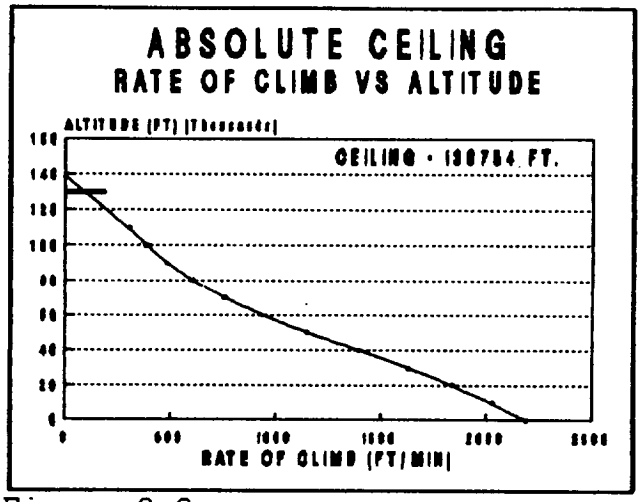

Figure 8.2

8.3 TAKE-OFF

Take-off distance is the distance required for an aircraft to accelerate from V=0 to take-off and climb over a 50 foot obstacle. The gross takeoff weight of 60,845 lbs, and the mission RFP demand the use of FAR Part 25 requirements for take-off and landing. Although there are no limits put on the take-off field length, it is controlled by the available engine power and stall velocity. The total take-off distance is the sum of the ground distance, rotation distance, transition distance and climb distance.

During the ground run the atmospheric conditions at 5000 feet were used for the takeoff analysis. The ground run friction coefficient of .3 was assumed for hard turf. The rotation time was assumed to be 3 seconds and the takeoff velocity as 1.2 times the stall velocity. The climb angle as discussed later in section 8.7 was approximated as 6 degrees.

The calculations done above assume all engines operative during takeoff. But federal laws require to compensate for the takeoff field length during an engine failure. This is shown using a balanced field length (Figure 8.3) where the distance to continue takeoff, following the recognition of an engine failure at V_1, is equal to the distance required to stop if the takeoff should be aborted. The complete takeoff diagram along with the expected and fulfilled requirements are shown in Figure 8.4.

SUMMARY OF CTOL TAKEOFF RULES
FAR Pt 25

ITEM	REQUIRED	CALCULATED
SPEEDS	V(TO.) >= 1.1 V(STALL) V(CL.) >= 1.2 V(STALL)	52.9>44 ft/sec. 97>44 ft/sec.
CLIMB	GEAR UP:300 FPM @ SL (AEO)	GEAR UP:1587 FPM @ SL (AEO)
FIELD LENGTH	T.O DISTANCE OVER 35 FEET	853.5 FEET

STALL VELOCITY = 44 ft./sec.
C-L max. = 1.3
WING LOADING = 3.1
THRUST LOADING =.25
ROLLING COEFFICIENT = .03

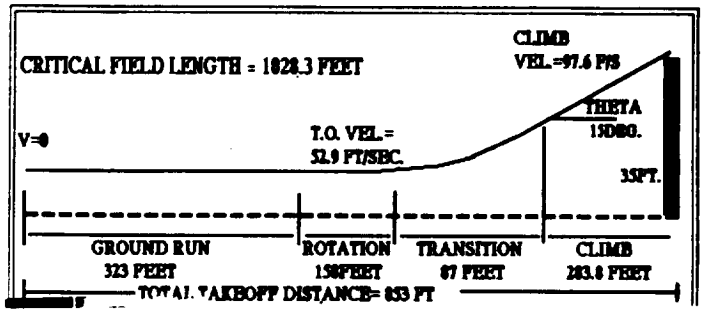

Figure 8.3

BALANCED FIELD LENGTH

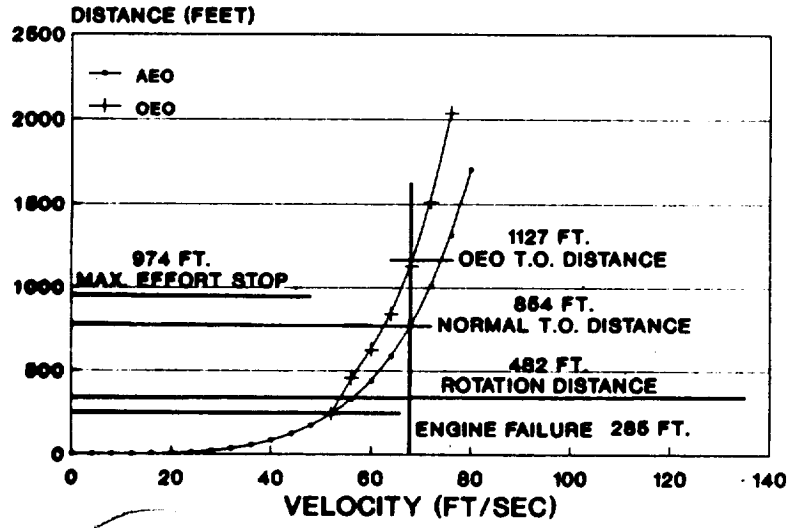

Figure 8.4

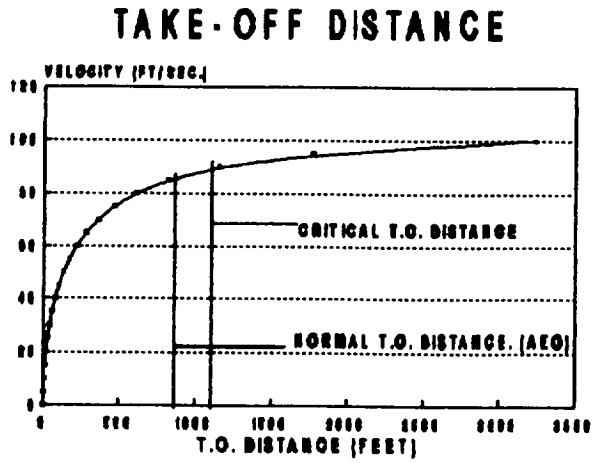

Figure 8.5

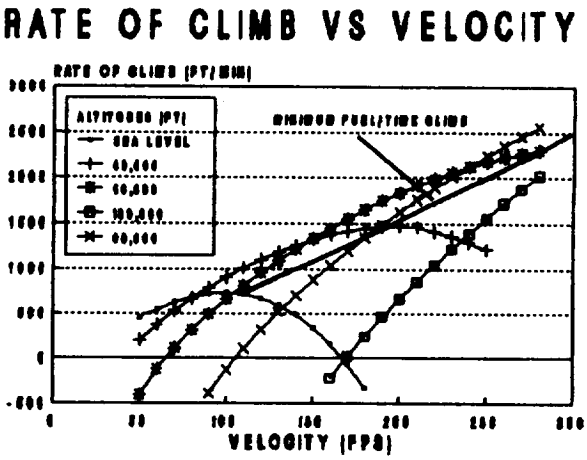

Figure 8.6

8.4 CLIMB

Higher density of the lower atmosphere, available power and the gross weight of the aircraft were among the main factors which required the fastest rate of climb under given power and the load factors. This relationship is shown in Figure 8.6 at different velocities and altitudes. The calculations were performed with all engines operative and under the conditions set by FAR Pt.23.

8.5 CRUISE

As cruise was the most critical part of the mission, the Global Sentry's design was optimized for this phase. The RFP required the maximum cruising altitude of 130,000 feet at Mach .7. Also among the cruising requirements was the option of either the range of 6000 nautical miles or at least 6 hours of cruising time.

This choice was made using several relationships between the given cruising altitude, available power, required Mach number and the weight of the aircraft. One of such relations is the range parameter. This relationship combines the cruise velocity, specific fuel consumption and the lift to drag ratio at the cruise altitude. The graphical representation is shown in Figure 8.7. This relationship indicates that the aircraft should fly at that velocity condition where the range parameter is maximum. This produces the best lift to drag

ratio of 17.71 during cruise and the optimum specific fuel consumption of .37. This lift to drag ratio was used to find the appropriate airfoil with required cruise lift coefficient; and the engine design was done such as to produce the required specific fuel consumption.

Another factor in the engine design was the required power during cruise. This relationship is shown in Figure 8.10 as a function of velocity and power required. The curves in this figure are the result of the power output by the designed engines, the maximum power at cruise is 3636 hp at Mach .7 where the required power amounts to 3288 hp.

8.6 DESCENT

The descent performance of the Global Sentry was analyzed for unpowered condition and different glide angles. This is shown in Figure 8.11. For unpowered condition, the best rate of descent was 1200 ft/min at the glide angle of 13 degrees. These values were chosen for maximum range during the glide descent. Therefore, the descent time is 1 hour and 48 minutes and the range is 4.94 nm.

8.7 LANDING

Although there was no RFP requirement for maximum landing distance, it was calculated for given Takeoff values of maximum lift coefficient, and atmospheric conditions. The

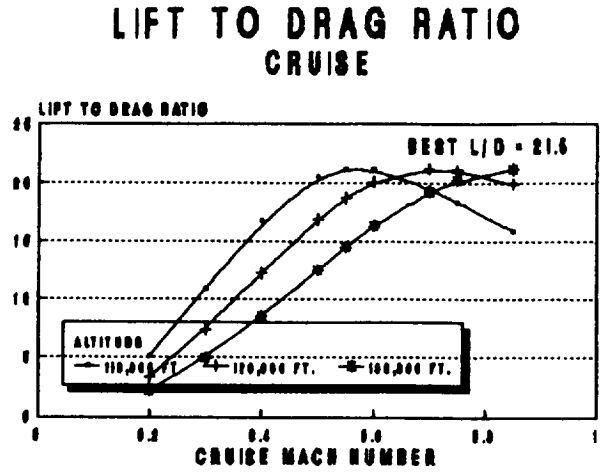

Figure 8.7

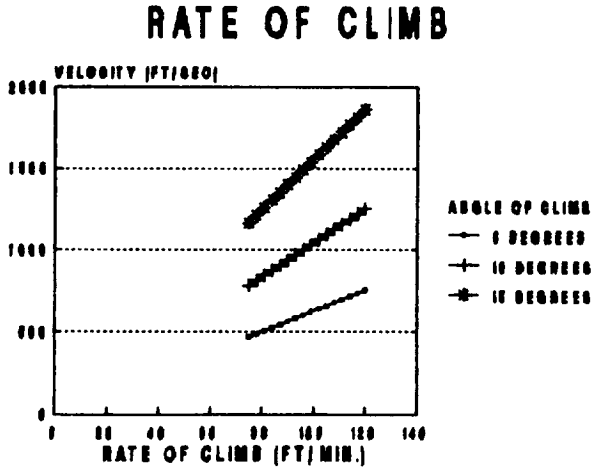

Figure 8.8

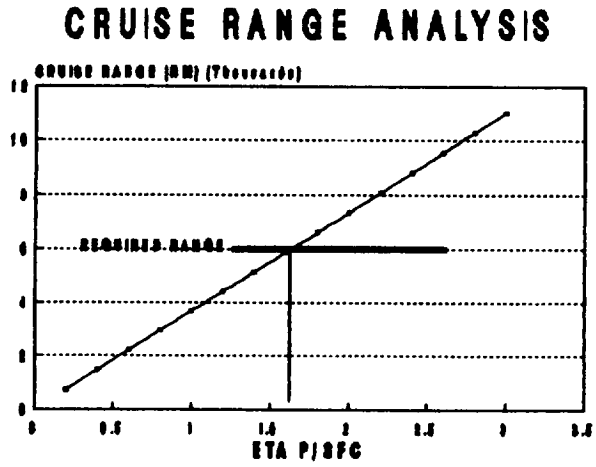

Figure 8.9

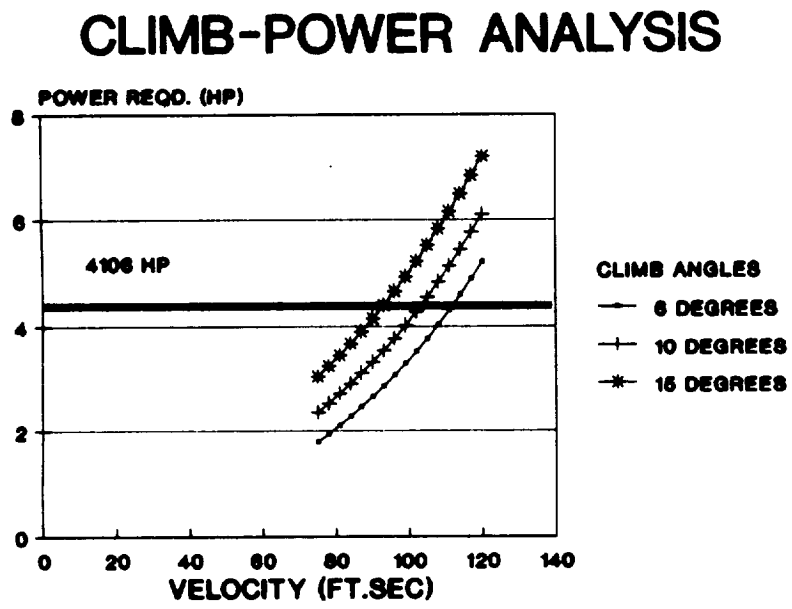

Figure 8.10

most important parameter for the landing was the breaking distance. Since the wing loading for the Global Sentry is relatively low it is sufficient to accommodate an appropriate landing distance. The complete results of the landing analysis are shown in Figure 8.12.

8.8 CRUISE RANGE

Brequet's range equation was used to determine the range distance. This relationship was plotted in Figure 8.13 for given propeller efficiency, specific fuel consumption, lift to drag ratio and weight fraction. To decide for the optimum range and cruise time, given values of available engine data and weights were taken into consideration. And the optimum range and cruise time were chosen for those values which satisfied the RFP as well as the given engine and weight limits.

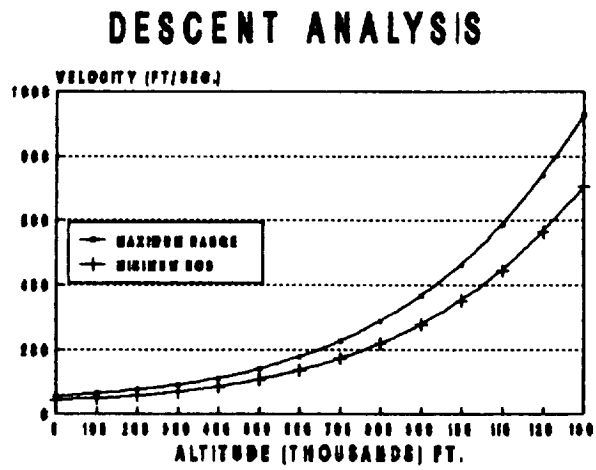

Figure 8.11

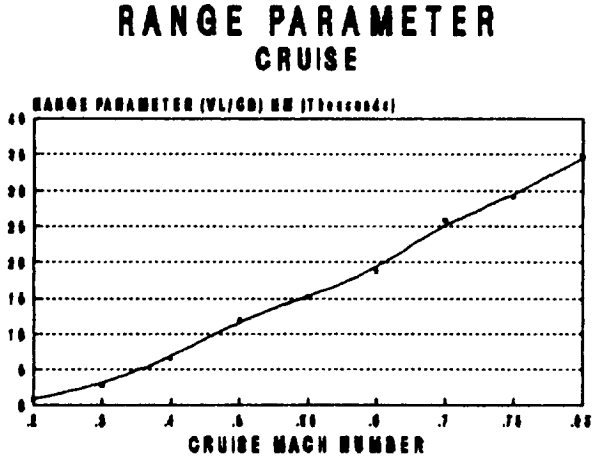

Figure 8.13

SUMMARY OF CTOL LANDING RULES
FAR Pt 25

ITEM	REQUIRED	CALCULATED
SPEEDS	V(35) >= 1.3 V(STALL) V(TD) >= 1.15 V(STALL)	.105> 69 ft/sec. 38.9> 61 ft/sec.
FIELD LENGTH	LAND. DISTANCE OVER 35 FEET	639.26 FEET

STALL VELOCITY = 33.85 ft./sec.
C-L max. = 1.3
WING LOADING =1.92
THRUST LOADING = .2
BRAKING COEFFICIENT = .1

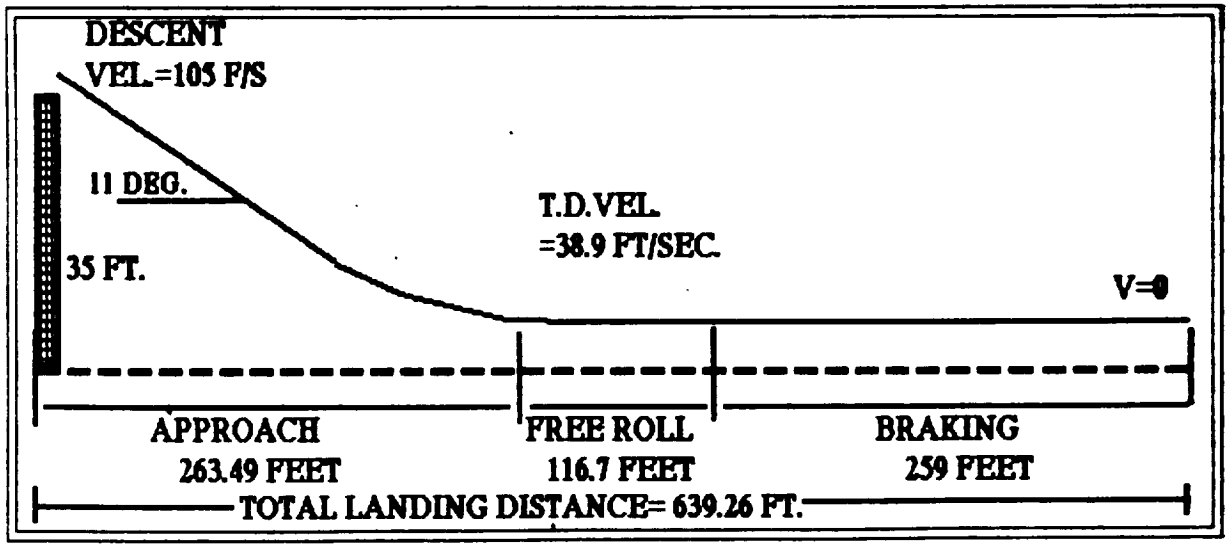

SCHEMATIC OF THE AIRCRAFT LANDING ANALYSIS

Figure 8.12

9.0 PROPULSION SYSTEM

The propulsion system requirements, selection, specifications, and performance will be described in the following sections.

9.1 SYSTEM REQUIREMENTS

The mission profile for this aircraft sets very stringent requirements for the propulsion system. At the operational altitude of 130,000 ft., ambient pressure is approximately 0.3% of standard sea level pressure. The required 0.7 Mach cruise at altitude yields a condition of low mass flow per unit area. In light of these conditions, the powerplant for this aircraft must be able to operate without large quantities of air, low specific air consumption. The 6,000 mile range requirement necessitates that the powerplants have a low specific fuel consumption to reduce the amount and weight of the fuel needed to complete the mission.

Since the aircraft is to operate at subsonic velocities and very high altitudes, the aircraft's wings will be large and heavy. This will require an engine that is capable of producing large amounts of power at altitude. The final requirements are to keep the engine and its systems as light as possible and to develop this system with current technology.

Figure 9.1 tabulates the requirements for the high altitude propulsion system.

Figure 9.1

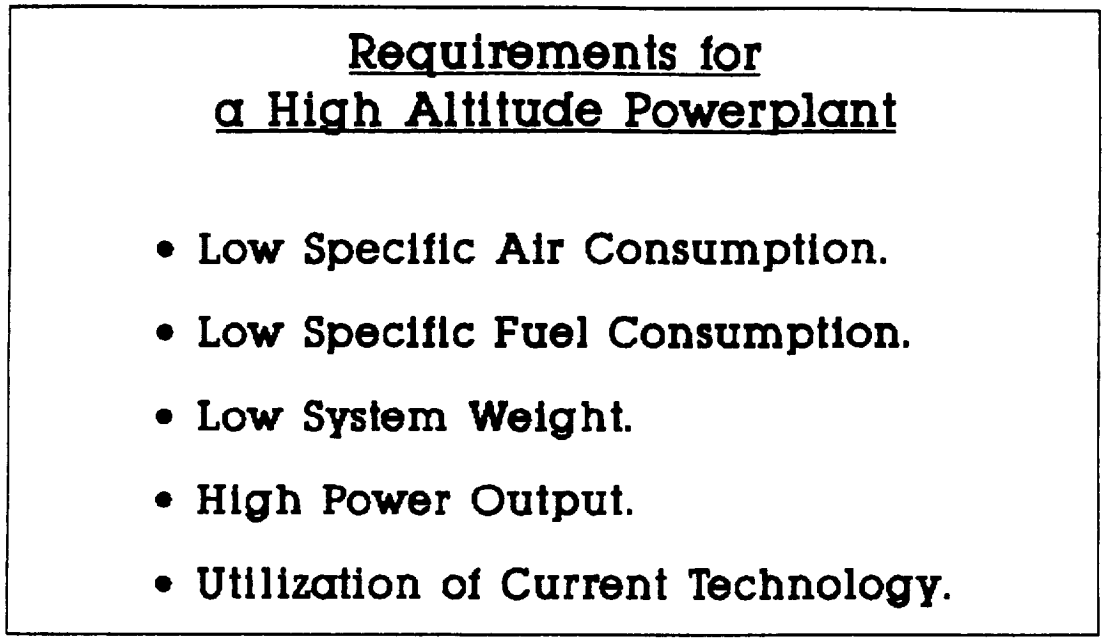

9.2 POWERPLANT SELECTION

Various engines were evaluated for their ability to satisfy the requirements for a high altitude propulsion system. The driving constraint in the engine selection process was the air consumption of the engine at altitude. The air consumption had to be low for the engine to produce power at altitude. Figure 9.2 shows typical specific air consumption (SAC) values for the engines examined. The second constraint was propulsion system weight. The system weight is the weight of the engine and weight of the fuel required for the mission.This had to be kept as low as possible. Figures 9.3-9.4 show typical specific fuel consumption (SFC) and specific weight values for the engines examined. The engines evaluated for this aircraft are described in the following sub-sections.

Figure 9.2

Specific Air Consumption for Various Engine Types

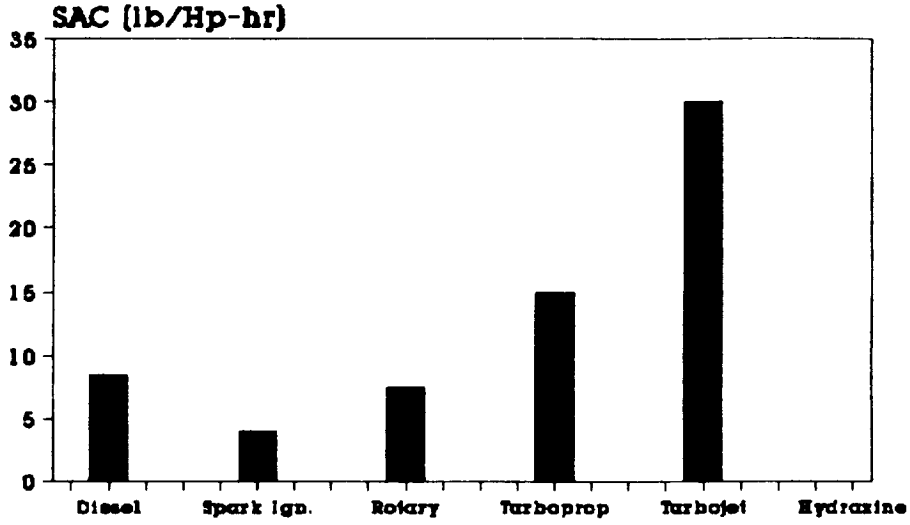

Figure 9.3

Specific Fuel Consumption for Various Engine Types

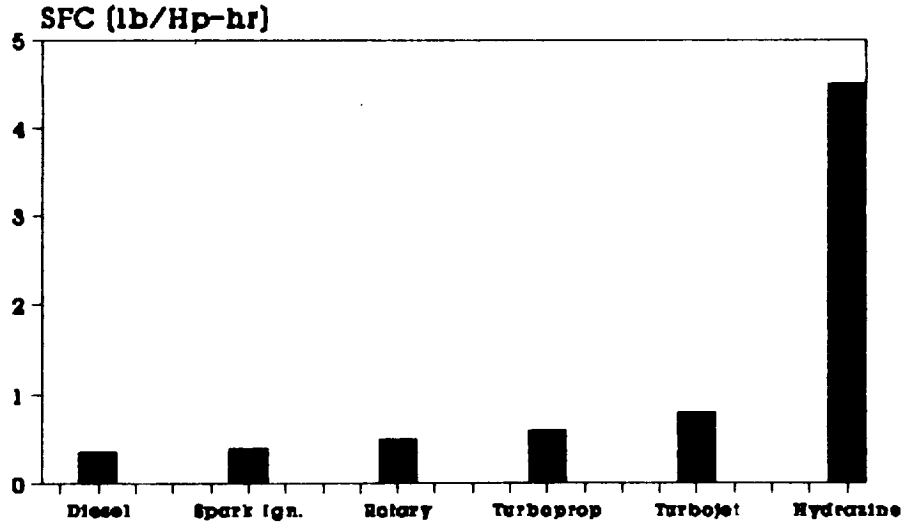

Figure 9.4

Specific Weight
for Various Engine Types

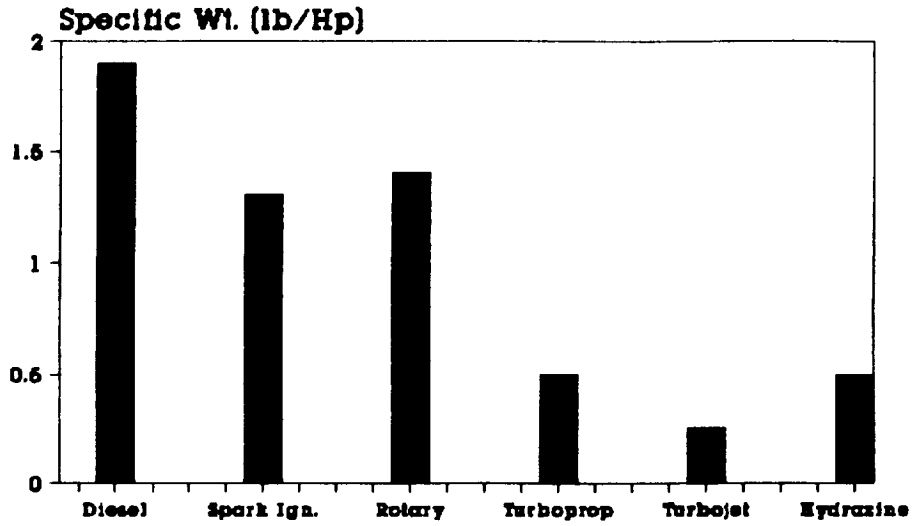

9.2.1 TURBOJETS/TURBOFANS

The use of turbojets or turbofans to complete the high altitude mission was first evaluated. The Pratt & Whitney J75 turbojet, the engine used on the U-2 and the TR-1, was the engine selected for examination. Figure 9.5 shows the performance of the engine with altitude. The J75's thrust goes from 17,000 lb. static sea level thrust to approximately 50 lb. of thrust at the cruise altitude of 130,000 ft.

The low density of the air at altitude and subsonic cruise velocity combined with the engine's high specific air consumption, make it impossible for any turbojet or turbofan engine to produce any meaningful thrust.

Figure 9.5

Thrust vs. Altitude
for a 17000 lb Thrust Turbojet

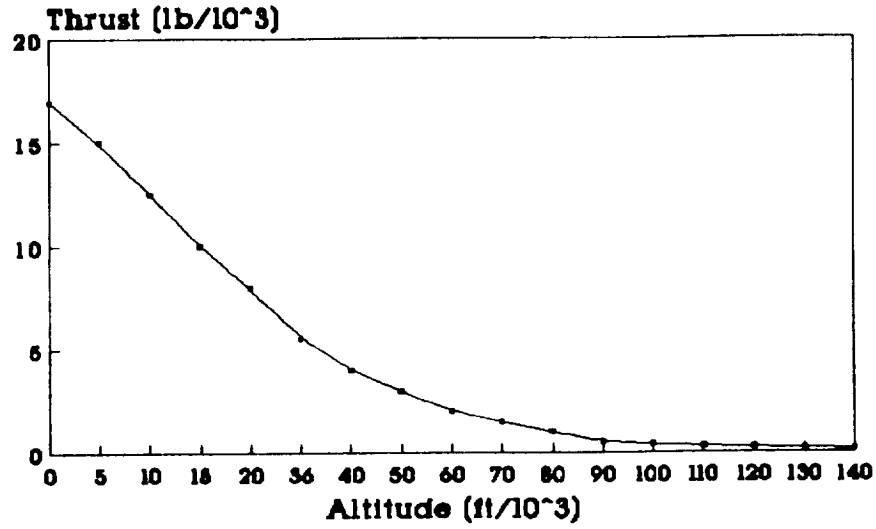

9.2.2 TURBOPROPS

After deciding that turbojets/turboprops were not feasible, attention was turned towards turboprops. Turboprops produce shaft power instead of accelerating air for thrust and have half the SAC of turbojets. However, turboprop engines still require more air than is available at altitude. Therefore, they follow the same power trend as the turbojet, Figure 9.5, producing little power at altitude.

9.2.3 HYDRAZINE ENGINE

The hydrazine monopropellant reciprocating engine was evaluated as a possible powerplant for the high altitude aircraft. This type of engine uses hydrazine as a fuel and does not require ambient air for combustion. The hydrazine

engine was developed by NASA for the Mini-Sniffer high altitude aircraft, Reference 15. The engine for the Mini-Sniffer generated 15 Hp. An engine for this aircraft would be a scaled up version of the Mini-Sniffer engine.

The hydrazine engine has an extremely high specific fuel consumption, Figure 9.3, compared to other types of engines. Hydrazine is also a toxic substance and must be specially handled. Despite these drawbacks, the hydrazine engine was considered for further study.

9.2.4 INTERNAL COMBUSTION ENGINES

Attention was given to exploring the feasibility of using internal combustion (IC) engines for a high altitude powerplant. IC engines have a relatively low SAC of 5-10 lb/Hp-hr. The fuel consumption of these types of engines are also attractively low, 0.3-0.5 lb/Hp-hr. Although these engines have a low SAC, they would be unable to produce enough power at altitude without some type of supercharging. The Lockheed HAARP Project, Reference 25, designed a turbocharging system to operate with an IC engine at an altitude of 100,000 ft. It was felt that such a system could also be designed for the required altitude of 130,000 ft.

A major drawback to IC engines is their high specific weight, Figure 9.4. The high specific weight of these engines added with the weight of the required turbocharging system will result in a propulsion system would be extremely heavy.

Of the three IC engines examined, diesel, rotary, and spark ignition, the spark ignition engine had the best mix of SAC, SFC, and specific weight. The spark ignition IC engine was selected for further study.

9.2.5 OTHER TYPES OF POWERPLANTS

Other engine technologies such as microwave propulsion, laser propulsion, nuclear propulsion, and electrical propulsion were examined. Practical versions of engines were not feasible with present day technology and received no further consideration.

9.2.6 SELECTION OF THE POWERPLANT

The two types of engines selected for further study were the hydrazine monopropellant reciprocating engine and the spark ignition reciprocating engine. Both engines were capable of operating at the required altitude of 130,000 ft and developing at least 500 Hp when scaled up. A system weight study was conducted to determine which of the engines would incur the least weight penalty completing a ten hour mission. Figure 9.6 shows the results of this study with both engines configured for operation at 130,000 ft.

The weight study showed that the spark ignition propulsion system was four times lighter than the hydrazine system. The main difference between the two engines is the fuel required for the ten hour mission. Thus the spark

Figure 9.6

Compairison of Estimated Total Propulsion Weight

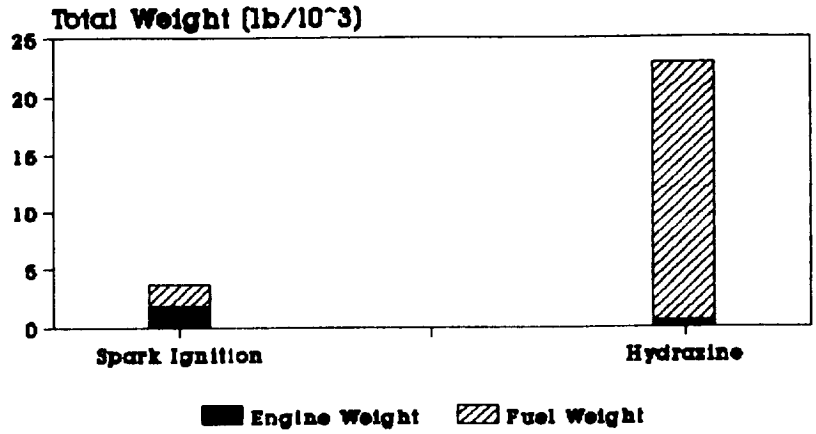

Note: 10 hour mission
600 Hp engine
Equipped for 130,000 ft.

Figure 9.7

Powerplant Configuration

- Reciprocating Spark Ignition.
- Horizontal Opposed Cylinders.
- Four Stage Turbocharged.
- Fuel Injected.
- Dual Ignition.
- Liquid Cooled.
- Geared Propeller Drive.

ignition IC engine was selected as the best choice for the high altitude propulsion system.

9.3 ENGINE CONFIGURATION

The configuration and details of the IC spark ignition engine developed for this project will be set forth in the following sub-sections. The engine configuration is shown in Figure 9.7.

9.3.1 TURBOCHARGING SYSTEM

The high altitude engine uses four stages of turbocharging to allow it to operate at altitude. Turbocharging was selected over supercharging so that the engine power would not have to be used. Figure 9.8 shows a schematic of the turbocharging system. Figure 9.9 tabulates the specifications of the system. The turbochargers are each composed of a radial compressor and a radial turbine. Each of the four turbocharger stages are intercooled with a crossflow air to air heat exchanger.

The full compression capacity of the system is only required at the cruise altitude. The pressure in the system is controlled by a waste gate installed between the engine and the high pressure turbine, Figure 9.8. The waste gate is designed to dump all exhaust up to a density altitude of 2800 ft. From 2800 ft. density altitude, the waste gate closes with the decrease in density. Full closure of the waste gate occurs

at a density altitude of 97,000 ft. As an added safety measure, an over pressure safety valve is incorporated between the high pressure compressor and the engine.This valve will release pressure if the pressure in the system becomes greater than 2140 psf. This protects the engine from a potentially disastrous over pressure from the turbochargers.

Figure 9.8

Schematic of the Four Stage Turbocharging System

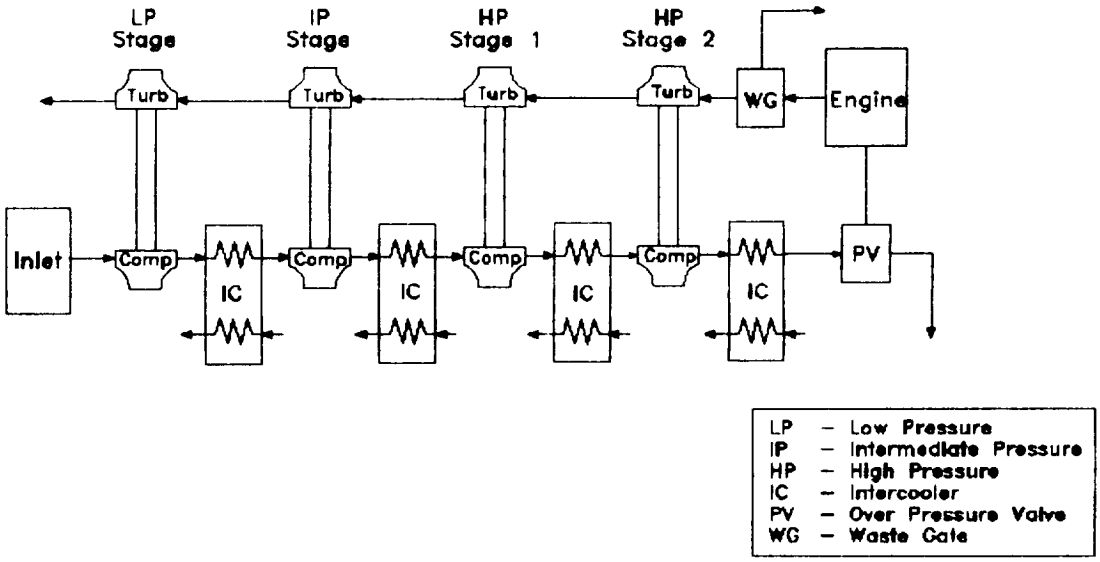

Figure 9.9

Specifications of the Four Stage Turbocharger System

Turbocharger Type	Radial
Over All Pressure Ratio	432:1
1st Stage Pressure Ratio	3:1
2nd Stage Pressure Ratio	4:1
3rd Stage Pressure Ratio	6:1
4th Stage Pressure Ratio	6:1
Maximum Mass Flow Rate	120.5 (lb/min)
Maximum Pressure Obtained at 130,000 ft.	1788 (psia)
Inlet Size	10.3 (ft^2)
System Weight	900 (lb)

9.3.2 ENGINE BLOCK AND CYLINDERS

The high altitude engine is arranged in a horizontal opposed configuration to reduce frontal area and allow an aerodynamic cowling to be fitted around the engine. The block is made up of two forged aluminum alloy pieces bolted together vertically. The crank shaft is a forged steel, twelve-throw, one piece design and is supported by seven journal bearings.

The engine has twelve, 10:1 compression ratio, aluminum alloy pistons displacing 1471 cubic inches. Each cylinder is made up of aluminum structure with a forged steel bore sleeve chrome plated to reduce wear and an aluminum alloy head. The cylinders are bolted separately to the block allowing for single cylinder replacement. There is one intake and one

exhaust valve per cylinder. The valve train is driven by a single camshaft geared to the crank. The valves are connected to the camshaft through a rocker arm pushrod setup.

9.3.3 LUBRICATION SYSTEM

The lubrication system for the high altitude engine is a pressure feed with a dry sump. The oil is pumped by a positive displacement gear type pump and the full flow is filtered. The oil receives cooling from a heat exchanger mounted in the front of the engine cowling. The oil used by the system is a 20/50 multi-grade.

9.3.4 COOLING SYSTEM

The cooling system used for the high altitude system is a pressurized liquid system. The coolant used is a 60/40 mix of Ethylene Glycol and water pressurized to 14 psig. The system uses a mechanical centrifugal pump capable of delivering 125 gal/min of coolant to the engine. The system has one radiator and a heat sink in the aircraft's fuel cell. The mean temperature of the coolant is 210 F and maximum system temperature is 265 F.

9.3.5 FUEL SYSTEM

The fuel system for the high altitude powerplant consists of a demand type mechanical pump with an electric

back-up pump. The fuel pump delivers the fuel to a electronic metering pump. This pump will vary the fuel inputs to the injectors to keep the correct air fuel ratio. There is one injector per cylinder injecting the fuel into the cylinder during the intake stroke. The fuel used by the system is 100 Low Lead aviation gasoline.

9.3.6 IGNITION SYSTEM

The ignition system for the engine consists of a dual electronic ignition system. Each circuit is totally separate and shielded with its own set of plug wires and plugs.

9.3.7 GEAR REDUCTION

A gear reduction box is employed to reduce the engine RPM down to and acceptable speed for the propeller. The gear reduction box is also used to mount and drive an auxiliary alternator. The gear reduction box has provisions for mounting other engine driven devices.

9.3.8 ELECTRICAL SYSTEM

The electrical system for the high altitude engine consists of a single mechanical 24 volt alternator powering dual 24 volt batteries and the engine sensors and aircraft systems. An extra alternator is driven by the engine to supply power for the payload package.

9.3.9 ENGINE CONTROL SYSTEMS

The engine control system for the high altitude engine is split in two parts, pilot controls and computer controls. The pilot controls the engine through dual throttles and pitch levers. The computer controls the engine's fuel mixture, ignition timing, and turbocharger waste gate to achieve the optimum performance.

The information on condition of the engine is displayed to the pilot through RPM gages, oil pressure gages, cylinder head temperatures, coolant temperature, and manifold pressure gages. Any engine faults are recorded by the computer for later retrieval.

9.4 PERFORMANCE SPECIFICATIONS

This section describes the performance of spark ignition engine developed for this aircraft.

The powerplant was modeled on an engine program modified from Reference 19. The program takes design parameters for the engine, preforms a cycle analysis, and outputs the performance of the designed engine. The program simulated the a twelve cylinder engine and turbochargers operating at 130,000 ft. Figure 9.10 shows the specifications and performance for the engine designed for this aircraft. Figures 9.11 and 9.12 show cycle information on the engines pressure vs. volume and heat transfer vs. gas temperature respectively.

Figure 9.10

Performance Specifications
1200 Hp Engine

Engine Type	IC Spark Ignition
Number of Cylinders	12
Cylinder Arrangement	Horizontal Opposed
Bore and Stroke	5.1 in and 6.0 in
Displacement	1470.4 cu in
Compression Ratio	10:1
Width and Height, Engine	37 in and 29.45 in
Width and Height, Installed	40 in and 66.53 in
Length and Frontal Area, Engine	57.96 in and 7.57 sq ft
Length and Frontal Area, Inst.	93.96 in and 17.87 sq ft
Engine Weight	1488 lb
Total Weight, Installed	2388 lb
Weight/Horsepower	1.93 lb/Hp
Fuel Grade	100 LL
SFC, Cruise and Max Power	0.374 and 0.403 lb/Hp-hr
SAC, Cruise and Max Power	5.467 and 5.625 lb/Hp-hr
Cruise Power	1202 Hp/3540 RPM @ 130k ft.
Max Power	1275 Hp/4570 RPM @ S.L.
	1240 Hp/4570 RPM @ 130k ft.

Figure 9.11

Pressure vs. Volume Diagram
1200 Hp Engine

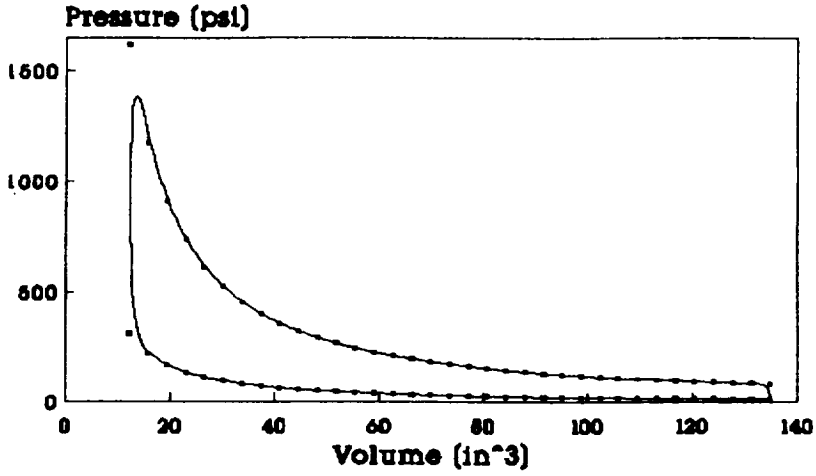

Cruise Conditions
Engine Displacement = 1470 cu.in.

Figure 9.12

Heat Transfer vs. Temperature
1200 Hp Engine

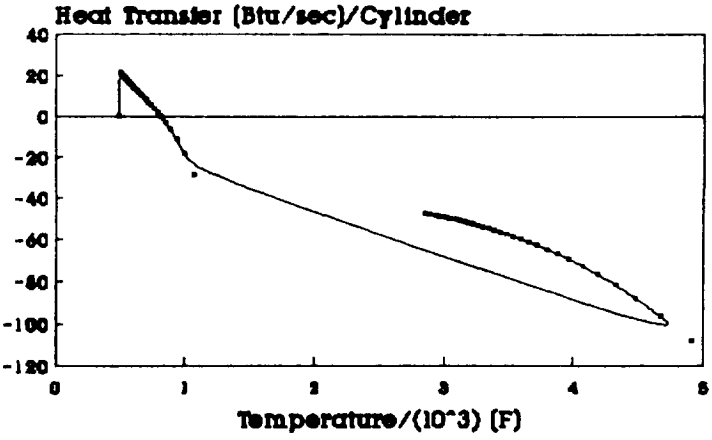

Cruise Conditions
Engine Displacement = 1470 cu.in.

9.5 Propeller Design

Research showed that, as in the design of a wing, the design of an efficient propeller is highly dependent on its operational speed. On the basis of momentum theory, the greatest efficiency is obtained by increasing the propeller diameter, and hence, reducing the induced velocity. However, a large propeller will have high tip speeds due to its rotational velocity that when added to its forward speed will produce transonic and supersonic speeds at the tip. Under these conditions, the effects of compressibility ignored by momentum theory can no longer be neglected. Thus, in order to avoid the heavy efficiency losses brought about by compressibility, the propeller blade speeds must not exceed the speed of sound.

The factors above indicate that the over-all shape of a propeller is determined by the maximum speed at which it must operate. For the Global Sentry, this implies that its propellers should be designed to have a large chord with the maximum amount of blade area concentrated in the minimum diameter (i.e., it should be short and stubby.) As a result,a high speed propeller is generally characterized by paddle-shaped blade tips that concentrate its area as far out as possible since this is where the major portion of the thrust is produced.

The design of a propeller to absorb a given power, as is the case in the design of a propeller for the Global Sentry, consists of determining the diameter and pitch of such a propeller. Reference 35 suggest a procedure which can be employed by using propeller test data. In a first attempt, to design a propeller of for the Global Sentry this was the approach taken. The procedure consists of a method built up on the use of nondimensional coefficients as outlined in References 3 and 36.

As a starting point, it was useful to determine the maximum rotational speed allowable for the propeller blades of the Global Sentry during cruise. Figure 9.13 is a presentation of the results. The vertical line on the figure represents the maximum rotational speed at which the propeller blades can operate without achieving sonic speeds. Since the diameter of the propeller is not yet known, the product ND, which is equivalent to the tip speed was used.

The results indicate that the maximum value ND the propeller blades can be subjected to is 14,000 ft.-rpm. This product was used because of the prevalent use of the factors N and D in the tabulation of propeller test data. N and D refer to the rotational speed and diameter of the propeller, respectively. With the maximum allowable rotational speed known several studies were conducted to determine if any existing propeller could be employed for propelling the Global

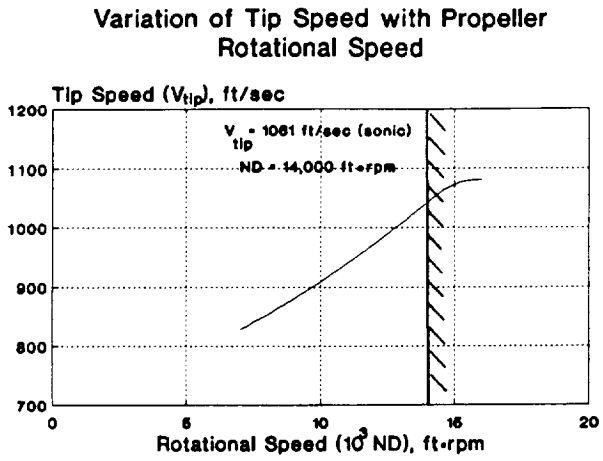

Figure 9.13: Propeller maximum velocity

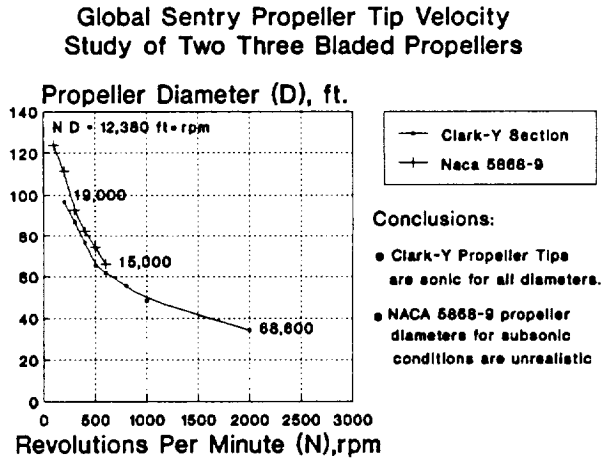

Figure 9.14: Tip velocity study of two propellers

Sentry. Figure 9.14 is the result of two such studies.

The study showed existing propeller charts cannot be employed in the design of a propeller for the this aircraft. As a result, further research will be needed to arrive at a feasible propeller design.

Upon further research, it was determined that the methods outlined in Reference 36 were suitable for estimating a propeller size and efficiency for the Global Sentry. The method provides a technique for adjusting the efficiency to account for compressibility effects of propeller tips which exceed the speed of sound. The following parameters were used in determining the propeller size of the Global Sentry:

Power Available: 1,202 Hp

Engine Speed: 4,000 rpm

Density: .8190E-05

Forward Speed: 742 ft/sec (Mach= .7)

The following are the results of the analysis:

Diameter: 27 ft.

Efficiency: 71%

Number of blades: 6

Section: NACA 16 series

Rotational speed: 1,500 rpm

Blade angle: - 75 degrees @ .3R

- 55 degrees @ .7R

Blade width: 3.2 ft. @ .7R

10. STRUCTURES

10.1 V-n DIAGRAM

In designing an aircraft and selecting the size and the material to be used, one must demonstrate the structural integrity of the aircraft subjected to the aerodynamic loadings that may exist throughout the V-n diagram. The velocity, V, in this diagram is expressed in term of equivalent air speed in knots, and n is the load factor. It is not practical to design an aircraft's structure to resist the highest possible load factors that it could produce, but base on experience, aircrafts are required to resist different limit load factors depending on its intended purpose. Besides these limit load factors, FAR Part 23 and 25 require a safety factor of 1.5 to be applied to the sizing of the structure, which definitely adds to the safety and integrity of the aircraft.

10.1.1. V-n MANEUVER DIAGRAM

The construction of this diagram is done following the outlined procedure given in Ref. 2. Any load factor, n, in this diagram is the load factor that can be achieved by maneuvering at that particular speed. As shown in Fig. 10.1, the highest load factor that Global Sentry may encounter in maneuvering is 2.5, and this means the structure must withstand at least this load factor. The design maneuvering

speed is referred as V_a, and the design diving speed is referred as V_d and they are also shown in the diagram.

10.1.2. V-n GUST DIAGRAM

The load factor, n, is the result of the gust encounter which increases the angle of attack of the wing thus causes an increase of lift and adds to the original lift in level flight. However, since one never encounters a truly sharp-edged gust, the gust velocity given is multiplied by a alleviation factor less than unity and thus reduces the acceleration due to gust. As shown in Fig. 10.2, the highest gust load factor that the Global Sentry may encounter is 5.9 and is higher than that of the maneuver diagram; therefore, the structure of Global Sentry must withstand 1.5 times this same load factor. As shown later in this report, the wing is modeled to withstand a load factor of 7.9 to assure structural integrity.

10.2 LANDING GEAR

Landing gears are important to an airplane because they provide the ability for ground maneuvering, absorb landing and taxiing shocks, allow for airplane towing, protect the ground surface, and provide for braking capability. In selecting the type of landing gear to be used in this airplane, three configurations were examined and analyzed,

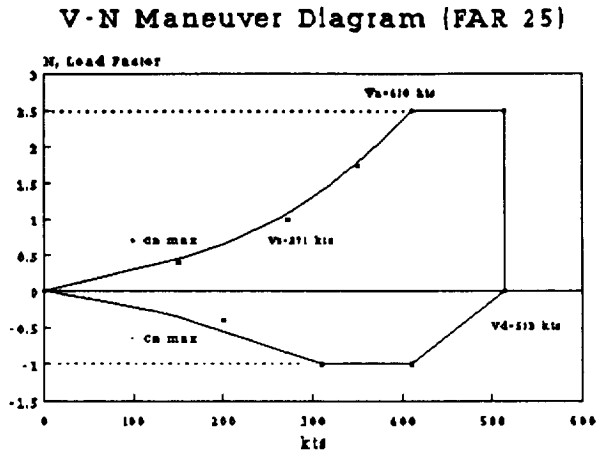

Figure 10.1

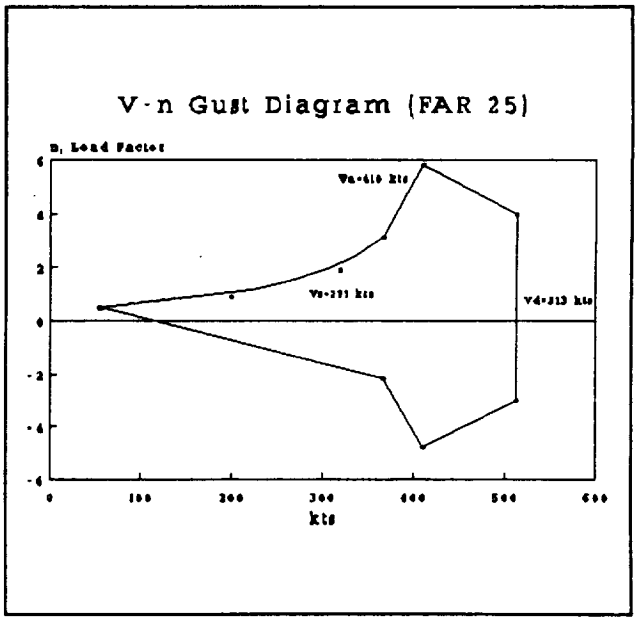

Figure 10.2

and they are taildragger, bicycle, tricycle, and quadricycle. The taildragger configuration was quickly ruled out because of poor visibility during ground operation and strong tendency to groundloop. The bicycle configuration, similarly, was ruled out because of the twin-fuselage configuration. The tricycle configuration was then analyzed, and it was found that because of the requirement that the maximum load the nose gear should take is 20% of the total weight (Ref. 37) and the forward locations of the center of gravity, the rearmost position of the main landing gears would be at about 47 feet from the nose of the airplane. If this configuration were chosen with the length of the landing gear of 105.2 inches, the aft part of the fuselage would bemxikely to touch the ground during landing or takeoff because an angle of 9.3 degrees would be formed between the aft-fuselage and the landing gear. Therefore, the quadricycle configuration was chosen (which is similar to bicycle configuration except for twin-fuselage), for this airplane, and the locations of the landing gears are shown in Figure 10.3. However, there are some disadvantages to this configuration. First, while the tricycle and the taildragger configurations are relatively low in weight, the quadricycle configuration is heavy because of its requirement of 45%-55% of load distribution between the front and rear gear that calls for a relatively heavy front gear. The next disadvantage is that the airplane is usually

hard to takeoff or lift its nose up because the front gear carrying 45% of the load. However, by using single tire per leg for both front and rear gears, a total of 520 lbs. were reduced since each tire weighs 130 lbs. And this airplane will not be likely to have any takeoff-rotation problem because of its tremendous wing span and area which means a small wing angle of incidence or deflection of elevator should get this airplane off the ground. The final configuration is shown in Figure 10.4.

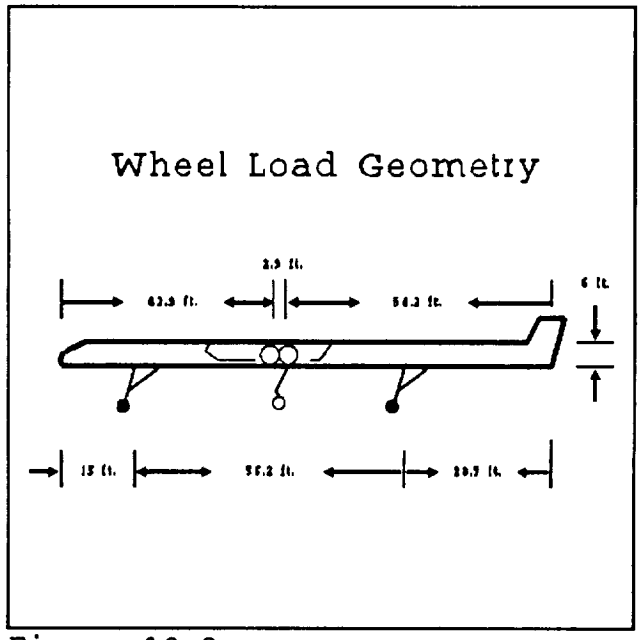

Figure 10.3

10.2.1. LOADS

The static and dynamic loads distributed to each of the landing gear were based on Fig. 10.4, which shows the positions of the gears based on the distribution of 45% of the loads to the front gear and 55% of the load to the rear gear in a quadricycle configuration. The static and dynamic loads of its members, namely oleo strut, drag brace, and side member were determined by pre/post-process the configuration in I-DEAS with the analysis performed by NASTRAN. The oleo strut and the top member were modeled as beam elements in I-DEAS since they resist bending moments,

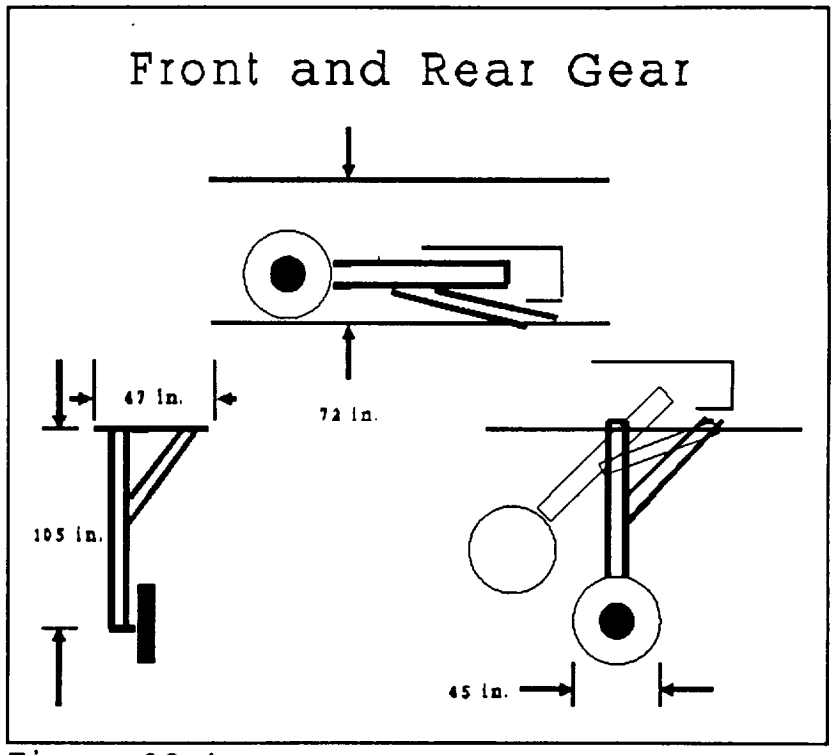

Figure 10.4

while the side member and the drag brace were modeled as rod elements. The material of the gear is steel alloy with Young's Modulus of 29E+6. Table 10.1 shows the final results of the landing gear loads including an increase of 7% as required by FAR 25, and Fig. 10.5 and Fig. 10.6 show the resulting loads on the members statically and dynamically, respectively.

Landing Gear Loads		
	Front Gear	Rear Gear
Maximum Static Load (per strut):	16185 lb.	17693 lb.
Minimum Static Load (per strut):	14474 lb.	-------
Dynamic Braking Load (per strut):	19115 lb.	-------

Table 10.1

10.2.2. TIRE SELECTION

With the determination of the static and dynamic loads, which now include an additional 20% of the load allowing for future growth of the airplane, the tire selection was done following the procedure outlined in Ref. 37. Table 10.2 summarizes the results keeping in mind that both the front and rear tire have the same dimensions.

Static Loads on Pts. of Constraint

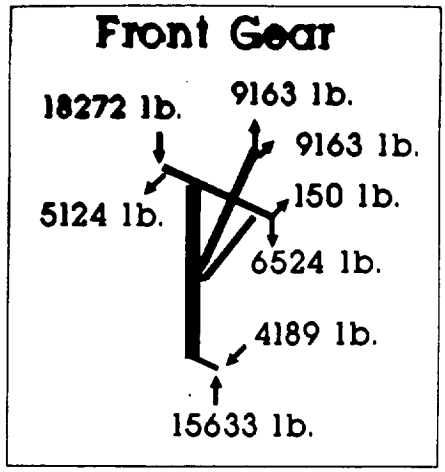

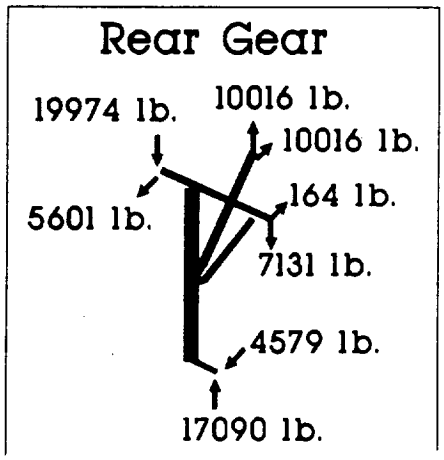

Figure 10.5

Dynamic Loads on the Points of Constraint

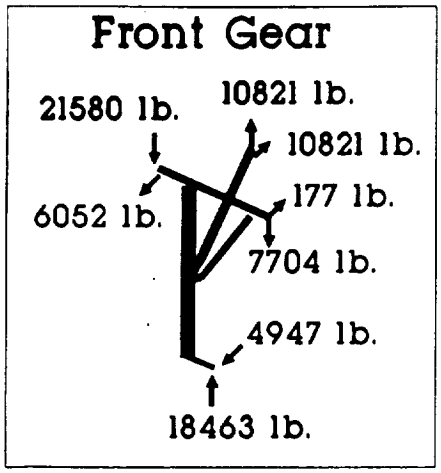

Figure 10.6

Tire Selection		
	Front Gear	Rear Gear
Maximum Load per Tire Required	20231 lb.	22116 lb.

Tire Data (B.F. Goodrich 15 X 15.5 - 20)			
Maximum Diameter	45.25 in.	Minimum Diameter	44.3 in
Maximum Width	16.0 in.	Minimum Width	15.0 in
Tire Pressure	105 psi.	Maximum Load	24000 lb.
Maximum Speed	160 mph	Rim Diamter	20 in.

Table 10.2

10.2.3. STRUTS

With the selection of oleo-pneumatic shock absorbers including the energy absorption efficiency of 0.8, the stroke (travel of the strut) and the diameter of the strut were found in Table 10.3 that can withstand a vertical descent of 12 fps and a landing gear load factor of 2 which are the requirements according to FAR 25.

Struts		
	Front Gear	Rear Gear
Diameter of the oleo strut	4.34 in.	4.18 in.
Stroke	21.22 in.	21.22 in.

Table 10.3

10.2.4. DEFLECTIONS

The static and dynamic deflections of the strut were determined using the NASTRAN program, and the results were post-processed by I-DEAS and are shown in Fig. 10.7 and 10.8. These results are based on the static and dynamic loads calculated above.

Table 10.4 summarizes the results.

Deflections		
	Front Gear	Rear Gear
Static	1.19 in.	1.30 in.
Dynamic	1.41 in.	--------

Table 10.4

10.2.5. LANDING GEAR RESPONSE

Fig. 10.9 shows the landing gear response using a spring constant of 270 lb/ft and a damping ratio of 180. There are

Landing Gear Static Deflection

Front Gear

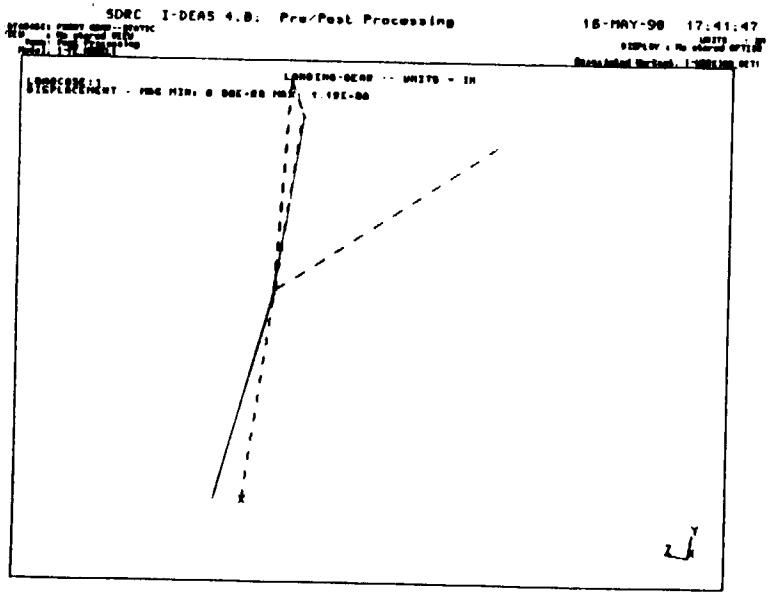

Rear Gear

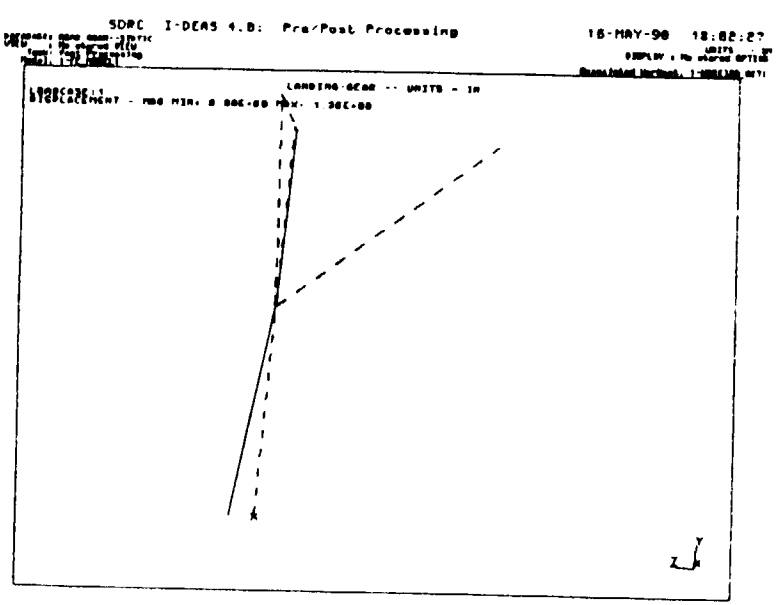

Figure 10.7

Landing Gear Dynamic Deflection

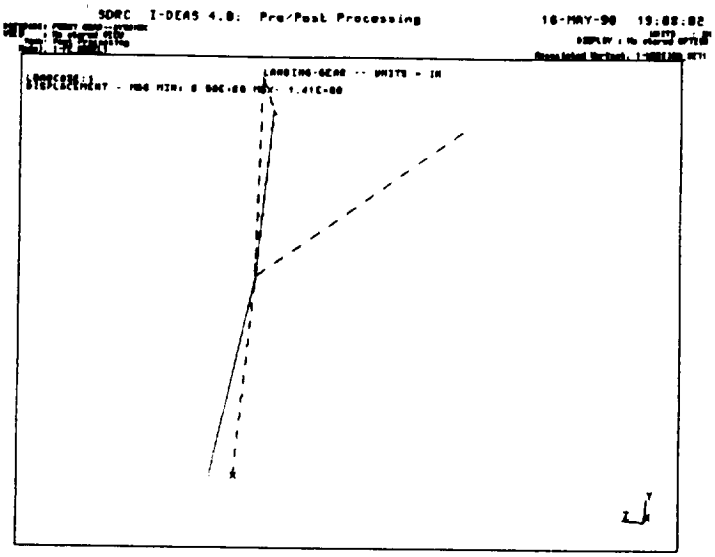

Figure 10.8

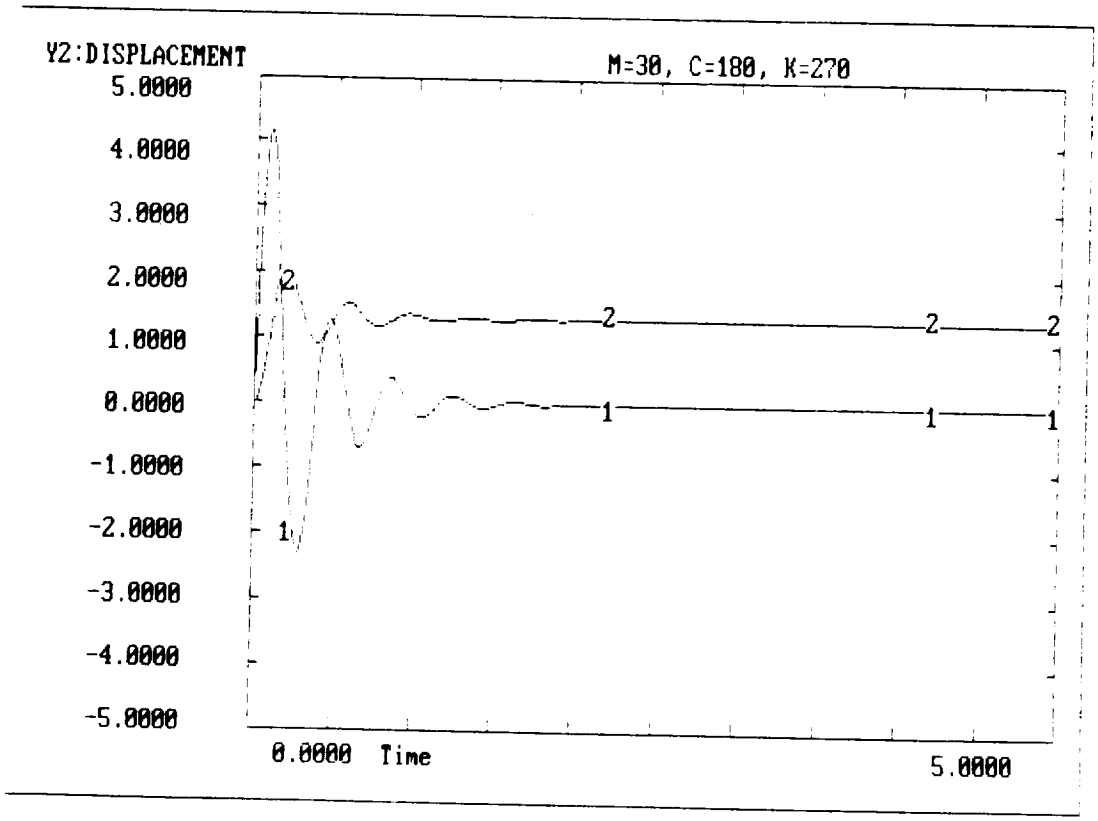

Figure 10.9

two axis shown in the figure with 1 representing the velocity and 2 representing the displacement or stroke. Recall that the maximum stroke calculated was 21.2 in., and Fig. 10.9 does show a maximum displacement of a little less than 2 feet.

10.3 WING STRUCTURAL ANALYSIS

Two analyses were performed using the finite element method to obtain the deflection, stress, and strain at various spanwise locations. The first analysis was done simulating a load factor of 7.9 loading on the structure, as required by the V-n Gust Diagram shown above, while the second analysis was done using the engine and structure weight to simulate the static deflection of the wing. Both of these analyses were pre-processed by I-DEAS's Supertab module, and then data files of MSC/NASTRAN Version 66A were generated by I-DEAS's Supertab module and sent for analysis. After the results were obtained, I-DEAS's Supertab module was used once again for post-processing. This means displacement, stress, and strain of the wing at the different spanwise locations were represented graphically and are shown later in this report.

10.3.1. WING MODEL (cross-section)

The airfoil used in this wing is divided into 18 segments on the upper surface and 17 segments on the lower surface. All of these segments are not spaced equally because their

locations depends on the curvature of the airfoil. This means that there are more segments to represent the more curved parts of the airfoil and fewer segments for the less curved parts of it. There are a total of 6 square stringers of 3 in. by 3 in. and are connected by CQUAD4 plates to resist bending.

10.3.2. WING MODEL

The top view of the wing is shown in Fig. 10.10, and it is seen that the wing is tapered in both leading and trailing edges. The wing has a semi-span of 173 feet, with a root chord of 49.6 feet and tip chord of 24.8 feet. The wing has a total of 20 webs of 8.9 feet apart and has a

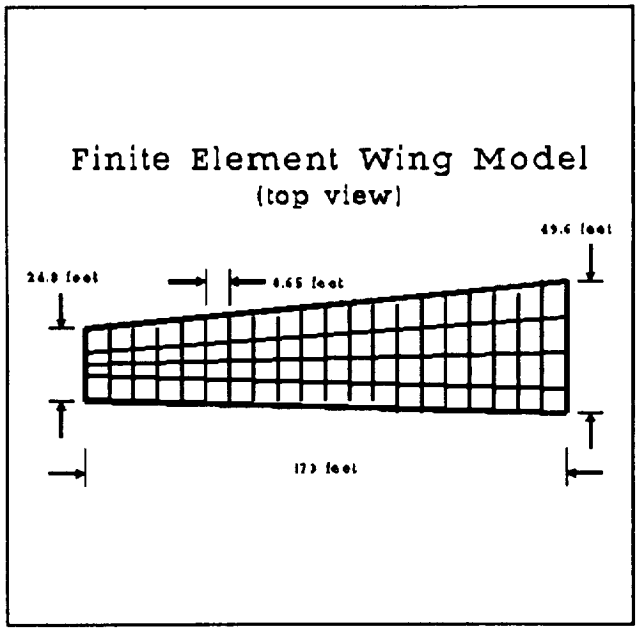

Figure 10.10

total of 6 stringers (3 stringers from the top view) extending from the root to the tip. The stringers are modeled with CBEAM elements while the skins and webs are modeled with CQUAD4 plates.

10.3.3. MATERIAL SELECTION

Composite materials are ideal for structural applications where high strength-to-weight and stiffness-to-weight ratios are required. In general, there are three commomly accepted types of composite materials :

1. Fibrous composites which consist of fibers in a matrix.
2. Laminated composites which consist of layers of various materials.
3. Particulate composites which are composed of particle in matrix.

Having high strength, stiffness in the fiber direction, low weight, corrosion resistance, wear resistance, and thermal insulation compare with aluminium, the laminated fiberous composites were used to model the wing's elements as following:

UPPER SKIN ..... graphite-epoxy

LOWER SKIN ..... graphite-epoxy

SPAR WEBS ..... graphite-epoxy

RIB SHEAR PANELS ..... graphite-epoxy

The composite material was modeled as a nine layer cross-ply composite laminae with equal thickness, and the layers oriented in the 0 and 90 degree of fiber directions for the wing structure. Such laminates are called regular symmetric cross-ply laminates which eliminated the coupling between bending and extension of the laminates. NASTRAN has the capability to model the entire stack of such laminae with a single plate or the shell element. Using the CQUAD, PCOMP and MAT8 bulk data cards, the user can define the fiber direction and the material properties of each laminate. NASTRAN analyzes a composite fiberous laminate based on the classical theory which incorporates the following assumptions:

1) The layers of a laminate are perfectly bounded together by the same matrix material that is used in the laminae.

2) The bonds are infinitesimally thin and displacements are continuous across lamina boundaries so that no lamina can slip relative to another.

3) Each lamina is assumed in a state of plane stress.

The following table define the material properties of the laminate.

Properties of Composite Material	
Tensile & Compressive Modulus of 0 deg.,E1(10^6 psi).	19.0
Tensile & Compressive Modulus of 90 deg.,E2(10^6 psi).	.900
In-plane Shear Modulus, G12 (10^6 psi)	.700
Poisson's Ratio	.250
Specific Weight (lb / in^3)	.055
Tensile Strenght of 0 deg. (ksi)	180.
Compressive Strenght of 0 deg. (ksi)	160.
Tensile Strenght of 90 deg. (ksi)	6.00
Compressive Strenght of 90 deg. (ksi)	20.0
In-plane Shear Strenght (ksi)	9.00
Interlamina Shear Strenght (ksi)	14.0
Cured Ply Thickness (in)	.030

Table 10.5

NOTE: 0 degrees orients the fiber direction

90 degrees orients the matrix direction

The following figure depicts the geometry of the graphite epoxy laminate:

Layer 9	0 deg.
8	90 deg.
7	0 deg.
6	90 deg.
5	0 deg.
4	90 deg.
3	0 deg.
2	90 deg.
1	0 deg.

10.3.4. PRE-PROCESSING

Pre-processing was done utilizing I-DEAS's Supertab module to generate the finite element model of the wing. The first thing in finite element modeling is to obtain all of the grid points (a total of 756 in this case). Then the 6 stringers were generated using CBEAM element and also the skins were generated using CQUAD4 element. Lastly, the webs were also constructed using CQUAD4 element to finish the structure of the wing. The spar webs are not hollow in this case because fuel is not store in this part of the wing but in the part between the two fuselages. Next, all the loads acting on the structure were accounted for with the assumption that they are acting on the stringers and webs only. These loads include the engine load, which was distributed on corresponding stringers and webs, and the lift, which was

distributed on the skin assuming an elliptical loading.

10.3.5. MODEL CONSTRAINTS

Since one-half of wing span from the left fuselage was modeled for the finite element analysis, the wing was constrained from all rotation and deflection at the wing's root. This meant the wing was modeled as a cantilever configuration. No contraints were applied at the wing tip.

It was necessary to restrain the quadrilateral elements from all rotation in the Z axis to avoid discontinuous slope at the boundaries of the element. This meant constraining all nodes from rotation in the Z direction.

10.3.6. LOADING THE MODEL

After defining all the geomtry and material properties of the wing, the loading of the model has to be resolved. The total lift load was based on the total weight of aircraft. The total weight of aircraft is 60,127 lbs, and a 7.9 gust factor and a 1.5 factor of safety were applied. This brought the total lift load to 475,003 lbs. From this value, the lift distribution per unit wing span was solved by assuming an elliptical spanwise load distribution acted at quater chord.

Next, the pressures over each plate of the upper and lower sufaces were resolved for the average pressures then

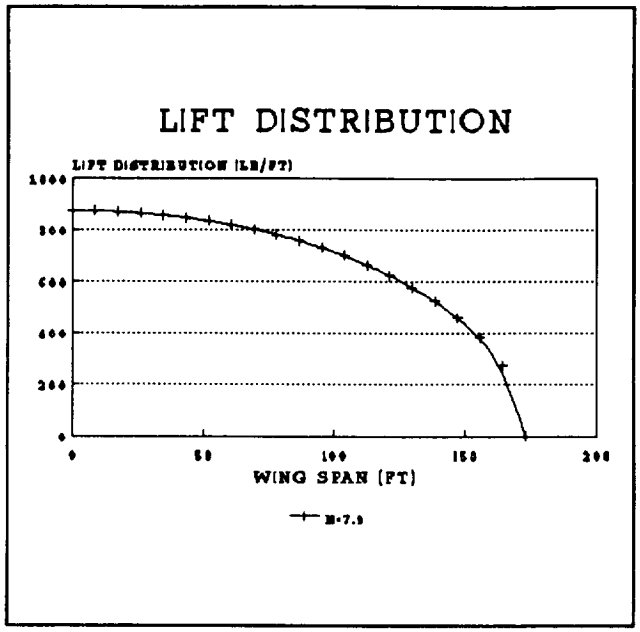

FIGURE 10.12

scaling their magnitudes to fit an elliptical spanwise loading. The pressures were scaled to represent a 2-g loading on the structure. The wing has to carry the loads perpendicular to its surface,but since there is a small amount of dihedral the horizontal components of lift were not accounted for to simplify matters. Therefore, the total lift forces were oriented in the positive vertical direction. The lift forces were input as distributed loads over quadrilateral plate for two dimensional. This was easy done by using the PLOAD2 bulk data card. The following figure depicts the load distribution versus wing span.

10.3.7. POST-PROCESSING

After the results were obtained from the NASTRAN

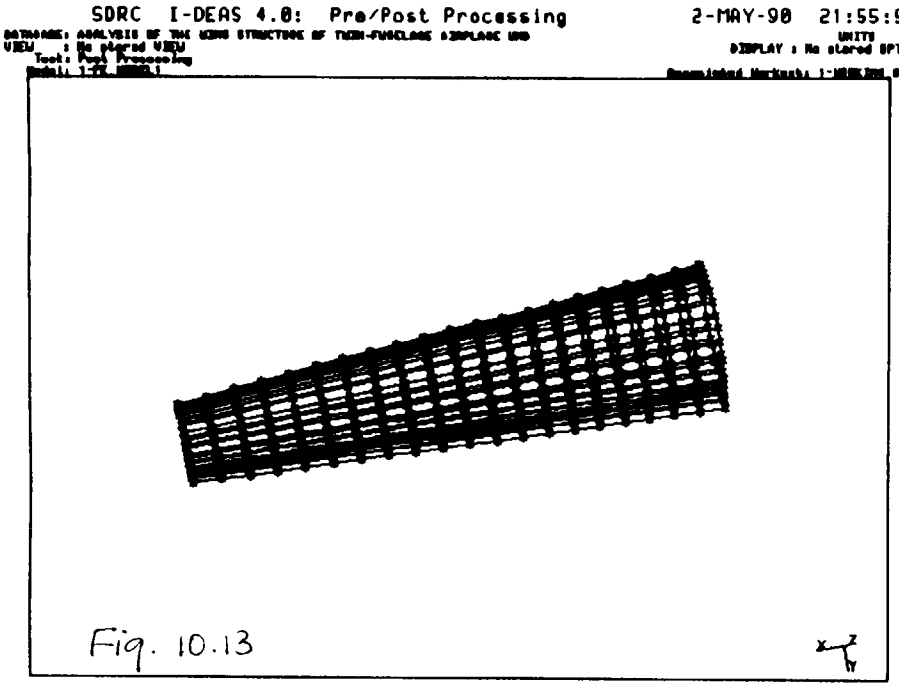

Fig. 10.13

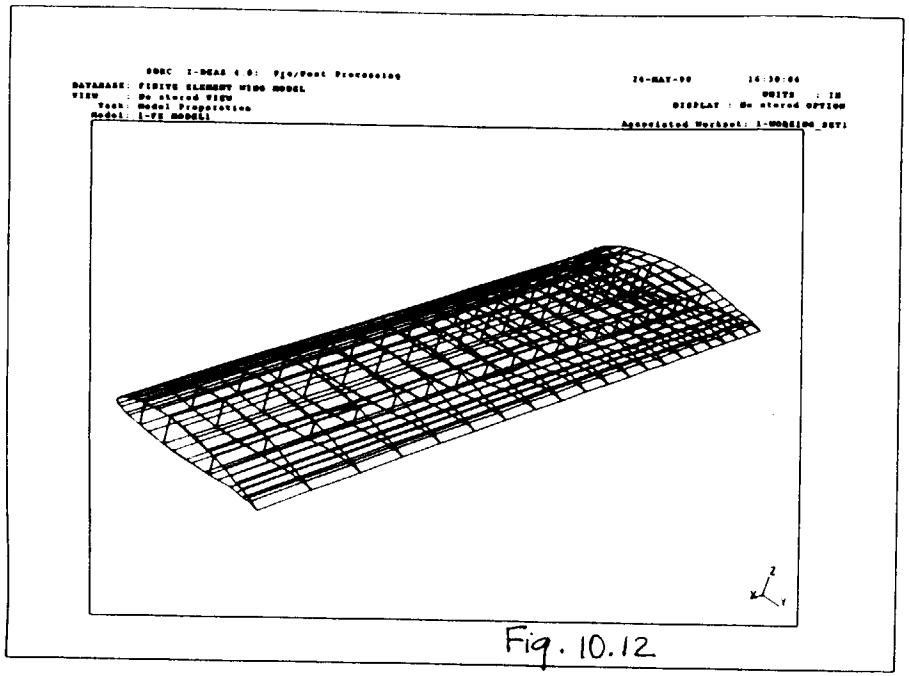

Fig. 10.12

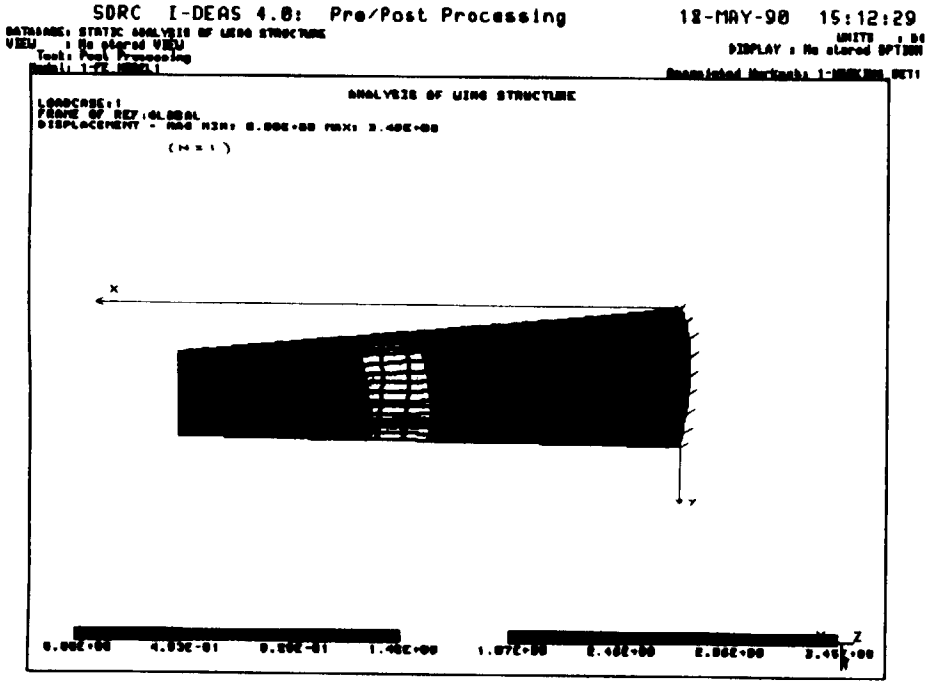

Fig. 10.14

analysis, post-processing was done utilizing I-DEAS's Supertab module and a graphic representation was obtained.

10.3.8. DISPLACEMENT

The maximum wing deflection occurs at the tip of the wing, while the minimum wing deflection is, of course, at the wing root. The results are summarized in Table 10.5, and graphically are represented in Fig. 10.14 and 10.15.

	Displacement	
	Load Factor=1	Load Factor=7.9
Maximum Deflection (at the tip)	3.45 feet	27.3 feet

10.3.9. STRESS

For the load factor of 7.9, the maximum stress occurs at the trailing edge of the wing root and is approximately equal to 13.5E6 ft-lb. This can be seen in Figures 10.16 and 10.17.

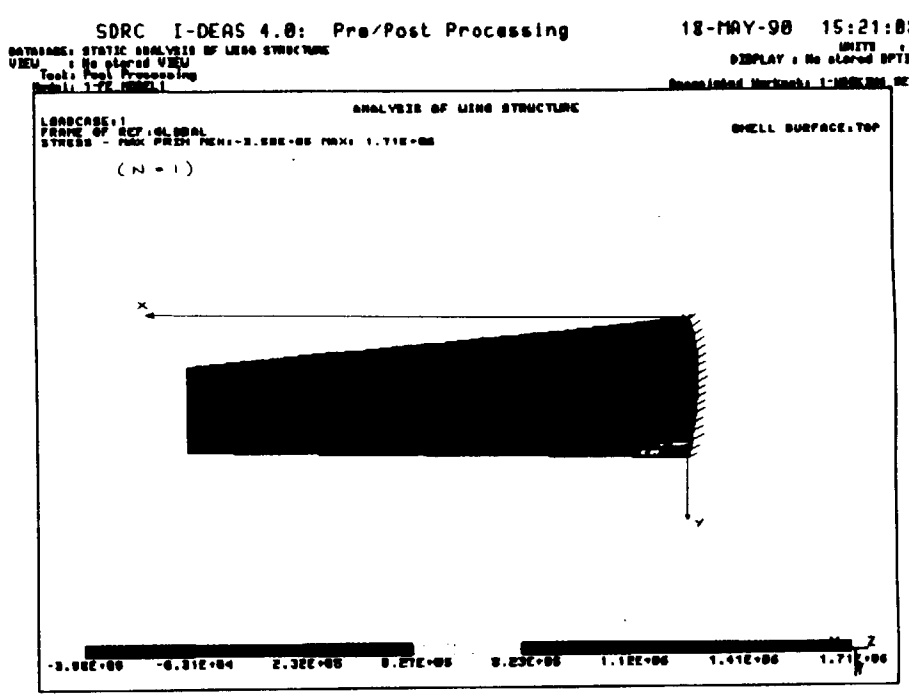

Fig. 10.16

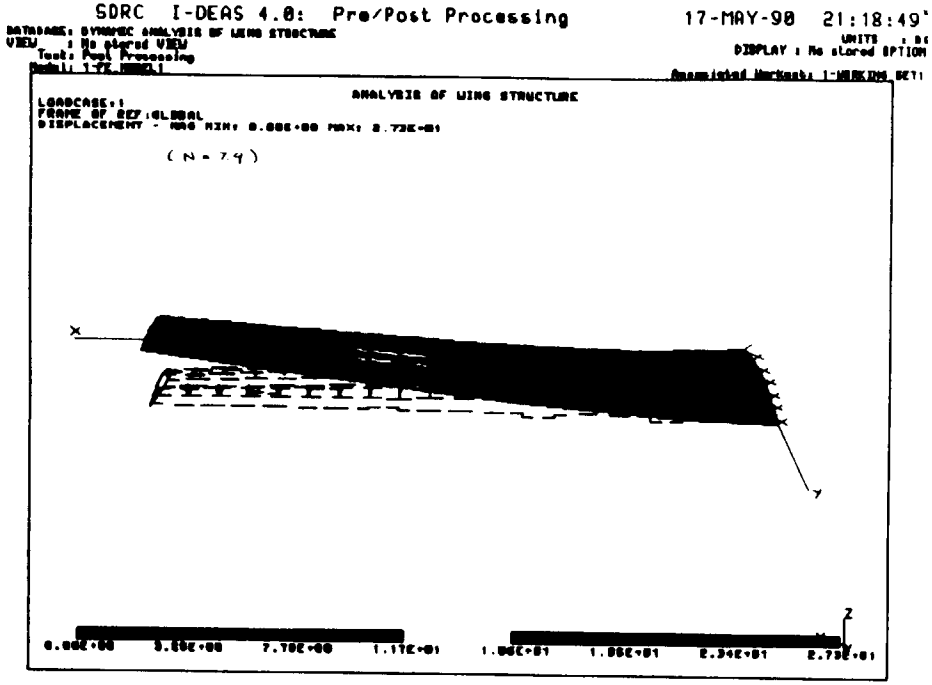

Fig. 10.15

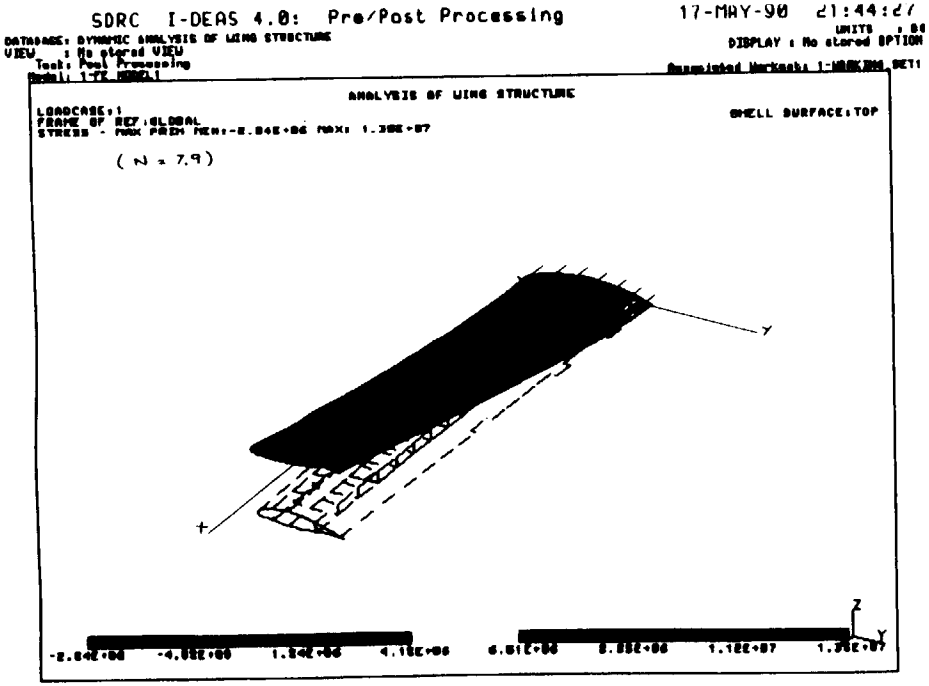

Fig 10.17

ORIGINAL PAGE IS
OF POOR QUALITY

11. COCKPIT, CONTROLS AND DISPLAYS LAYOUT

11.1 COCKPIT LAYOUT

The following cockpit considerations, and assumptions specifications have been taken from Reference 41. The cockpit layout is shown in Figure 11.1.

11.1.1 DESIGN CONSIDERATIONS

1. The pilot will be positioned so that he can reach all controls comfortably, from some reference position.
2. The pilot will be able to see all "flight essential" instruments without undue effort.
3. The pilot's communication by voice or by touch will be possible without undue effort.
4. Visibility from the cockpit will adhere to certain minimum standards.

11.1.2 DESIGN ASSUMPTIONS

Some assumptions need to be made for the cockpit design of the high altitude aircraft.

1. Male crew member in a pressure suit at all times.
2. The crew member will be in his sitting position during the entire flight mission.
3. The work envelop will be within reach by the pilot.

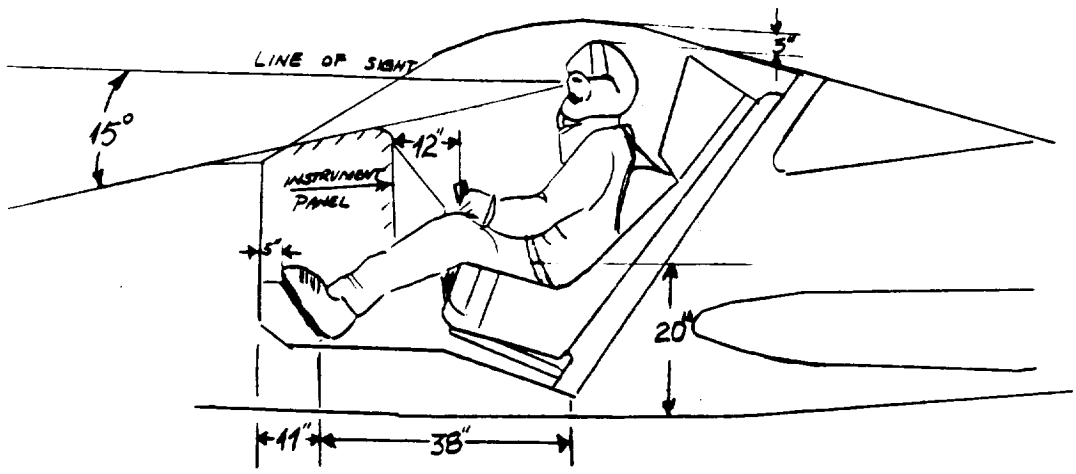

Figure 11.1 Cockpit Layout

11.2 COCKPIT CONTROLS AND DISPLAY LAYOUT

For ease of pilot operation, the throttle switches and stick controls have been used in the design of the cockpit

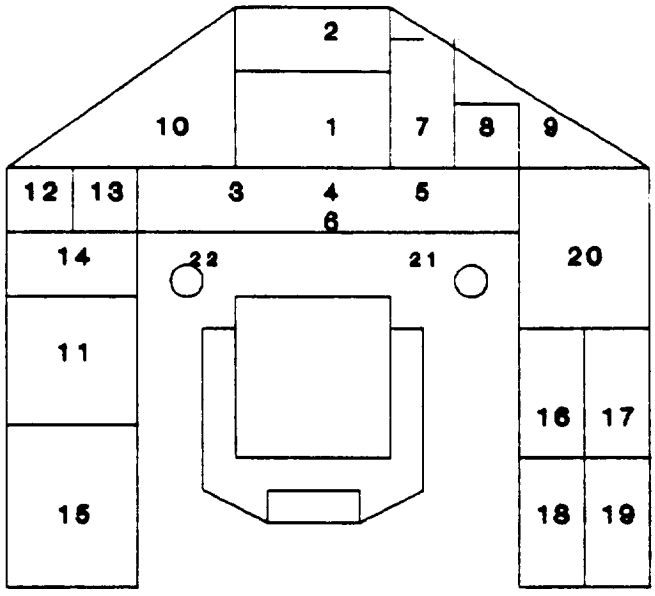

MAIN PANEL

1 CRT
2 HUD
3 Altitude
4 Speed
5 Altimeter
6 Attitude
7 Temperature
8 Fuel Flow
9 Oil Pressure
10 Engine Starter

CONTROL STICK

21 Stick Control
22 Stick Control

LEFT SIDE PANEL

11 Radar Control
12 Fuel Control
13 Throttle
14 Radio Transmitter
15 Speed Brake

RIGHT SIDE PANEL

16 Engine Control
17 Oxygen Regulator
18 Environmental Control System
19 Cabin Temperature Control
20 Warning Panel

Figure 11.2 Cockpit Layout Displays and Controls

displays and pilot interfaces. Figure 11.2 illustrates the layout of the cockpit displays. All instruments have been grouped according to their functions. The Head-Up-Displays (HUD) concept has been used due to the interaction between technological progress, economics and safety, due to the laminar fuselage the HUD will increase the visibility of the pilot.

11.2.1 MAIN PANEL DESIGN

The "Basic T Panel" has been used in the design of the main panel Figure 11.3. This panel is configured on the fast and accurate scanning of four basic parameters simultaneously - speed, attitude, altitude and heating.

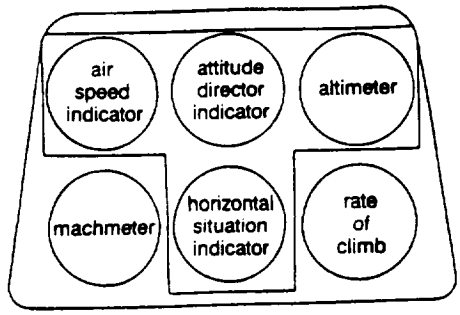

Figure 11.3 "Basic T Panel"

11.2.2 SWITCHES DESIGN

Since switches should be easy to access on the control panels, the concept of a forward-on and sweep-on are used in

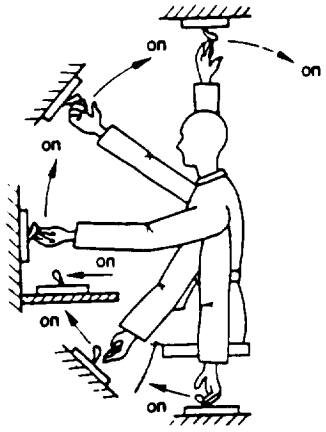

Figure 11.4 The 'Sweep-on' and 'Foward-on' switch.

11.3 HUMAN FACTORS

11.3.1 HUMIDITY

Humidity is an environmental problem in high altitude flight aircraft of low relative humidity (RH). This results from the very low water content of the air at the high altitudes. To resolve this problem, an installation of humidifiers is recommended in the cockpit design.

11.3.2 LIFE SUPPORT SYSTEMS

The Life Support Systems (oxygen, suit faceplate heat, suit-cooling air, and air conditioning) must be within reached distance by the pilot to prevent any hazard occur. The cockpit pressurization must not exceed 29,000-ft cabin altitude at its maximum altitude for manned flight.

11.3.3 FOOD AND FLUID STORAGE

A storage area for foods and fluids for the pilot is to

design within reaching distance. The foods and fluids recommended are high in carbohidrate and protein, and considering the long flight caffeine liquids would be welcome.

11.4 MAINTAINABILITY

For years, the maintenance tasks could be simplified for mechanics, or made better, or just made the job performance easier for the individual. As time went by, all the maintenance programs were put on the paper before any performance due to the high cost in maintenance. With this in mind, the maintainability design is very important to the industry.

A computer programming language has been developed to solve for the Up-Time-Ratio, maintenance increment, equipment availability, mission availability, and the system reliability. Figure 11.5 shown the maintainability of landing gear, fuselage, and the airframe.

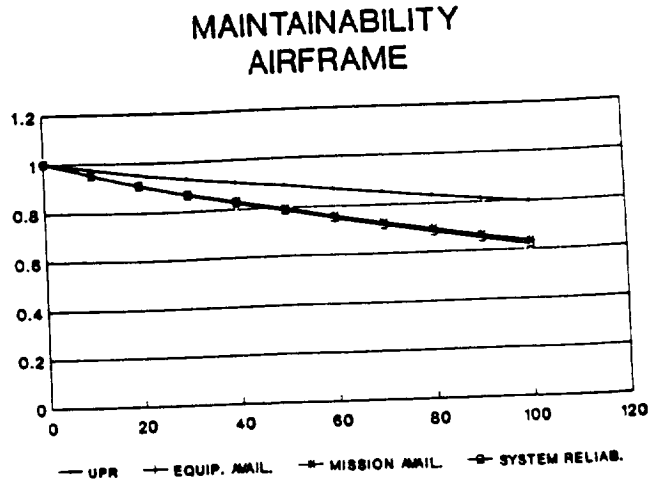

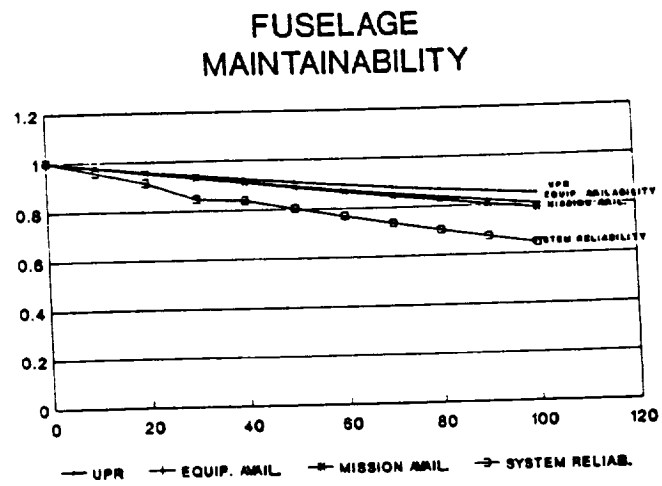

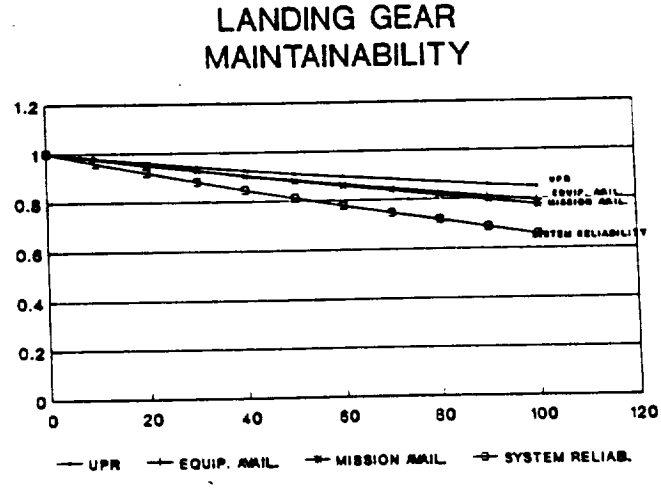

Figure 11.5 The Maintainability of Airframe, Fuselage, and Landing Gear.

12. MANUFACTURING AND MANAGEMENT STRUCTURE

12.1. MANUFACTURING

Figure 12.1 shows the production and final assembly layout for the Global Sentry. The facility will be 300.000 square feet. The first step will involve the manufacturing of the fuselage structure. The assembling of the fuselage will be followed by the assembly of the center wing and the vertical tail. The next step is to install control and install the landing gear which will be followed by the installation of electronic and control systems of wings and the instrumentation of fuselage. Finally, the engines will be inducted which will come after quality control check. Vertical tails, engines, control surfaces, and nose cones will be received from a vendor.

Since the facility is large and to be cost effective it is recommended that such a facility should be built where land is inexpensive and property taxes are low. If such a facility was to be built in Southern California, San Bernardino County would be cost effective for such a project.

12.2 MANUFACTURING STRUCTURE

The management structure for the Global Sentry aircraft will be a matrix organization type structure. This type of structure will closely monitor each and every department

creating a efficient working environment. Weekly meeting should be held by each department manager to ensure production schedule and progress of the project.

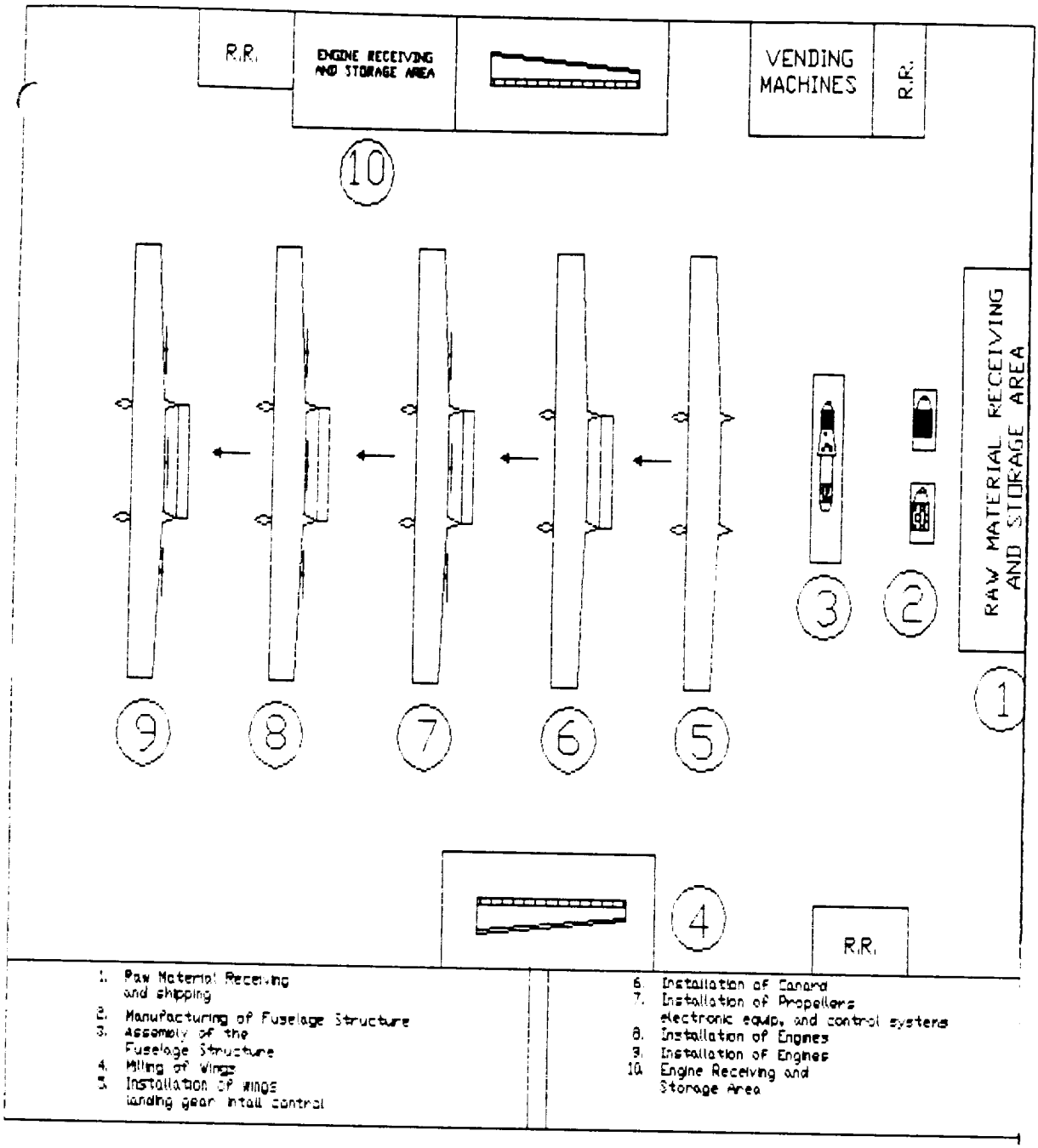

Fig. 12.1

SENTRY PROJECT MANAGEMENT STRUCTURE

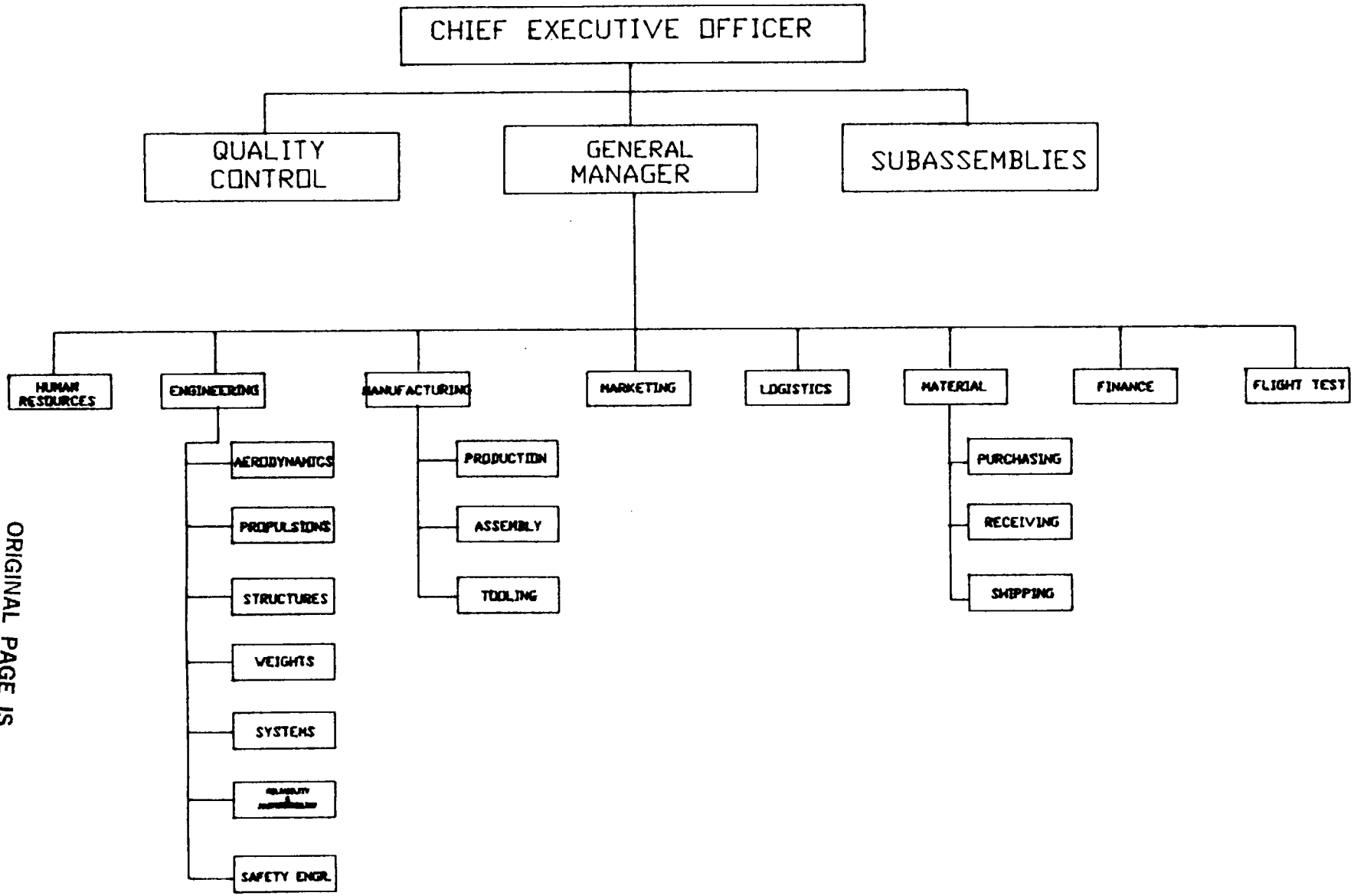

13. COST ESTIMATION

A computer program has been developed which allows you to input such factors as the number of aircraft for production, the years allocated for the project, and the number of prototypes needed. The program calculates the total cost of the project and computes the cost per aircraft. It takes into account the learning curve theory as well as the inflation rate which varies yearly and is based on the Aerospace Price Index.

These various costs are all calculated in term of future dollars when the project is to be completed. Different vendors were contacted in order to get an estimate for the engineering, tooling and manufacturing cost involved in the design and production of this aircraft. The total cost of the plane is subdivided into various costs such as the materials, production development, quality control, manufacturing labor, test flight operations, engineering and tooling.

The manufacturing material cost includes the raw materials, hardware and purchased parts required for the fabrication and assembly of the major structure of an aircraft. Quality control is closely related to direct manufacturing labor, but is estimated separately. Quality control is simply estimated as a proportion of manufacturing labor. It is estimated to be 13% of total labor man hours dedicated to this project. Tooling cost includes all costs

allocated to tool design, tool planning, tool fabrication production test equipment and the maintenance of tools. Manufacturing labor cost includes all costs necessary to machine process, fabricate and assemble the major structure of an aircraft and to install purchased parts. The engineering cost includes activities such as design studies and integration, shop and vendor liaison, materials and process specifications, and reliability. The cost of development support is the cost of manufacturing labor and material required to produce mock-ups, test parts, and other items of hardware that are needed for airframe design and development work. This cost is related to IMPURE weight speed and the quantity of aircraft in the development contract. The flight test operations cost element comprises all costs incurred by the contractor to carry out flight tests except the cost of the test aircraft. It includes engineering planning and data reduction manufacturing support,instrumentation, and pilot's salary. Table 13.1.1 presents the cost estimation for building a prototype and does not include the cost associated with engines or avionics.

Table 13.1.1

Cost Estimate for 3 aircraft and 1 prototype	
Prototype Cost	
Development Cost	12,072,330
Material	5,456,822
Quality Control	1,680,964
Test Flight Operation	6,004,768
Engineering	22,660,640
Tooling	8,315,523
Manufacturing Cost	12,930,500
Total Prototype Cost	69,121,440

Table 13.1.2 presents the cost associated with the production of three aircraft.

Table 13.1.2

Production Cost Estimate ($ Millions)	
Development cost	521,660,800
Material	1,101,186,000
Quality Control	143,154,100
Manufacturing Labor	658,933,830
Test Flight Operation	187,775,700
Engineering	640,067,800
Tooling	612,039,400
Total Production Cost	44,768,610,000
Cost Per Aircraft	150,397,300

Figures 13.1.1 and 13.1.2 presents charts of the costs associated with the production of the Global Sentry Aircraft.

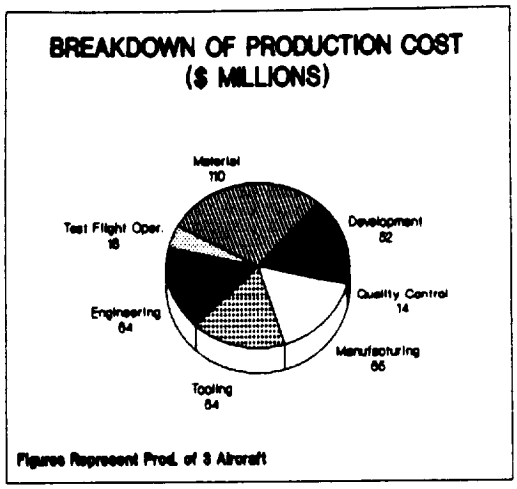

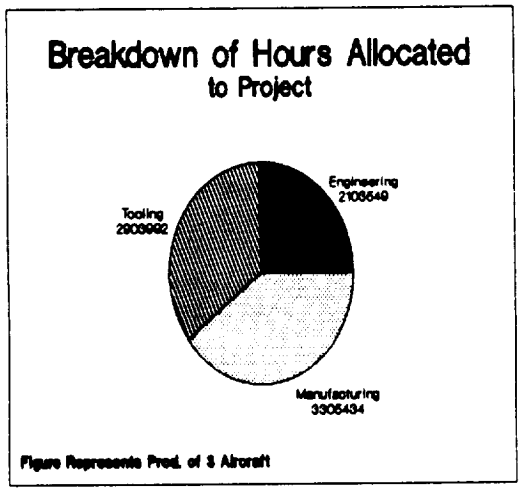

Fig. 13.1.1

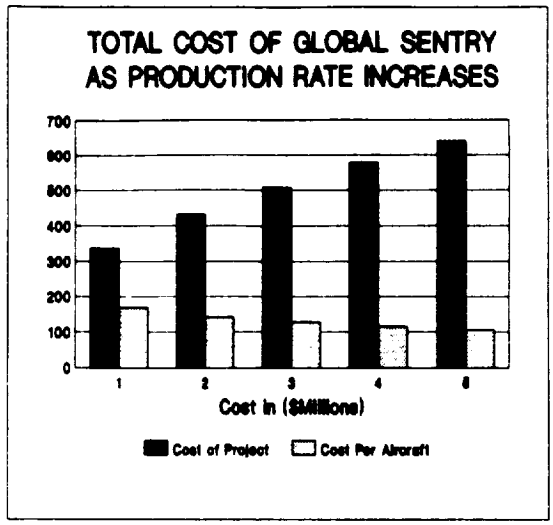

Fig. 13.1.2

14 RELIABILITY

14.1 Reliability

Design engineers play an important role with respect to reliability in system design. Since there are difficulties in motivating design engineer for reliability Figure 14.1.1 displays guidelines to design for a reliable system which needs to be included in the manufacturing process of this aircraft.

The historical data for a T-38 trainer was obtained from Northrop Aircraft. This was the simplest aircraft for which complete reliability analysis was available. The data for the T-38 was a starting point to calculate the reliability of each and every component that is critical for proper functioning of the Global Sentry aircraft. Since the two planes are so different a complexity factor was assigned to each of the components. This factor is needed in order to justify the end result. For example, the reliability of the airframe was determined by calculating the mean time between failures for the T-38. The Global Sentry was broken down into several different components which were external pressure, geometry of the aircraft, material, and structure. These were then ranked accordingly to their importance.

A computer program was used to find the reliability of each critical component in the aircraft. The airframe reliability for the Sentry was calculated to be .95. Similar

type of analysis was used to calculate the reliability of other components of the airplane. It was assumed that each of the components is in a series type of system with no redundancy where if one component fails the plane is unreliable. The reliability of the plane as the mission time increase is displayed in Figure 14.1.

RELIABILITY ANALYSIS

SYSTEM	MTBF	R(6)	R(10)
Airframe	210	0.972	0.9535
Fuselage	230	0.9743	0.9575
Landing Gear	240.5	0.9754	0.9593
Flight Control	180.6	0.9673	0.9462
Power Supply	270.4	0.978	0.9637
Lighting System	10000	0.9994	0.999
Fuel System	500	0.9881	0.9817
Instruments	340.4	0.9825	0.9711
Radio	18000	0.99967	0.9994
Engines	433.3	0.9862	0.977
Interphone	310	0.9808	0.968
TOTAL RELIABILITY		0.8198	0.7196

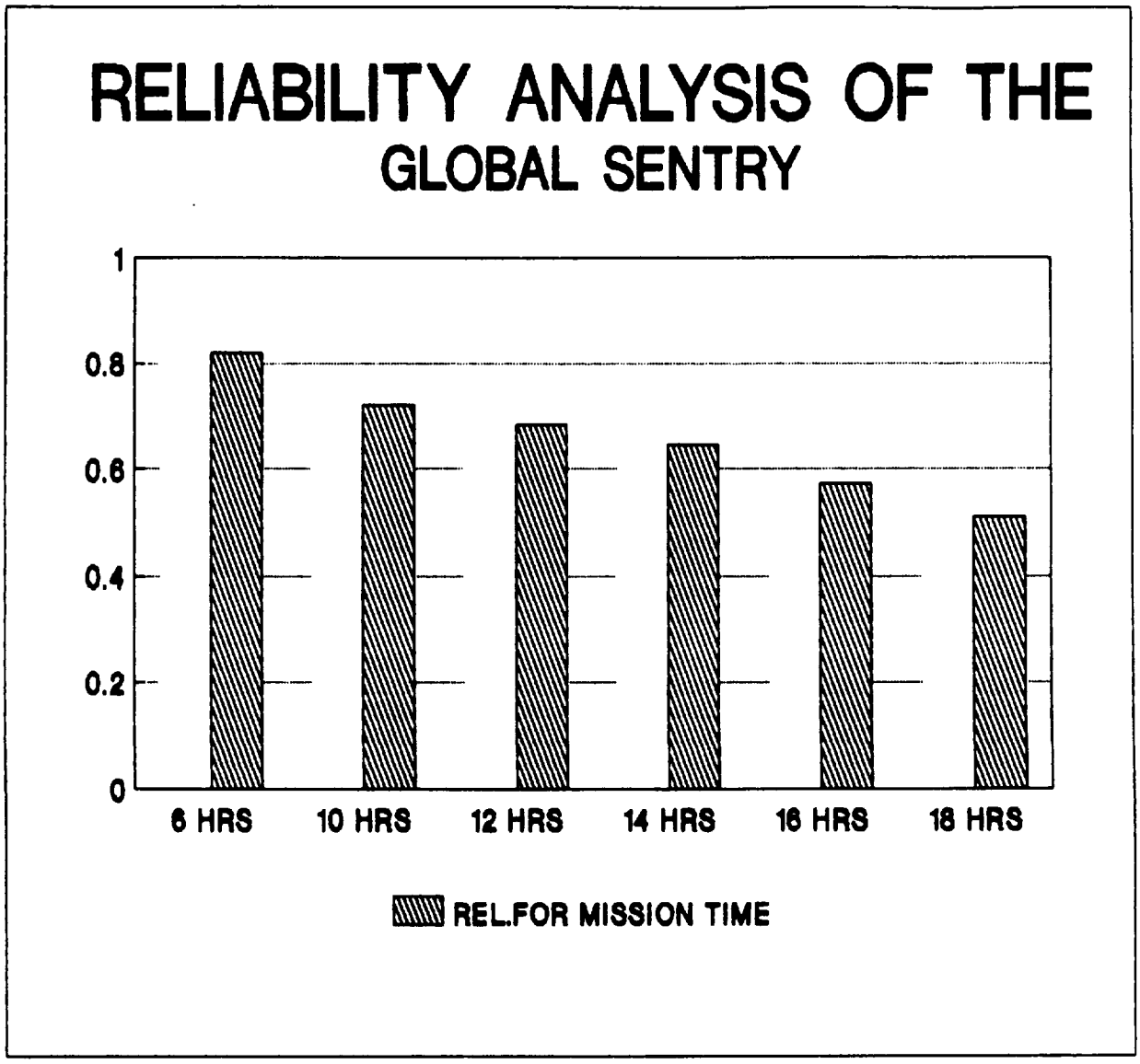
RELIABILITY ANALYSIS OF THE
GLOBAL SENTRY
1
0.8
0.6
0.4
0.2
0
6 HRS
10 HRS
12 HRS
14 HRS
16 HRS
18 HRS
REL.FOR MISSION TIME

Fig. 14.1

15. CONCLUSION

As it was seen in this report, it is possible to achieve the required cruise altitude utilizing conventional technology. Altitudes of 130,000 feet can be achieved, but further study needs to be conducted in the area of propulsion. For the propulsion system, the emphasis is on the cooling system, engine weight and ram drag.

Other areas that need further investigation are:

- reduce the wing span or find an adequate airport that would support a wing span of 400+
- improve the reliability of the aircraft (possible by reducing the flight mission hours)
- investigate the effects of radiation on the aircraft and pilots

16. REFERENCES

1. **Nicolai, Leland M.**, Fundamentals of Aircraft Design, Mets,Inc., San Jose, Ca., 1984.

2. Roskam,J., Airplane Design: Part I, Preliminary Sizing of Airplanes, Roskam Aviation and Engineering Corporation, Route 4, Box 274, Ottawa, Kansas.

3. McCormick , Barnes W., Aerodynamics, Aeronautics, and Flight Mechanics, John Wiley & Sons, New York, 1979.

4. Eppler, Richard, and Somers, Dan M., Airfoil Design for Reynolds Numbers Between 50,000 and 500,000, NASA Langley Research Center, Hampton, Va.

5. Hoak, D. E. et al., USAF Stability and Control DATCOM, Flight Control Division, Air Force Flight Dynamics Laboratory, Wright Patterson Air Force Base, Ohio, 45433, Sept. 1970.

6. Raymer, Daniel P., Aircraft Design: A Conceptual Approch, AIAA Educational Series, New York, 1989.

7. Roskam, J., Airplane Flight Dynamics and Automatic Flight Controls: Part I, Roskam Aviation and Engineering Corporation, Route 4, Box 274, Ottowa, Kansas, 66067, 1979.

8. Roskam, J., Methods for Estimating Stability and Control Derivatives of Conventional Subsonic Airplanes, Roskam Aviation and Engineering Corporation, Ottowa, Kansas, 1971.

9. Lord, P., Ruggles, Diamante, Tamango, STADERP Program.

10. Hudson, Ray, Aircraft Flight Dynamics Analysis (AFDA) Program.

11. Blakelock, John, Automatic Control of Aircraft and Missles, John Wilex & Sons, Inc., New York, 1965.

12. California Technological Institute, Program CC

13. Akkerman, J.W., Hydrazine Monopropellant Reciprocating Engine Development, NASA Lyndon B. Johnson Space Center, Houston, Texas, January 1976.

14. Kerrebrock, Jack L., Aircraft Engines and Gas Turbines, MIT Press, Cambridge, Massachusetts, 1987.

15. Taylor, C.F., The Internal Combustion Engine in Theory and Practice, Volume 1, MIT Press, Cambridge, Massachusettes, 1985.

16. Taylor, C.F., The Internal Combustion Engine in Theory and Practice, Volume 2, MIT Press, Cambridge, Massachusettes, 1985.

17. Benson, R.S. and Whitehouse, N.D., Internal Cmbustion Engines, Pergamon Press Inc., New York, 1979.

18. Kays, W.M. and London, A.L., Compact Heat Exchangers, 3rd Edition, McGraw-Hill Book Company, New York, 1984.

19. Zinner, K., Supercharging of Internal Combustion Engines, Springer-Verlag, New York, 1978.

20. Janota, M.S. and Watson, N., Turbocharging the Internal Combustion Engine, John Wiley & Sons Inc., New York, 1982.

21. Cambell, Ashley S., Thermodynamic Analysis of Combustion Engines, John Wiley & Sons Inc., New York, 1979.

22. Benway, Ralph B., Design an Development of a Light Weight, High Pressure Ratio Aircraft Turbocharger, SAE 871041, 1987.

23. High Altitude Atmospheric Research Platform, Information Package, The Lockheed Corporation, Burbank, California, February, 1990.

24. Wilkerson, Paul H., Aircraft Engines of the World 1958/59, Washington D.C., 1958.

25. Rymer, Daniel P., Aircraft Design: A Conceptual Approach, AIAA Education Series, Washington, D.C., 1989.

26. Joyner, Upshur T., Mathematical Analysis of Aircraft Intercooler Design, NACA TN-781, October, 1940.

27. Benson, R.S., Annand, J.D., and Baruah, P.C., A Simulation Model Including Intake and Exhaust Systems for a Single Cylinder Four-Stroke Cycle Spark Ignition Engine, International Journal of Mechanical Science, Pergamon Press, 1974.

28. Strange, F.M., An Analysis of Ideal Otto Cycle, Including the Effects of Heat Transfer, Finite Combustion Rates, Chemical Dissociation, and Mechanical Losses, SAE 633D, January, 1963.

29. Kurtz, Oskar, Research and Design Problems Introduced by Increased Power Output, NACA TM-840, April, 1937.

30. Wasielewski, E.W. and King, J.A., Effect of Several Supercharging Control Methods on Engine Performance, NACA Tn-795, February, 1941.

31. Kutzbach, K., Adaptation of Aeronautical Engines to High Altitude Flying, NACA TN-142, May, 1933.

32. Incropera, Frank P. and DeWitt D.P., Fundamentals of Heat and Mass Transfer, John Wiley & Sons Inc., New York, 1985.

33. Sonntag, R.E. and Van Wylen, Gordon, Intoduction to Thermodynamics Classical and Statistical, John Wiley & Sons Inc., New York, 1982.

34. Wolgemuth, C.H. and Olson, D.R., A Study of Engine Breating Characteristics, SAE 74348, 1974.

35. Diehl, Walter S., The Application of Propeller Test Data to Design and Performance Calculations, NACA Report 186.

36. Gilman, Jean, Jr., Propeller-Performance Charts for Transport Airplanes, NACA TN 2966, 1953.

37. Roskam, J., Airplane Design Part IV: Layout Design of Landing Gear and Systems, Roskam Aviation and Engineering Corporation, Route 4, Box 274, Ottawa, Kansas, 1985.

38. Jones, Robert M., Mechanics of Composite Materials, Hemisphere Publishing, New York, 1975.

39. Lubin, George, Handbook of Composites,Van Noshand Reinhold Company, New York, 1982.

40. Anderson, William J., MSC/NASTRAN Interactive Training Manual, John Wiley & Sons Inc., New York, 1983.

41. Frank, Hawkins H.,Human Factors in Flight, 1987.

42. Roskam, J., Layout Design of Cockpit, fuselage, wing & Empennage: Part III, Roskam Aviation and Engineering Corporation, Route 4, Box 274, Ottowa, Kansas, 66067, 1979.

43. Gordon, Vail T., Design of Maintainability, SAE Technical Paper Series.

44. Billinton, Roy and Ronal, Allan N., Reliability Evaluation of Engineering Systems.

45. Global Stratospheric Change, Requirements for a Very-High Altitude Aircraft for Atmospheric Research, A Report of the Workshop Sponsored by NASA Ames Research Center Truckee, California, 1989.

46. Bedworth, David, and James Bailey, Integrated Production Control Systems, New York: John Wiley 1987.

47. Tomkins, James, and John White, Facilities Planning, New York: John Wiley 1984.

48. Carter, A.D., Mechanical Reliability, New York: John Wiley, 1972.

49. Stewart, Rodney, Cost Estimating, New York: John Wiley, 1982.

50. Dhillon, Balbir, Quality Control, Reliability, and Engineering Design, Dekker 1985.